Low field Nuclear Magnetic Resonance Spectroscopy of Hyperpolarized Spin Systems

Von der Fakultät für Mathematik, Informatik und Naturwissenschaften der RWTH Aachen University zur Erlangung des akademischen Grades eines Doktors der Naturwissenschaften genehmigte
Dissertation

vorgelegt von
Dipl. Chem.
Johannes Franz Peter Colell

aus Engelskirchen

Berichter:
Universitätsprofessor Stephan Appelt
Universitätsprofessor Bernhard Blümich

Tag der mündlichen Prüfung
29.04.2015

Contents

1 Theoretical Background **10**

1.1 Magnetostatics . . . 10

1.2 The Signal - Induction, Amplification and Origin of minimal Noise . . . 16

1.2.1 Coil detected NMR . . . 16

1.2.2 Signal-to-Noise Ratio . . . 17

1.3 Formal quantum mechanics . . . 19

1.3.1 Hilbert spaces . . . 19

1.3.2 Basic definitions . . . 20

1.3.3 The density matrix . . . 22

1.3.4 Nuclear Magnetic Resonance . . . 24

1.3.5 Secondary spin interactions . . . 27

1.3.6 Manipulation of spin systems with radiofrequency pulses . . . 28

1.3.7 Description of complex NMR experiments - Product Operators . . . 29

1.4 Para Hydrogen in NMR spectroscopy . . . 33

1.4.1 The Para Hydrogen Molecule . . . 33

1.4.2 Para Hydrogen Induced Polarization . . . 34

1.4.3 A chemical viewpoint of Para Hydrogen Induced Polarization . . . 36

1.4.4 Analytic description of the PHIP process . . . 38

2 Results **41**

2.1 Construction and Evaluation of a new shimmed Electromagnet system for high-resolution NMR spectroscopy . . . 41

2.1.1 Simulation of the magnet . . . 42

2.1.2 Evaluation of the magnet and shimming system . . . 45

2.1.3 The new current source - improvement of temporal homogeneity . . . 50

2.1.4 Experimental Homogeneity limits . . . 52

2.2 Spin Polarization induced Nuclear Overhauser Effect . . . 56

2.2.1 SPINOE-Equations . . . 56

2.2.2 Experimental procedure . . . 57

2.2.3 SPINOE Hyperpolarization of organic molecules . . . 58

2.2.4 SPINOE Hyperpolarization of Ionic compounds . . . 60

2.2.5 Ion SPINOE and strongly coupled systems . . . 62

2.3 Para Hydrogen Induced Polarization . . . 68

2.3.1 Introductory remarks . . . 68

2.3.2 Experimental verification of the heteronuclear three spin density matrix . . . 70

2.3.3 The model system . . . 72

2.3.4 Experimental procedure for ^{1}H experiments . . . 73

2.3.5 Field-dependent Ethoxyethylene spectra . . . 74

2.3.6 Derivation of the three-spin density matrix . . . 79

2.4 Styrene 81
2.4.1 PHIP-Hyperpolarization of Heteronuclei 83
2.4.2 Matching conditions 84
2.4.3 Experimental Studies 85

3 Conclusion and Outlook **89**

Statement of authorship

I herewith affirm that I have written this dissertation independently. All passages and sentences that have knowingly been taken literally or by meaning from other sources have been used with explicit declaration of origin. Furthermore I affirm that, this dissertation has not been submitted by me or another individual at a university or been published elsewhere.

Johannes Colell[1]

Aachen, 29.04.2015

[1] This Statement of authorship is valid without signature.

Additional information

Selected results presented in this thesis have already been published. In particular, the results described in the para-hydrogen induced polarization section are available in

J. Colell, P. Türschmann, S. Glöggler, P. Schleker, D. Budker, A. Pines, B. Blümich, S. Appelt, *Fundamental Aspects of Parahydrogen Enhanced Low-Field Nuclear Magnetic Resonance*, Phys. Rev. Lett. **110**, 137602 (2013).

P. Türschmann, J. Colell, T. Theis, B. Blümich, S. Appelt, *Analysis of para-hydrogen polarized spin systems in low magnetic fields*, Phys. Chem. Chem. Phys. **16**, 15411 (2014).

In addition it was moved for funding sponsored by the Bundesministerium für Bildung und Forschung (BMBF) in conjunction with the Deutscher Akademischer Austauschdienst (DAAD) resulting in the Academic Student and Scientist Exchange Network "ACalNet".

In the course of this thesis the RWTH Seed fund "Hyperpolarized Ions as Biosensors" was raised. Furthermore it was moved for the DFG grant "New atomic magnetometers for nuclear magnetic resonance" in collaboration with the Institute of Photonic Technology Jena and Ben Gurion University of the Negev.

The Exploratory Research Space (ERS) visit of Dr. S. Knappe was organized which will hopefully lead to fruitful collaboration between the ITMC and IWE1 of the RWTH Aachen University and the National Institute of Standards and Technology (NIST).

From 06/01-09/01/2012 I assisted the ERS Theodore von Karman fellow Dr. T. Theis with low field experiments regarding singlet state lifetimes in low magnetic fields. The variable Larmor-frequency and, in principle, free access to any nucleus offered by resistive magnet units offered unique research possibilities.

A scientist is supposed to have a complete and thorough knowledge, at first hand, of *some* subjects and, therefore, is usually expected not to write on any topic of which he is not a master. This is regarded as a matter of *noblesse oblige*. For the present purpose i beg to renounce the *noblesse*, if any, and to be freed of the ensuing obligation...

Erwin Schrödinger, What is Life?

Things will become clear to you... at least clearer than they are at the moment.

Slarty Bartfast, Hitchhikers Guide to the Galaxy by *Douglas Adams*

Acknowledgments

In the course of my thesis many people helped me be it in performing experiments, developing theoretical models, writing software or construction and development of hardware. I would like to acknowledge everyone who contributed to this work and express my appreciation for their support.

Thanks to my colleagues Stephan Appelt, Bernhard Blümich, Stefan Glöggler, Meike Emondts, Pierre Türschmann, Phillip Schleker and Martin Süfke.

I thank K. Ishikawa and B. Patton for their assistance with SPINOE experiments.

The financial support from the Jülich Research Center, especially the mechanics workshops of the ZEA I and II, is greatly appreciated. Construction an optimization of the new NMR magnet system would not have been possible without their excellent technical assistance.

The financial support from Prof. Blümichs group is gratefully acknowledged.

Finally I would like to convey my most sincere appreciation to my parents Franz und Vera Colell for their continued support.

Introduction

Over the last decades nuclear magnetic resonance (NMR) spectroscopy has established itself to be one of the most commonly used methods for investigation of molecular structures and dynamics. Since the discovery of the proton nuclear spin in 1933, for which O. Stern was awarded the Nobel price in 1943, another four Nobel prizes have been awarded in this field. The importance of NMR based methods originates mainly from the versatility of the method. The versatility originates from the low energy dissipation in a sample, as most materials do not interact with magnetic fields in a way that their molecular structure is altered and excitation impulses are radio-frequency fields of comparably low energy. The most widely known application of NMR is magnetic resonance imaging (MRI), and Lauterbur and Mansfield have been awarded a Nobel price in recognition of their achievements. Albeit most popular, imaging is hardly the most common application of NMR: NMR spectroscopy is widely in use as a means of structure elucidation and more dimensional spectroscopy has found widespread use in structural biology, as it allows for determination of rather complex molecular structures and has been awarded two Nobel prices.

It should be noted that structure elucidation means something different for NMR spectroscopy than for X-ray diffractometry or high resolution microwave spectroscopy in the gas phase. NMR is an indirect method applicable for condensed phases with a large number of interacting particles. The spectra do usually not allow determination of structure in a theoretical chemists sense - that is either a determination of the full set of coordinates for each nucleus for an isolated molecule or coordinates and translational order/space group in a crystal[2] - but instead refers to the possibility to reconstruct the sequence and connectivity of the nuclei from a spectrum which effectively enables determination of a structure. This restriction is reasonable, as for organic compounds in solution the available thermal energy, proportional to $k_B T$, is often sufficient to allow for free rotation (or tunneling) of bonds. An NMR spectrum will thus be an ensemble average over all rotamers. Ensemble averaging is one of the characteristics of NMR theory in general and will be discussed at a later stage, albeit not all details will be discussed.

Traditionally NMR related experiments are carried out in high magnetic fields and field strengths range from 9.3 to 28 Tesla in common, and 50 Tesla in exotic applications. The rationales for favoring high field strengths are abundant and the development of low-field NMR has long been impeded. Firstly, the NMR methods have inherently low sensitivity which can be partially alleviated by using high magnetic fields to obtain correspondingly high polarization. The parameters used for structure elucidation in the liquid state historically constituted the most important argument for high fields. One important parameter, the chemical shift of a nucleus in a given environment, is proportional to the magnetic field while the other important parameter, the scalar J-coupling, may often not be resolved in low fields as a result of an effect known as roof-effect which occludes both chemical shift and coupling information when the ratio of absolute frequency shift to the coupling (both in Hertz) is close to, or smaller than, unity.

However, advances in the quality of microelectronics, development of new sensors types including atomic magnetometers and nitrogen-vacancy based sensors, and hyperpolarization technology have rekindled the interest in low field methods and made it an increasingly popular field of research in the last two decades. The first NMR experiment in very low magnetic fields has been carried out as early as 1954 by Packard and Varian, who were able to observe an NMR signal of water in the weak magnetic field of the Earth, quite an accomplishment given that the Earth's magnetic field only has a flux density of 0.5 Gauss, or $5 \cdot 10^{-5}$T[50]. There is, however, no strict definition of what is to be considered a low-field experiment. In this thesis methods where a magnetic field of less than 1000 G is applied shall be deemed low field NMR, but from a neutral point of view 0.1 Tesla already constitutes a significant magnetic field. With respect to the possibilities offered by NMR it is important to differentiate between methods requiring a homogeneous and static magnetic field - the spectroscopic methods - and those requiring a gradient field of some sorts, which includes imaging and diffusion measurements.

For the present purpose we shall restrict the ensuing discussion to spectroscopy in low magnetic fields, as

[2] Note that it is sometimes possible to determine structural details in solid state NMR, but X-ray or neutron methods are not limited to certain space groups and remain superior.

this thesis is unconcerned with methods requiring static or pulsed gradient fields and high-field NMR is rarely used. It is evident from the acronym NMR that in order to perform an experiment at the very least a nucleus and a magnetic field are required[3]. The most important factor for spectroscopy is always spectral resolution. In NMR the resolution is defined by the linewidth as a fraction of the overall spectral width characteristic for a given nucleus on the one hand, and the Signal-to-Noise ratio (SNR) on the other, as SNR determines the visibility of a line. The overall spectral width of a nucleus is defined by the magnitude of its observable J-coupling and its maximum chemical shift range, where both are characteristic for a given isotope of a nucleus, whereas linewidths are a function of the magnetic field homogeneity. It should be noted that chemical shifts are given as parts per million (ppm) frequency shifts to an external reference (Tetramethylsilane for ^{1}H and ^{13}C). In order to resolve chemical shift, one of the important parameters for structure elucidation, the magnetic fields homogeneity should evidently be comparable to that quantity, meaning that all inhomogeneities over the sample need to be less than one ppm. The first task for a low-field NMR experiment is thus to construct a magnetic field system, which may consist of one or more coils, that allows to generate and maintain a highly homogeneous field. Explicit calculations based on magnetostatics are required for the construction of magnets providing high homogeneity. The theory will be briefly reviewed and details of the construction and evaluation of the shimmable electromagnet with variable field and modular probes constructed in this thesis shall constitute the first part of the experimental section.

Regarding the inherently low sensitivity of the method the fundamental quantity is the Signal-to-Noise ratio (SNR). It evidently depends on the number of molecules that are being investigated, but higher number of nuclei always means larger sample volumes. If a larger sample diameter is chosen maintaining field homogeneity over the sample becomes problematic and often times spectral resolution will have to be sacrificed with large volume samples. Other factors influencing the SNR can be attributed to other aspects, such as characteristic constants of nuclei and microelectronic devices. For the nuclei the important quantity is the gyromagnetic ratio, as it is connected with the magnetic moment which will define the voltage in a coil resulting from induction. Microelectronic devices used in the amplifier stages have a characteristic current noise i_n and voltage noise e_n and will constitute a noise source. For coil detected (standard) NMR, the origin of the signal is Faraday induction caused by the magnetic fields of atomic nuclei with a non-zero magnetic moment placed inside a coil while precessing in an external magnetic field. Hence quantum mechanical and electrodynamical aspects are important for understanding an NMR experiment. And lastly the sensitivity of the method is only inherently low when spin alignment is achieved by brute force - exposure to strong magnetic fields. It can sometimes be circumvented by hyperpolarization methodology. Hyperpolarization is generally defined by coupling of nuclei to an external reservoir with very high polarization and this is where the rationale favoring low-field NMR comes into play. Coupling to the external reservoir of high polarization may be more efficient in low fields, as coupling involves matching of frequencies. It may be easier from a technical viewpoint to perform a hyperpolarization experiment in low fields, as, for example field distortions caused by diamagnetic metallic building blocks influence field homogeneity less significantly. And finally it may simply be cheaper not to have to use several cryocooled superconducting magnets.

Established methods of hyperpolarization are interaction of nuclei with organic radicals, where an unpaired electron is continuously excited by means of microwave irradiation to an equilibrium state (Dynamic Nuclear Polarization: DNP), coupling to a highly polarized Laser beam with subsequent transfer from polarized electron spins to a nucleus (Spin Exchange Optical Pumping: SEOP), interaction of highly polarized nuclei with low polarization nuclei by either dipolar interaction (Spin Polarization Induced Nuclear Overhauser Effect) or by preparing a system into a pure state (such as a singlet state in the hydrogen molecule) and enforcing a direct interaction by means of forming a chemical bond between those compounds leading to non-equivalent hydrogen positions in the reaction product, thus creating a large measurable magnetization (Para-Hydrogen Induced Polarization). With the exception of DNP, all means of hyperpolarization have been used to some extent within the course of this thesis. DNP requires extensive construction of suitable hardware.

[3] In more exotic applications, the zero-field methods, similar experiments can be performed in absence of a magnetic field, as the J-coupling exists independent of the field.

Chapter 1

Theoretical Background

For the reasons discussed in the introduction NMR requires critical inspection of multiple points which can each be attributed to a different field of scientific or engineering disciplines. Firstly an NMR experiment requires a magnetic field to be well known, as field homogeneity is the decisive factor for spectral resolution. Essential details of magnetostatics theory shall be briefly reviewed and the origin of magnetic fields will be derived from first principles. This will be required for understanding the general procedure of performing the simulations for the following construction of the electromagnet and shimming system. Furthermore the characteristics of battery-driven resistive magnet units for low-field NMR spectroscopy can only be understood in the framework of magnetostatics theory.

Any magnetic resonance experiment needs to be detected in one way or another and the operating principle of coil detected NMR, where the signal is the voltage induced by precessing nuclear spins placed within this coil, will be discussed. The law of induction will be stated, and origin of signal and noise will be discussed in some detail.

The third part will be covering relevant quantum mechanical aspects of NMR spectroscopy and introduce the common mathematical framework of NMR theory. A description in terms of a density matrix is of special relevance for reasons that will become evident.

Finally a brief description of catalytic hydrogenation reactions in homogeneous phase is relevant for the understanding of the Para-Hydrogen Induced Polarization (PHIP) effect.

1.1 Magnetostatics

This section covers the theoretical background information relevant to construct a magnetic field coil suitable for spectroscopy purposes. Magnetostatics theory is a part of electrodynamics, one of the classical disciplines of theoretical physics. Magnetic effects are long known and date back to the lodestone (6th century BCE), a compound intrinsically magnetized and ordered resulting in permanent magnets (consisting of the magnetic mineral Magnetite Fe_3O_4), but a rigorous description of magnetism has not been successful for many centuries. Literature attributes the problems with a mathematical description of magnetism and its origins to the fact that, in contrast to electrostatic phenomena where electrons as a monopole with an elemental charge q may be defined as the origin, no magnetic monopole or elemental magnetic charge exists.[35, 48, 31]

Magnetostatic fields are caused by *stationary electrical currents*, where *stationary* is to be understood as currents having a constant current density that does not change in time. Magnetism is thus a property related to *moving* charges, rather than the presence of surplus charge or inhomogeneous charge distributions. All definitions have historically been made for moving positive charges, the electron has a charge of $-e$. As this section serves as a means to introduce some concepts important for NMR it should initially be noted that special attention should be payed to the occurrence of the current strength I in equations relating magnetic fields to the current. Unique to low-field NMR with electromagnets is the concept of temporal field homogeneity, as the

mean field should be a magnetostatic field which can only be obtained by *stationary* currents[1]. This constitutes an additional problem over the the spatial homogeneity requirements briefly discussed in the introduction.

The movement of charge carriers is described by the current density $\vec{j}$

$$\vec{j} = nq\vec{v}, \tag{1.1}$$

where n is the number of electrons with elemental electrical charge $q = -e$ in a volume increment V that flow parallel to the normal vector on the conductor cross section area A with average velocity $\vec{v}$. The definition of a current is straightforward. It includes the conductor cross section area G to yield[2]

$$\vec{I} = nq\vec{v}G. \tag{1.2}$$

However, the movement of a charge carrier along a trajectory is generally a directed quantity. In simple cases it is thus a vector and in general a time and spatially dependent vector field. The generalized expression is

$$\vec{j}\left(\vec{r},t\right) = \varrho\left(\vec{r},t\right)\vec{v}\left(\vec{r},t\right), \tag{1.3}$$

where $\varrho\left(\vec{r},t\right)$ is the charge density, which is defined by the number of charges in a volume increment $d^3\vec{r}$. The reason for a directed flow of charged particles, with an average velocity $\vec{v}\left(\vec{r},t\right)$, must be a potential difference between two points in space

$$\varphi\left(\vec{r}\right) - \varphi\left(r_0\right) = -\int_{r_0}^{r} \vec{E}(\vec{r'}) \cdot \mathrm{d}\vec{r'}, \tag{1.4}$$

where $\varphi\left(\vec{r}\right)$ is the scalar electrical potential and $\vec{r'}$ is the vector to the relevant point in space. This potential difference defines the voltage. The integral is to be understood in terms of a line integral, where at every point along the connection formed by the vector $\vec{r'}$ the *scalar product* between vector and vector field $\vec{E}(\vec{r})$ is to be calculated.

The fundamental problem of magnetostatics is to calculate the field of magnetism, the magnetic induction $\vec{B}$, which is caused by the current density $\vec{j}$ through a conductor of defined geometry[48, 35]. If we consider two closed loops, say C_1, C_2 carrying currents I_1 and I_2, the interaction of two magnetic fields will result in a force between the magnets described by Ampere's Law, which is a physical quantification of everyday experience with magnets. Furthermore a current, or more generally a current density, will also result in a magnetic induction defined by Biot-Savarts law

$$\vec{B}\left(\vec{r}\right) = \frac{\mu_0}{4\pi}\int \vec{j}\left(\vec{r'}\right) \times \frac{\vec{r} - \vec{r'}}{|\vec{r} - \vec{r'}|^3}\mathrm{d}\vec{r'}^3 \tag{1.5}$$

This equation introduces the magnetic induction, magnetic flux density or magnetic field $\vec{B}$, the directly measurable quantity in magnetic phenomena. It is connected to the more abstract notion of an underlying vector-potential $\vec{A}$. Calculation of the vectorpotential resulting from a specific conductor geometry allows to obtain the magnetic field at a point in space, and thus designing a magnet suitable for NMR spectroscopy. However, an expression for the vector potential and the connection to magnetism is required. Unfortunately there is no shortcut to derive the relevant relationships. The relevant differential equations need to be introduced and elucidated upon their solution, as is done in the literature [48, 35]. It is

$$\frac{\partial \varrho}{\partial t} + \vec{\nabla} \cdot \vec{j} = 0. \tag{1.6}$$

The Nabla-Operator, also called divergence, is the sum of the partial differentiation of the components F_i

[1] A similar problem arises when permanent magnets are used for NMR. Material properties like expansion coefficients of materials and the dependency of the magnetic field on the temperature have similar effects. If a magnet is not exposed to significant temperature changes or mechanical force the time-scale is different, changes occur more slowly.

[2] Note that this definition leads to some difficulties. A wire is described as a mathematical object, say a line, which does by definition not have a cross-section.

$(i = x,\, y,\, z)$ of a quantity $\vec{F}$ to its respective coordinates

$$\vec{\nabla} \cdot \vec{\mathbf{F}}\,(\vec{r}_0) = \frac{\partial F_x}{\partial x}\,(\vec{r}_0) + \frac{\partial F_y}{\partial y}\,(\vec{r}_0) + \frac{\partial F_z}{\partial z}\,(\vec{r}_0) \tag{1.7}$$

and here it quantifies the flux of the vector field along the vector $(\vec{r}_0)$, thus the name divergence. Any change of the charge density in time must be caused by a flow of a number of charged particles out of (or into) the volume increment and, as the name magneto*statics* implies, stationary currents result in no change of the charge density at any point in space. This means $\partial\varrho/\partial t = 0$ and thus

$$\vec{\nabla} \cdot \vec{j} = \operatorname{div} \vec{j} = 0. \tag{1.8}$$

Equation (1.8) constitutes the first fundamental differential equation of magnetism, the homogeneous Maxwell-equation also referred to as continuity equation. The second fundamental equation

$$\vec{\nabla} \times \vec{B} = \operatorname{rot} \vec{B} = \mu_0 \vec{j} \tag{1.9}$$

is the inhomogeneous Maxwell-equation and connects the magnetic field to the vector potential $\vec{A}$

$$\vec{B} = \operatorname{rot} \vec{A}. \tag{1.10}$$

Now that the magnetic field has been introduced and a connection to moving charges has been established it is sensible to briefly review some experimental facts about magnetic fields and solenoid coils before elaborating on simulations of an electromagnet system suitable for NMR spectroscopy.

A solenoid coil of a finite length will never result in a magnetic field with no change along its spatial dimensions. Along the axis of rotational symmetry the field has a parabolic shape with its maximum field strength in the middle of the twine. This seems reasonable, as the contribution to the field strength made by each turn of the twine[3] adds up to give maximum field strength in the geometric middle. However, magnetic fields may add up or compensate for each other at a point in space, as magnets are dipoles rather than monopoles.

The shimming process for an NMR-magnet can be understood as a puzzle, where the question is how to generate magnetic fields that, when the superposition of the fields is taken, result in a magnetic field of a desired magnitude at a position in space with changes to the field strength along the spatial coordinates that are smaller than $10^{-6} = 1\,\text{ppm}$ of the value of the field at this position. Modern high-field NMR machines allow to obtain parts-per-billion homogeneity over small samples[4]. As this field may be a superposition of fields generated by several coils, the puzzle is defined by how to combine coils of different geometries to yield a desired result.

[3] The winding of the coil. Twine is more commonly used for thread.

[4] Conventional high-field NMR sample tubes have inner diameters of 4.94-4.96 mm.

Modelling of the magnet unit

It was reasonable to assume that superposition of fields generated by solenoids would allow for a very homogeneous magnetic field along a cylinder length axis, given that curvature of the magnetic field of the additional coils compensates for the curvature of the main field. The first important task was to determine a way to analytically describe the problem at hand.

A solenoid coil consists of a number of helices, where the number of helices is identical to the number of layers. A helix is a space curve with the parametric equations for its coordinates defined by $x = r\sin v;\ y = r\cos v;\ z = ct$. Two helices with different diameters are shown in Fig. 1.1 and constitute a rather realistic scenario for a solenoid coil with two layers[5]. The separation of the helix loops is given by $2\pi c$. In an actual construction the lower limit is given by the wire diameter d_w, that is saying every loop is in direct contact with its neighbors.

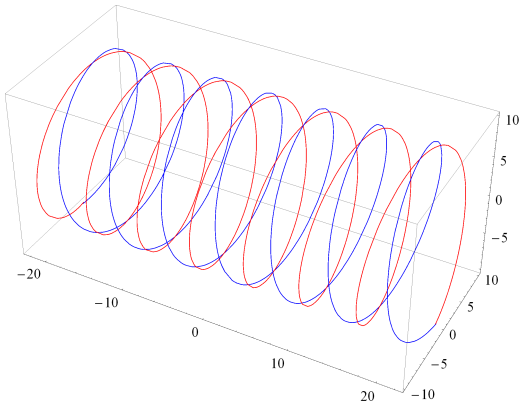

Figure 1.1: A two layer solenoid consisting of two helices. For clarity the separation of helix loops $2\pi c$ has been chosen to be much larger than in the actual construction.

An analytic description relating to actual construction details is required for several reasons. The current I and the radius of a loop a are the defining quantities for resistive magnets. The result of explicit calculation will yield the *driving currents* necessary to obtain a desired magnetic field strength obtained from a coil with a number of loops. The radius of the wire needs to be adapted to the driving current. In a resistive magnet Joule-heating with a power dissipation P will occur. The power P converted from electrical to thermal energy is given by $P = \Delta V I = I^2 R$, with ΔV as the voltage drop over the element, current I and resistivity R. The resistivity for directed, stationary currents is given my $R = l/G\rho_{Cond}$, and thus a function of the length of a wire l, the wire cross section area G and a the conductivity ρ_{Cond}, a material constant of the conducting material. This imposes restrictions on the wire diameter required for a given current. Knowledge of the current allows to define the wire diameter which will allow to calculate the number of turns required to obtain a field of given strength. This will evidently require an iterative procedure, as, for example, a change of the wire diameter will change the number of turns and the applicable maximum current.

As shown by the sequence in Fig. 1.2, a helix can be approximated by an number of parallel loops. It should be expected that the approximation becomes better with smaller ratio of wire diameter and coil support diameter, as the approximation of parallel wires becomes better[6].

This way the first step in the problem of constructing a magnet suitable for high resolution low-field NMR-spectroscopy can be reduced to a problem extensively discussed in the literature - the vector potential and magnetic field of a current carrying loop - by approximating the solenoid as a number of parallel loops[7].

Due to the symmetry of a loop it is reasonable that mathematical details are most conveniently described in geometry adapted coordinates. Analytic calculation of magnetic fields requires an analytic function describing the current in a loop, defining the spatially dependent vector field of the preceding section.

In the coordinate system shown in Fig. 1.3, with the loop placed in the x, y-plane of the Cartesian coordinate frame, the current will only have an x- and a y-component. If the symmetry center of the loop is placed at the coordinate frame origin, the current can be written as a function of only ϕ, as the velocity of the charge

[5] There are still deviations at the end of each turn where the winding is inverted for the second layer. Using two sine-functions with different sign leads to a discontinuity at the point where the wire changes form one layer to another, a kink not present in a real solenoid. This is one of the reasons why, apart from the apparent problems with analytic mathematical description, a simpler approach seemed appropriate.

[6] A special type of wire was used for the mean field coil. It has a rectangular cross section allowing for orderly stacking of coil layers. Spatial dimensions are 1.5 x 2.6 mm. Wires are arranged to allow for a maximum number of turns per layer, that is the smaller one of the aforementioned values (1.5 mm) defines the wire spacing.

[7] Which can be justified by considering that the coil support cylinder has a diameter of 200 mm and the wire diameter is 1.5 mm.

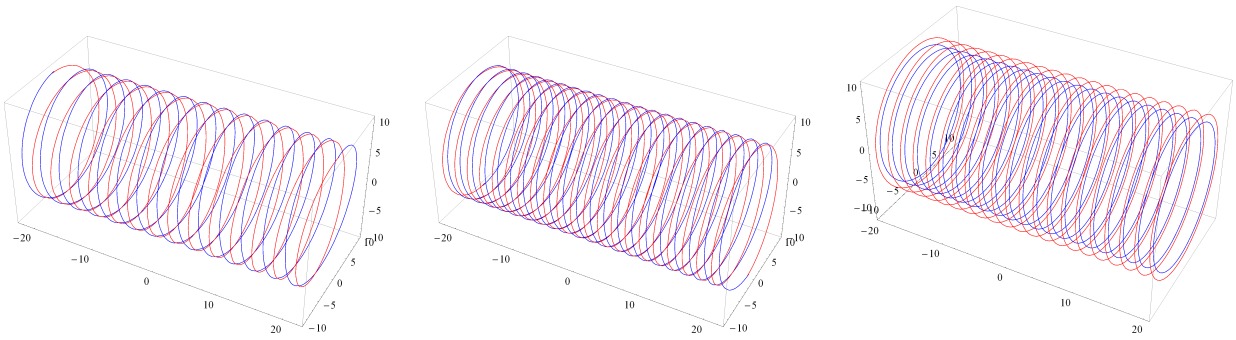

Figure 1.2: From left to right: Reduction of loop displacement per turn results in a smaller angle between the wires of two layers. As shown on the right hand side, a solenoid consists of parallel wires in the limit of infinitely small wire diameters (radius of the red loops on the r.h.s. has been chosen larger for clarity). The wire diameter defines the distance between nested loops in the simulation.

carriers is given by the angular velocity. A vector that is tangential to the loop at every point of the loop can be constructed using the unit vectors $\vec{e}_x, \vec{e}_y$ and trigonometric functions thereby describing the movement of charge carriers trajectory on a loop analytically.

It is

$$\vec{j} = -j_\phi \sin\phi' \, \vec{e}_x + j_\phi \cos\phi' \, \vec{e}_y \tag{1.11}$$

The missing term j_ϕ needs to restrict the current vector to the loop. This is most conveniently realized by introducing the Dirac-Delta function δ.

$$\begin{aligned} \delta(x-a) &= 0 \qquad \text{for } x \neq a \\ \int \delta(x-a)\mathrm{d}x &= \begin{cases} 1 & \text{if } x = a \text{ is in the integration region} \\ 0 & \text{otherwise} \end{cases} \end{aligned} \tag{1.12}$$

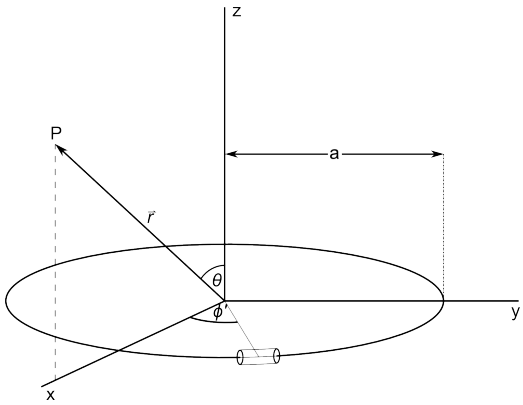

Figure 1.3: A loop representing the conducting wire placed in the x, y-plane of a coordinate frame. For a loop placed in a way that its center is at the origin of the coordinate frame a DC-current is described by a change of the ϕ-coordinate - the current only has a ϕ-component. The current needs to be restricted to the conductor, that is coordinates ϕ', θ' and $|\vec{r}| = a$. All coordinates denoted with ' are on the loop.

The Dirac δ-function is a distribution that can be understood as the limit of a function with one well defined maximum, say a Gauss-function, that gets narrower and higher while the integral remains normalized to unity. The strict mathematical definition is defined by a series of normalized functions $\delta_n(x)$. Explicitly a series of Gaussian functions

$$\delta_n(x) = n e^{-\pi n^2 x^2} \tag{1.13}$$

constitutes one valid example[35]. The rigorous definition is

$$\lim_{n\to\infty} \int \delta_n(x-a) f(x) \mathrm{d}x = f(a), \tag{1.14}$$

and thus the Dirac-delta function may be defined to be

$$\int \delta(x-a) f(x) \mathrm{d}x = f(a). \tag{1.15}$$

It is now applicable to define the missing term j_ϕ using the δ-function and

$$j_\phi = I\delta(\cos\theta') \frac{\delta(|\vec{r'}| - |\vec{a}|)}{|\vec{a}|}. \tag{1.16}$$

From the coordinate choice in Fig. 1.3 it is evident that $\theta = 90° = \theta'$ thus restricting the current to the x, y-plane with the first δ-function and to a radius a with the second one.

The vector potential and magnetic field of a single loop are known from the literature [35]. Due to the rotational symmetry of a loop and the well defined behavior of x, y-components of the current according to Eq. (1.11) the vector potential is a function of θ and $\vec{r}$.

But as the current is a function of ϕ so is the vector potential A_ϕ. In cgs. units, which are more convenient for low magnetic fields which are more conveniently given in Gauss and defining $|\vec{r}| = r$, it is

$$A_\phi(r,\theta) = \frac{I}{ac}\int r'^2 \mathrm{d}r'\mathrm{d}\Omega' \frac{\cos\phi'\delta\cos\theta'\delta(r'-a)}{|(r^2 - 2rr' + r'^2 - 2ar\sin\theta\cos\phi')^{1/2}|}, \tag{1.17}$$

where c is the speed of light. The explicit solution of the integral is performed by integration over the δ-functions. Using the definition of the Dirac-delta function from Eq. (1.15) means that integration over r'^2 will simply yield a^2. Similarly the integration over $\cos\theta'$ is trivial, as $\theta' = 90° = 0$. The integration over the delta-functions thus results in

$$A_\phi(r,\theta) = \frac{Ia}{c}\int_0^{2\pi} \frac{\cos\phi'\mathrm{d}\phi'}{(a^2 + r^2 - 2ar sin\theta\cos\phi')^{1/2}} \tag{1.18}$$

This integral can be expressed by the complete elliptic integrals of the first and second kind $K(k)$ and $E(k)$.

$$A_\phi(r,\theta) = \frac{4Ia}{c(a^2 + r^2 + 2ar\sin\theta)}\left[\frac{(2-k^2)K(k) - 2E(k)}{k^2}\right] \tag{1.19}$$

The argument k of the elliptic integrals is defined by

$$k = \frac{4ar\sin\theta}{a^2 + r^2 + 2ar\sin\theta}. \tag{1.20}$$

The solutions of these integrals are known and implemented in common software packages[8]. Making use of the solutions allows to obtain the magnetic induction and its components are

$$\begin{aligned} B_r &= \frac{1}{r\sin\theta}\frac{\partial}{\partial\theta}\sin\theta A_\phi \\ B_\theta &= -\frac{1}{r}\frac{\partial}{\partial r} r A_\phi \\ B_\phi &= 0. \end{aligned} \tag{1.21}$$

The magnetic field of a solenoid can now be obtained by summation over the contribution from each loop. The position of the first loop is placed at the x, y-plane of a coordinate frame and all other loop positions are defined by the choice of wire diameter d_w, where the z-position of the n-th loop is simply $z_n = nd_w$.[9]

To conclude this section the important results shall be briefly discussed. The rationale why solenoid coils with a small displacement per loop can be approximated by parallel current carrying loops has been established. Secondly, the prefactor of the integral in Eq. (1.17) shows that the value of the magnetic field will be directly proportional to the driving current. Current drifts must thus be avoided if a homogeneous field is to be obtained - irrespective of the theoretical limit to field homogeneity resulting from conductor geometry. This statement follows directly from $A_\phi(r,\theta) \propto I$ and defines *temporal* field homogeneity. It is important to keep in mind why currents need to be very homogeneous, that is stationary, to obtain a homogeneous field applicable for NMR spectroscopy, as defined by the prefactor of the integral in Eq. (1.17). A convincing example of spectra obtained with different current sources will illustrate the temporal homogeneity issue.

[8] Such as Wolfram Mathematica or Mathworks Matlab. Implementation has to be handled carefully, as to internal parameter declarations characteristic to the programs are not identical with the ones commonly found in the literature.

[9] There is a small error here. The length of a helix exceeds the length obtained from simulation by one wire diameter, as one full turn ends exactly one wire diameter displaced from the starting point. The number of turns in the experimental setup are thus not the calculated number but one turn per layer less. For example, the solenoid shimming coil has 398, rather than the calculated 400 turns, as it is a two layer solenoid.

1.2 The Signal - Induction, Amplification and Origin of minimal Noise

Whereas Biot Savart's law defines the magnetic field generated by a current density, Faradays Law of induction deals with its reversal. In 1831 Faraday performed experiments to clarify whether, if a moving charge causes a magnetic field, a magnet moved relative to a fixed detector shouldn't also result in an observable current.[10]

A magnet that is moved past a fixed detector causes a varying magnetic field at the detectors position in space and the law of induction is

$$\oint_C \vec{E} \cdot \mathrm{d}\vec{r} = -\frac{\mathrm{d}}{\mathrm{d}t} \int_{F_C} \vec{B} \cdot \mathrm{d}\vec{f} \tag{1.22}$$

so that integration of an electrical field $\vec{E}$ over a closed conductor loop C yields the time dependence of the corresponding magnetic field. In the following the left hand side of this equation shall be referred to as electromotive force ξ, the right hand side is the rate of change of the magnetic flux ϕ through an area F_C whose boundary is the closed conductor loop, where $\mathrm{d}\vec{f}$ is the normal vector on F_C.

Induction is the basis of coil based signal detection in NMR experiments. The combined magnetic moments of aligned precessing nuclear spins[11] result in a voltage in the coil which is amplified and recorded.

1.2.1 Coil detected NMR

Any signal received by a detector will always consist of at least two parts, where one is the ideal undistorted signal and the other part is noise. In real applications there may be multiple causes for the noise, where the most prominent ones are i) the receiver picking up noise from external sources ii) the conductor itself iii) the amplifier itself. In the following we need to pay great attention to properly discriminate between the notion of a signal, which may refer to the measured signal including noise or the undistorted signal.

The undistorted signal is quantum mechanical in origin and, from a physicists viewpoint, it is the induction of a electromotive force (emf) ξ, caused by precessing spins in proximity to a conductor causing a time varying magnetic field. If a closed conductor loop C, carrying unit current i, is considered this loop will produce a field $\vec{B}_1$ at the position of a fictive dipole $\vec{\mu}$. It is

$$\xi = \frac{\partial}{\partial t} \vec{B}_1 \cdot \vec{\mu}, \tag{1.23}$$

As Faraday's-Law demands equality between time variation of a magnetic field and the emf ξ, it can immediately be stated that a current in a closed conductor loop will result in a magnetic field. If the situation is reversed, meaning an oscillating dipole causing an emf exists in the proximity of a conductor, the description must also remain valid. However a real sample does not contain just one spin and the induced emf will result from all spins, the net magnetization, and the relative position of all spins in space. This leads to the necessity to integrate over the sample volume V_s, where the value of the $\vec{B}_1$-field is at any point in the sample needs to be known. If the spins in a sample have been subjected to a 90°-pulse the magnetization is only a function of a known mean magnetic field B_0 and, assuming a perfect pulse, the value of $\vec{B}_1$ will be identical at all points in the sample. Therefore integration over sample volume and time is a trivial task (relevant parameters are constants) and solution of the first order differential equation yields

$$\xi = K\omega_0 (B_1)_{xy} M_0 V_s \cos(\omega_0 t), \tag{1.24}$$

where a factor K, accounting for B_1-field inhomogeneity, has been introduced. The scalar quantity $(B_1)_{xy}$ is the part of the magnetic field of all dipoles that actually contributes to the emf, that is the component of the field B_1 perpendicular to the mean field.[12]

It should be noted that the outlaid theory can, in principle, be used to calculate the signal for different coil

[10] This is a simplification based on modern perception, which allows to see induction in context. The original experiments dealt with the behavior of currents in time dependent magnetic fields originating from permanent and electromagnets.

[11] The net magnetization will be formally introduced later on.

[12] Mind the dot (scalar) product in the definitions. Dot products of parallel vectors yields maximum values, whereas orthogonal alignment yields zero and can be neglected.

geometries. Results will only be an approximation if skin and proximity effects are neglected. The skin effect is the phenomenon that current densities of alternating currents in a conductor are not distributed uniformly over the cross section of the conductor, but higher on the surface. This leads to an increase of the effective resistivity of a conductor that becomes more prominent with increasing frequency. The proximity effect results from the spatial proximity of loops of a coil to each other and is caused by the mutual influence of current densities of the loops of a coil.

It is interesting to note that no analytic theory for coils with many layers and a high number of turn accounting for the proximity effect has been derived so far. This has the annoying result that when a low-field NMR experiment is performed with two (seemingly identical) coils they can have different properties in an experiment[13]. This is a result of Thompson's formula for resonant L, C-circuits $\omega = 1/\sqrt{LC}$, where the resonance frequency of a circuit used for signal detection imposed restrictions on the coil inductivity L and capacitance of the matching capacitator C. Every wire has a residual value of C, which may not become infinitely small and hence usually a large value of L is required at low magnetic fields and low frequencies. As the inductivity scales with the number of turns of the detection coil large coils are required at low frequencies.

1.2.2 Signal-to-Noise Ratio

The noise is the part of the voltage that is fluctuating randomly. It will generally be unavoidable that different noise sources exist. If a system is perfectly designed, the emf in the conductor wire should only be superimposed by the thermal noise of the conductor itself. The thermal noise of conductors, also called Johnson-Nyquist noise, is of the white noise type and thus frequency independent - the time averaged voltage is identical at each frequency[14]. This noise voltage V_n of thermal noise of the conductor is given by

$$V_n = (4k_B T_w \Delta\nu_d R)^{\frac{1}{2}} \tag{1.25}$$

with temperature of the conductor T_w, detection bandwidth $\Delta\nu_d$, resistivity R and Boltzmann's constant k_B.

The semiconductors that are part of the e.g. operation amplifiers in the circuitry constitute additional noise sources. The additional noise is a characteristic property of the component and manufacturers give specific values for voltage noise e_n and current noise i_n, which are important parameters for the design of low noise electronics. Any experimenter or electronics designer needs to pay attention to the tradeoff between components with high i_n and low e_n, and vice versa, and where to use which component in an amplifier circuit.

The signal is originating from quantum mechanics and proportional to the magnetization of the nuclei. For thermally polarized spin systems it is a function of the magnetic field strength B_0.

$$M_0 = N_s \gamma_i^2 \hbar^2 I(I+1) \frac{B_0}{3k_\mathrm{B}T} \tag{1.26}$$

γ_i is the gyromagnetic ratio of the observed nucleus i, N_s the spin density[15] T the thermodynamic temperature of the sample, not the conductor, B_0 the magnetic field strength, $\hbar$ is Planck's quantum divided by 2π and here I refers to the spin angular momentum quantum number of the nucleus.

The Signal-to-Noise ratio (SNR) is defined by the peak signal strength and the root mean square noise in terms of a voltage ratio

$$SNR = \frac{S}{N} = \frac{K(B_1)_{xy} V_s N_s \gamma \hbar^2 I(I+1) \frac{\omega_0^2}{3k_\mathrm{B}T}}{\sqrt{2}\, V_\mathrm{noise}}. \tag{1.27}$$

Use of the root mean square noise introduces the factor $\sqrt{2}$. The term $(B_1)_{xy}$ is more commonly found as B_1/i

[13] Usually this simply means the effective measure of an NMR experiment, the Signal-to-Noise ratio, varies between two coils with many layers and many turns even if the number of turns is identical. These variations can be surprisingly large and depend on how a coil has been manufactured.

[14] As opposed to pink noise, very relevant for extremely low-frequency applications such as SQUID MEG or NMR with SERF atomic magnetometers close to zero-field. Pink noise intensity is a hyperbolic function of the frequency

[15] The number of spins per unit volume. The notion of a spin density might seem a little weird, especially to a chemist who would look for a molar quantity, but the product of sample volume and spin density is the number of NMR active isotopes in the sample.

and referred to as coil sensitivity due to the occurrence of the unit current i. From Eq. (1.27) it is evident that the product of sample volume V_s and spin density N_s, as well as the Larmor-frequency ω_0, strongly influence the SNR. The signal is proportional to the square of the Larmor-frequency $\omega_0 = \gamma_i B_0$, and thus the magnetic field strength. The expression V_{noise} may generally be rather complex, as it is the contribution of the noise generated by *all* noise sources[16].

For hyperpolarized spin systems the expression for the noise remains unaffected, as it is not connected to the polarization of the spin system but the systematic error resulting from choice of a specific detection system, that is magnet and spectrometer in a given location[17]. The signal, however, is a function of the magnetization and for hyperpolarized spins the expression becomes

$$SNR = \frac{k_0 \gamma \frac{B_1}{i} V_s N_s \hbar \omega_0 P_N}{\sqrt{2}\, V_{\text{noise}}}. \tag{1.28}$$

Equation (1.28) shows that the SNR depends linearly on the polarization P_N, the number of NMR active nuclei, the Larmor-frequency and the coil sensitivity. The polarization, and thus magnetization, has been replaced by an expression reflecting on a polarization method other than brute force alignment by magnetic field exposure. It is then given by

$$M_0 = \frac{1}{2} n_s \gamma \hbar P_N. \tag{1.29}$$

P_N is the polarization of the spin ensemble[18] mentioned in the introduction and can range from $P_N \in [0, 1]$. If P_N is 1 the system is said to be in a pure state.

[16] A statement typically made in that context is that all electronics prior to digitalization will add additional noise and there is no noise increase after digitalization.

[17] The location matters, as it will be responsible for the external noise sources.

[18] Which may be a Laser, a para-hydrogen molecule, another nucleus with a higher polarization or a dynamic phenomenon resulting in polarization, as in DNP.

1.3 Formal quantum mechanics

1.3.1 Hilbert spaces

In order to understand the concepts of NMR theory, especially product operators and their geometrical meaning, some introduction to the basic concepts of quantum mechanics is in order. Quantum mechanics is a rather formal discipline of physics and makes use of concepts developed in the early 1920's by several mathematicians concerned with the problem of generalization of Euclidean space and calculus to higher dimensional spaces[19]. The existence of a Hilbert space is the rigorous mathematical foundation of quantum mechanics. Before one can introduce the wave function as the entity allowing for a rigorous mathematical description and calculation of all properties of a quantum mechanical problem it is reasonable to review the mathematical framework, especially with respect to the basic definitions that are absolutely necessary for further discussion. It will become clear at several points throughout the theory that quantum mechanics consists mostly of rotations in the complex plane and using basic definitions while making use of the properties of the Hilbert space. The probably most fundamental quality of Hilbert space for its application in quantum mechanics is that any oscillating wave may be described as exactly one point. This property is stated without proof[20] because it is relevant for reasons that will become evident.

The properties of a Hilbert space may be understood as generalization of vector algebra and calculus in two and three dimensions to any finite or infinite number of dimensions[21]. Thus, the existence of an inner product, in analogy to the dot product

$$< \vec{u}, \vec{v} >= const. \tag{1.30}$$

is one essential property of a Hilbert space. This statement is equally valid in the $\mathbb{R}^n$ and $\mathbb{C}^n$, where in the latter case the vector $\vec{u}$ has to be taken as its complex conjugate $\vec{u}^*$. The dot product has the same interpretation as in trigonometry, where $|\vec{u}||\vec{v}|\sin\theta$ is the angle between vectors. The same concept holds in Hilbert spaces and, although Hilbert spaces may be complex, the concept of angles remains strictly defined. Furthermore the definition of a norm (length) of any vector, in the same sense known from Pythagorean metrics

$$|\vec{f}| = \sqrt{< \vec{f}, \vec{f} >} \tag{1.31}$$

is one essential property of a Hilbert space. The concepts of lengths, distances and angles have thus been established by introduction of norm and inner product. Furthermore the space needs to be complete in order to allow for the rules of calculus to hold[22]. The importance of Hilbert spaces for applications in quantum mechanics is that they allow for the definition of any pure state, which is thus one oscillating wave rather than a superposition of many, as a single point in a suitable Hilbert space, where there are sub-types of Hilbert spaces depending on the properties of the quantum particle. In NMR this will generally be the complex space of spinors. A state can then be defined by a state vector which is itself strictly defined up to a phase factor. Observables are obtained by action of a self adjoined linear operator on the state space, the result is an eigenvector of the operator with corresponding eigenvalue of the observable. In quantum mechanics the inner product between two states yields a probability amplitude, a complex number with no direct significance, where the square of the absolute value of probability amplitudes describes the probability of the wave function to collapse during a measurement thereby joining initial and final states. In real applications initial states are rarely pure, but statistical mixtures of pure states best described by density matrices (vide infra). Using the principles of norm and inner product established above the rules of calculus and linear algebra may be used without restrictions

[19] The concept was established between 1904 and 1910 by David Hilbert, Erhardt Schmidt, Henry Lebesque, Friegyes Riesz and others. For historical reasons mathematical spaces fulfilling these rules are referred to as Hilbert space

[20] rather lengthy and difficult.

[21] In the context of quantum mechanics this is often restricted to countably infinite number of dimensions. This means it has the same number of elements as the natural numbers.

[22] Completeness in the mathematical sense means that any Cauchy series converges to a value within a metric space, where metric means that any two elements have a number, its metric, and the difference may be interpreted as a distance. In a less formal sense it just means the space has no gaps.

to generality. For a complex vector space V operators are linear projection to themselves of the form

$$f : V \to V. \tag{1.32}$$

f is called an endomorph, the property endomorphism. Any vector $\vec{v} \neq 0$, where zero is always true, where a scalar multiple c of itself is obtained by the projection f is automatically an eigenvector

$$f(\vec{v}) = c\,\vec{v}. \tag{1.33}$$

The scalar constant c is called the eigenvalue. The process may be understood as a form of scaling, the result is the same vector with a scaling factor, its eigenvalue [33, 39]. The general action of an operator is a combination of rotation and scaling. With explicit calculations in mind it is more important to note that for any finite dimensional vector space one may describe the endomorphism by a quadratic matrix $(n \times n)$ $\boldsymbol{M}$, under which circumstance the equation above becomes

$$\boldsymbol{M} \cdot \vec{v} = c\,\vec{v} \tag{1.34}$$

with the column vector $\vec{v}$. The analogy between endomorphic projections and the action of operators is relevant for the definition of matrix-forms, elements of matrices and action of operators in matrix form.

1.3.2 Basic definitions

Quantum particles possess both properties known from classical mechanics and properties bearing similarity to those of classical physics yet intrisically quantum mechanical in origin and devoid of a classical analogue. Stern and Gerlach performed an experiment where elemental silver was evaporated and a beam of silver atoms passed through a magnetic field gradient. Classically, the atoms would be allowed to take any orientation to the external field. Physicists at that time would have expected a blurred line on the detector. However two sharp lines were observed so it was concluded that quantum particles possess an intrinsic angular momentum that is similar to the angular momentum of a classical spinning object, but the intrinsic momentum can only take certain, quantized, values. Quantization, restriction of observables to certain values, is what defines quantum mechanics. With respect to magnetic resonance the important property is referred to as spin, a property a nucleus needs to exhibit to be NMR active. Several other experiments at the beginning of the 20th century clearly showed that when extremely small numbers of particles or extremely small length scales were involved classical physics broke down[23]. Thus a new theory based on the essential postulate that all properties of a system are covered by a wave function[24] was developed which bears similarity to the theory of electromagnetic waves in electrodynamics. Valid wave functions can be directly obtained from the time dependent

$$i\hbar\frac{\partial\Psi_n}{\partial t} = \widehat{H}\Psi_n \tag{1.35}$$

and the time independent

$$\widehat{H}\Psi_n = E\Psi_n \tag{1.36}$$

Schrödinger equations (Eqs. (1.35) and (1.36)). The latter equation states that application of an operator, which is usually just the differential operator analogue to the same quantity from classical mechanics, to a wave function will yield a definite value, the so called eigenvalue. If the Hamiltonian $\widehat{H}$ is used this value will be the energy E. The former equation states that the time development of a wave function is governed by its Hamiltonian. The time dependent wave functions are denoted as Ψ_n and $\hbar$ is Planck's quantum $h = 6.626$ Js

[23] Most notably the photoelectric effect and Planck's solution to the blackbody radiation problem.

[24] In literature there are several postulates of quantum mechanics (see. e.g Atkins, Friedmann - Molecular quantum mechanics). I personally do not agree, as i feel that other definitions referred to as postulates have a clear physical meaning within the Copenhagen interpretation of the wave function.

divided by 2π, which is the fundamental unit of quantum discreteness.[25]

The wave functions my be separated into a time dependent and independent part by integration. Using the[26] property of the imaginary number $1/i = -i$ allows to write the argument of the exponential in the common form (as frequency $E_n/\hbar$) and yields

$$\Psi_n(t) = \mathrm{e}^{-\frac{i}{\hbar}E_n t}\psi_n(q) \tag{1.37}$$

with the later term being a function of only the coordinates, while introducing the configuration space q. Equation (1.37) naturally introduces *stationary* wave functions identified by the small letter ψ_n corresponding to an stationary state n. These are the state vectors. In order to make calculations possible the basis functions are chosen to be orthonormal, that means orthogonal (the dot product of unlike vectors is zero) and they have a norm (the dot product with itself is unity). In shorthand notation this is expressed by Kronecker's Delta

$$\delta_{ij} = \begin{cases} 0 & \text{if } i \neq j \\ 1 & \text{if } i = j, \end{cases} . \tag{1.38}$$

The meaning of Eq. (1.38) is that a basis state is one that is linearly independent of other states - it cannot be expressed by linear combinations of the other state vectors and thereby constitutes a unique possibility of the system - a state. The time derivative in quantum mechanics, in flagrant discrepancy to classical physics, cannot be connected to measurement of a property at two adjacent points in time, as if one enforces a value for a property at one time it will generally not have a value at an adjacent point in time as a result of the uncertainty principle. This problem is connected to the quantum mechanical treatment of transitions, as a transition is a change in the system which necessarily requires a time increment for the transition to happen. The value of the average time derivative $\bar{\dot{f}}$ is defined as the time derivative of the average $\dot{\bar{f}}$. It is

$$\bar{\dot{f}} = \dot{\bar{f}} = \frac{\mathrm{d}}{\mathrm{d}t}\int \Psi^* \hat{f} \Psi \mathrm{d}q = \int \frac{\partial \Psi^*}{\partial t}\hat{f}\Psi \mathrm{d}q + \int \Psi^* \frac{\partial \hat{f}}{\partial t}\Psi \mathrm{d}q + \int \Psi^* \hat{f}\frac{\partial \Psi}{\partial t}\mathrm{d}q \tag{1.39}$$

The expression for the time derivative of the wave function is unambiguously defined by the time dependent Schrödinger equation Eq. (1.35) and thus

$$\bar{\dot{f}} = \int \Psi^* \frac{\partial \hat{f}}{\partial t}\Psi \mathrm{d}q + \frac{i}{\hbar}\int \widehat{H}^* \Psi^* \hat{f}\Psi \mathrm{d}q - \frac{i}{\hbar}\int \Psi^* \hat{f}\widehat{H}\Psi \mathrm{d}q. \tag{1.40}$$

The Hamiltonian is a Hermitian operator, where Hermitian means

$$\int \widehat{H}^* \Psi^* \hat{f}\Psi \mathrm{d}q = \int \Psi^* \widehat{H}\hat{f}\Psi \mathrm{d}q. \tag{1.41}$$

As a result of Hermiticity the time derivative of an operator f can be immediately identified to be

$$\hat{\dot{f}} = \frac{\partial \hat{f}}{\partial t} + \frac{i}{\hbar}(\widehat{H}\hat{f} - \hat{f}\widehat{H}). \tag{1.42}$$

This formal derivation *naturally* introduces one of the most important shorthand notations in quantum mechanics and its meaning. The so called commutators

$$(\widehat{\mathrm{H}}\hat{f} - \hat{f}\widehat{\mathrm{H}}) = [\widehat{\mathrm{H}}, \hat{f}], \tag{1.43}$$

define the time development of a system for any operator without explicit time dependency. Thus the commutator with the Hamiltonian is connected to the measurement process, as states are not directly observable in

[25] It is interesting to note that the unit of Planck's quantum is an action with the dimension [energy][time]. Actions are relativistic constants, that is hyper-rectangles, 4 dimensional constants. For a nice non-mathematical viewpoint to quantum mechanics discussing this problem see: J. Gribbin, In Search of Schrödinger's Cat - Quantum Physics and Reality. Black Swan, Revised Edition Edition (1985).

[26] very interesting

quantum mechanics (only transitions between states are observable). As a result a zero-commutator means a quantity is measurable.

The matrix elements of operators may be identified by making use of knowledge of the time development. The wave function can be written as a superposition of stationary states - the basis functions Ψ_n

$$\Psi = \sum a_n \Psi_n, \tag{1.44}$$

where a_n are coefficients which can generally be real or complex. The expectation value $\langle f \rangle$ for an operator $\hat{f}$ for compounds with a discrete energy spectrum expanded in this basis can then be written as

$$\langle f \rangle = \sum_n \sum_m a_n^* a_m F_{nm}(t) \tag{1.45}$$

where the entire set of combinations for all possible n and m defined by

$$F_{nm}(t) = \int \Psi_n^* \hat{f} \Psi_m \mathrm{d}q \tag{1.46}$$

is the matrix of the quantity f with operator $\hat{f}$ where $f_{nm}(t)$ is one matrix element. Mind that the wave functions denoted by Ψ are time dependent.

For operators without explicit time dependency only the wave function is time dependent and can be separated into a time dependent and independent part. The time dependency of the matrix elements becomes

$$\dot{f}_{nm}(t) = f_{nm} \mathrm{e}^{i\omega_{nm}t} \tag{1.47}$$

and the time derivative can be easily calculated to be

$$\dot{f}_{nm}(t) = i\omega_{nm} f_{nm} \mathrm{e}^{i\omega_{nm}t}. \tag{1.48}$$

with the now time independent matrix elements f_{nm}. For real physical quantities, identified by the action of the respective operator on the wave function, the complex conjugate $f_{nm}^* = f_{nm}$. Time dependency of wave functions is accounted for by time dependent coefficients $a_n(t)$. The valid solutions of the time dependent Schrödinger equation Eq. (1.35) cover time dependency in terms of first order natural exponentials. These are, to my knowledge, the most well behaved functions in mathematics as irrespective of the number of differentiations natural exponentials with exponents linear in the differentiation argument reproduce upon differentiation and are, in a mathematical sense, smooth. Smoothness means that the function can be continuously differentiated and will always be defined over all values of the variable - no discontinuities exist[27] As a result the solutions for time dependency must always be functions with no discontinuities and are typically exponentials or trigonometric functions - natural processes on a quantum scale have no bumps but due to the fundamental unit of quantum discreteness $\hbar$ in the equation they may only take specific values.

1.3.3 The density matrix

The most thorough description of a system in the framework of quantum mechanics is knowledge of the wave function. If a system, which is a subsystem of an isolated bigger system, is described in terms of a wavefunction the general expression is $\Psi(q, x)$, where the set of x-coordinates refers to the subsystem and q to the rest of the coordinates. This wavefunction cannot be separated into a product of two wave functions $\Psi(q)\Psi(x)$, as this would restrict generality to non-interacting functions.

If the operator $\hat{f}$ is for an observable property of the subsystem it needs to act only on the configuration

[27] The non-mathematician is referred to: R. Penrose, The Road to Reality - A complete Guide to the Laws of the Universe. Knopf, 2005.

space of the subsystem, in this syntax x, and the expectation value is

$$\langle \hat{f} \rangle = \int \int \Psi^*(q,x) \hat{f} \Psi(q,x) \mathrm{d}q \, \mathrm{d}x. \tag{1.49}$$

That the operator acts only on x allows to introduce a function defined by

$$\rho(x,x') = \int \Psi(q,x) \hat{f} \Psi(q,x)^* \mathrm{d}q \tag{1.50}$$

and integration is restricted to dq. This function is called the *density matrix* of a system.

The importance of the density matrix for NMR cannot be underestimated, as its is generally the case that only a fraction of the nuclei in a system will need to be treated. For example if an NMR experiment with Boltzmann polarization is performed only a small number of nuclei contributed to the magnetization and is manipulated by radiofrequency pulses (vide infra). In many para-hydrogen experiments only a fraction of molecules are hydrogenated - a density matrix treatment does nevertheless allow to calculate a correct spectrum.

Although the syntax used in Eqs. (1.49) and (1.50) is helpful to identify why the density matrix is the only suitable means for describing NMR experiments, it is not very well suited for quantitative calculations.

Several properties of the density matrix are most easily understood by inspection of the expansion theorem. Introducing the bra-ket notation

$$\langle \Psi | \Psi \rangle = \int \Psi(x)^* \Psi(x) \mathrm{d}x, \tag{1.51}$$

and allows a shorthand notation for integrals. The content of the expansion theorem is

$$\langle \Psi | \Psi \rangle = \sum_i \langle \Psi | \varphi_i \rangle \langle \varphi_i | \Psi \rangle. \tag{1.52}$$

This expression means that any inner product of the form $\langle \Psi | \Psi \rangle$ can be expanded by a complete set of orthonormal states. It is easy to see from Eqs. (1.50) and (1.51) that the complete set of states $|\varphi_i\rangle\langle\varphi_i|$ in expression Eq. (1.52) is connected to the density matrix. The state functions φ_i must themselves be legitimate quantum mechanical functions, that is they must be expandable as defined by Eq. (1.44) and time dependency must be separable as defined by Eq. (1.37). For explicit calculations, concerned with the expectation value of an operator it is important to note

$$\begin{aligned} \langle \Psi | \hat{f} | \Psi \rangle &= \langle \sum_m a_m \psi_m | \hat{f} | \sum_n a_n \psi_n \rangle \\ &= \sum_m \sum_n a_m a_n^* \langle \psi_m | \hat{f} | \psi_n \rangle \\ &= \sum_m \sum_n \rho' f_{mn} \\ &= Tr\{\rho' f_{mn}\} \end{aligned} \tag{1.53}$$

that is a coefficient matrix $\sum_m \sum_n a_m a_n^* = \rho'$ is obtained. The ensemble average of ρ' is called the density matrix.

The significance of this coefficient matrix will be briefly derived. First, a density operator

$$\hat{\rho} = \overline{|\Psi\rangle\langle\Psi|} \tag{1.54}$$

is introduced. The expansion theorem may be used in a reciprocal form and the φ_i identified as legitimate wavefunctions Ψ according to the first postulate of quantum mechanics yielding

$$\rho_{mn} = \langle \psi_m | \overline{|\Psi\rangle\langle\Psi|} | \psi_n \rangle. \tag{1.55}$$

The state $|\Psi\rangle$ may be developed after the basis functions ψ_m, as may be $\langle\Psi|$ to yield

$$\begin{aligned}\rho_{mn} &= \overline{a_m a_n^*}\langle\psi_m|\psi_m\rangle\langle\psi_n|\psi_n\rangle \\ &= \overline{a_m a_n^*}.\end{aligned} \tag{1.56}$$

As such the density matrix only has relevance for ensemble averages (denoted by the bar). The probabilty of finding a system in a state is given by the action of the operator on that state and as such the diagonal elements of the density matrix ρ_{mm} are occupations of a state. As a result of normalization the trace Tr, the sum of the diagonal elements, must be unity, as the system has to be in one of its allowed states.

As the density matrix is the most suitable tool for NMR evaluation and the measurement process intrinsically requires time, the time development of the density matrix is of special interest. It is defined by the Liouville von-Neumann equation

$$\frac{\mathrm{d}\rho}{\mathrm{d}t} = -i\hbar[\hat{H}, \rho], \tag{1.57}$$

which is very similar to the time derivative of general operators defined by Eq. (1.39). The solutions of the Liouville von-Neumann equation are straightforward if operators have no explicit time dependency. The formal definition of the density operator $\overline{|\Psi\rangle\langle\Psi|}$, and recognition that the Schrödinger equations allowed to express time dependency by an exponential as defined by Eq. (1.37), allows to write the solutions as

$$\rho(t) = e^{i\hbar\hat{H}t}\rho(0)e^{-i\hbar\hat{H}t}, \tag{1.58}$$

where $\rho(t)$ is the density matrix at a time $t_0 + t$ and rho_0 the initial state of the system prior to development. This formula is often called sandwich-formula, the terms $e^{i\hbar\hat{H}t}$ (and complex conjugate) propagators, as they define the time development. Equation (1.58) will be encountered in more detail again.

In the following the operators relevant for nuclear magnetic resonance will be discussed.

1.3.4 Nuclear Magnetic Resonance

Most chemical elements exist naturally as a mixture of isotopes with the same proton but different neutron number in the nucleus. Out of the isotopes of an element one or more may have a intrinsic angular momentum usually referred to as spin and quantization of values is once again observed for both angular momentum and spin. The spin may be characterized by a spin quantum number which may be either an integer number including zero or a half integer number. As stated above the existence of a non-zero nuclear spin, usually referred to as I or S, is the requirement for occurrence of the magnetic resonance effect. Spin and angular momentum are closely connected, as the quantum mechanical expressions follow the same set of rules - they are described an analogous operator and follow identical transformation rules[39]. The space itself is isotropic and homogeneous which means that no preferential direction exists ab-initio. Thus the Hamiltonian may not change upon a rotation of the entire system by any angle. An operator that does not change for infinitesimally small angles is sufficient to account for any angle. The angular momentum operator is hence defined by

$$\hbar\hat{L} = -i\hbar\,\vec{r}\times\vec{\nabla} \tag{1.59}$$

where the capital letter $\hat{L}$ means that the same rules apply to angular momentae of single particles (usually denoted with a small letter, e.g. l) and systems of composite particles (capital letter).

Switching to the more commonly used syntax in NMR the spin operators are in the following referred to as I, S and their components as $I_i;\ i = x, y, z$. Expressed in spherical polar coordinates, more convenient for reasons that will become evident later (Eq. 1.67) the eigenvalue problem becomes

$$-i\hbar\frac{\partial\psi}{\partial\phi} = l_z\hbar\psi. \tag{1.60}$$

The transformation rules for both spin and angular momentum are given by the cyclic permutation relations

for the components

$$[I_y, I_z] = iI_x, \;\; [I_x, I_y] = iI_z, \;\; [I_z, I_x] = iI_y. \tag{1.61}$$

As the commutator is related to the time derivative of quantum mechanical properties, and thus to the measurement process itself, non-zero commutators show that not all three components may be measured simultaneously. ψ is obtained by integration of expression Eq. (1.60) and yields

$$\psi = f(r, \theta) \mathrm{e}^{il_z\phi} \tag{1.62}$$

where f may be any function of r and θ. The exponential describes a rotation and is connected to the polar form of complex numbers, where $l_z\phi = 2\pi$ identifies a complete rotation in the complex plane.[28] This periodicity in the argument of the exponential in Eq. (1.62) restricts the possible values of l_z to

$$l_z = m, m = 0, \pm 1, \pm 2..... \tag{1.63}$$

m is often referred to as magnetic projection quantum number and may take $2I{+}1$ values from $-I, ..., I$. In full analogy to the angular momentum there will be $2S{+}1$ values from $-S, ..., S$. The angular momentum J of a quantum mechanical system is now given by an angular momentum part L and a spin part S and is thus given by $L + S$ where the use of capital letters implies composite particles.
A similar treatment with an analogous operator for the spin results in an additional non-spatial variable σ in the wave function. For the $s = 1/2$ spins, which are relevant in the following, the operators required for explicit calculations can be written as $2s{+}1$ row matrices - the Pauli matrices. They are

$$\hat{\sigma}_x = \begin{pmatrix} 0 & 1 \\ 1 & 0 \end{pmatrix}, \;\; \hat{\sigma}_y = \begin{pmatrix} 0 & -i \\ i & 0 \end{pmatrix}, \;\; \hat{\sigma}_z = \begin{pmatrix} 1 & 0 \\ 0 & -1 \end{pmatrix}. \tag{1.64}$$

These matrices have interesting properties with respect to the generation of complex space. The spin functions for one spin 1/2 particle are

$$\psi = \begin{pmatrix} \psi(1/2) \\ \psi(-1/2) \end{pmatrix} = \begin{pmatrix} \alpha \\ \beta \end{pmatrix} \tag{1.65}$$

Similar to the concepts established in the magnetostatics section the magnetic moment $\vec{\mu}$ of a nucleus must be connected to moving charges. It has been briefly noted that nuclei are composite particles of spin 1/2 quarks but, apart from the spin, quarks also carry a charge of either $2/3e$ or $-1/3e$, where e is the elemental charge of a proton. The concepts of magnetostatics also hold for elemental particles and without elaborating further on details about internal structure of atomic nuclei it should just be noted that theory is thus internally consistent. The operator for the angular momentum has no explicit time dependency and the magnetic moment is time independent

$$\vec{\mu} = \hbar\gamma_i \hat{I}. \tag{1.66}$$

This equation reveals that the gyromagnetic ratio γ_i, a constant for a given isotope, can be understood as a kind of scaling constant that modifies the absolute length of the vector μ which is the strength of the dipolar field of a given nucleus. From electrodynamic theory it is known that a magnetic moment exposed to an external magnetic field $\vec{B}$ will experience a torque given by vector product of the field and the magnetic moment μ. Thus the vector of the magnetic moment will not be static in time and

$$\frac{\mathrm{d}\vec{\mu}}{\mathrm{d}t} = \vec{\mu} \times \vec{B} \tag{1.67}$$

is the classical equation of motion for an isolated magnetic moment, where isolated means that the magnetic moment may only interact with the field. The interaction energy depends on the relative orientation of the magnetic field and the orientation of the magnetic moment and the Hamiltonian, which is the quantum mechanical

[28] This is shown later on in conjunction with product operators. It did not seem reasonable to show the figures multiple times.

analogy to the classical treatment, is

$$\widehat{H} = -\vec{\mu} \cdot \vec{B}. \tag{1.68}$$

If the z-axis is chosen as preferential direction[29] the Hamiltonian of the Zeeman-interaction becomes

$$\hat{H} = -\hbar\gamma_i \begin{pmatrix} 0 \\ 0 \\ B_0 \end{pmatrix} I_z = -\hbar\gamma_i B_0 I_z. \tag{1.69}$$

and allowed energy eigenvalues are

$$E = -\hbar\gamma_i B_0 m \tag{1.70}$$

where the occurrence of m shows that a finite number of equally spaced energy levels exists. At this point the net magnetization M_0, resulting from the energy difference between spin orientation upon field exposure [1], can be formally introduced as a result of quantum mechanics and yields the expression

$$|\vec{M}_0| = N_s\gamma\hbar \frac{\sum_{m=-I}^{I} m e^{\frac{\gamma\hbar B_0 m}{k_B T}}}{\sum_{m=-I}^{I} e^{\frac{\gamma\hbar B_0 m}{k_B T}}}. \tag{1.71}$$

N_s is the number of spins in the sample, k_B is Boltzmann's constant and T the thermodynamic temperature. Note that, although $\vec{M}$ is a vector, this equation refers to the projection of the Magnetization vector on the arbitrarily chosen z-axis and therefore is the z-component of m. Due to the occurrence of $\hbar$ in this equation linear expansion of the exponential is valid (as the exponent is typically extremely small) and yields the commonly used expression for the net magnetization in the high temperature approximation already used in Eq. (1.26)

$$M_0 = N_S\gamma^2\hbar^2 I(I+1)\frac{B_0}{3k_B T}. \tag{1.72}$$

Note that this definition of the magnetization holds only for spins in thermal equilibrium with some lattice, and systems which can be characterized by a spin temperature[59].[30] Valid wave functions of the Zeemann-Hamiltonian can be obtained from Eq. (1.35) to be defined by

$$\Psi_{I,m}(t) = \mathrm{e}^{-\frac{i}{\hbar}E_m t}\psi_{I,m} \tag{1.73}$$

with m ranging from -I to +I.
The general wavefunction is the linear superposition of all possible eigenstates meaning all possible values of m, as also recognizable in the partition function defining the magnetization Eq. (1.71).

$$\Psi(t) = \sum_{m=-I}^{m=I} c_m\psi_{I,m}(t) = \sum_{m=-I}^{m=I} c_m\psi_{I,m}e^{-\frac{i}{\hbar}E_m t}. \tag{1.74}$$

The expectation value of an observable with operator $\hat{f}$ is given by the integrals of the type

$$\langle f\rangle = \int \Psi^* \hat{f}\Psi \,\mathrm{d}q, \tag{1.75}$$

where the integration is over the configuration space, which is just the suitable Hilbert space. Quantum mechanically the precession of nuclei around a static magnetic field along the z-axis can be derived by calculating

[29] Due to the uncertainty relation a quantum mechanical property cannot be completely determined. Generally one component and the absolute value are measurable simultaneously. Therefore the field will appear bold, whereas a component of a field is a scalar quantity and therefore emphasized as italic letters.

[30] Specifically, this definition does not hold for spin systems subjected to para-hydrogen and chemical reaction, where the concept of a spin temperature is not valid.

the expectation values of the x, y components of $\vec{\mu}$. The expectation value of μ_x is given by

$$\langle \mu_x(t) \rangle = \hbar \gamma_i \int \Psi^* I_x \Psi \, \mathrm{d}q \tag{1.76}$$

with $\mu_x = \hbar \gamma_i I_x$. Using the wave function Eq. 1.74 and considering that operators act as endomorphic projections while introducing the bracket notation for integrals of this type, as the seemingly more explicit integral notation is inaccurate, because the configuration space q is 3N-dimensional, where N is the number of particles. Thus one would have to write 3N integral symbols. The expression

$$\langle \mu_x(t) \rangle = \sum_{m'} \sum_{m} \gamma_i \hbar c^*_{m'} c_m \langle m' | I_x | m \rangle \mathrm{e}^{\frac{i}{\hbar}(E_{m'} - E_m)t}, \tag{1.77}$$

reveals that the exponential function once again describes a rotation in the complex plane, due to its time dependency sometimes referred to as complex oscillation, and therefore the expectation value $< \mu_x >$ is evidently time dependent. The double sum shows that a number of oscillations will exist, where using Bohr's relation $\hbar\omega = h\nu = E$ results in the possible transition frequencies given by $E_{m'} - E_m/\hbar$. In order to yield an observable transition there needs to be a nonzero matrix element of an operator joining the initial and final state and the selection rule is $\Delta m = \pm 1$.

1.3.5 Secondary spin interactions

As a result of quantum mechanics electron densities in atoms are not just a spherical charge distribution around the nucleus, but are best described by atomic orbitals consisting of a radial function $R_{n,l}(r)$ and spherical harmonics $Y_l^m(\theta, \phi)$ with the quantum numbers l, m. In molecules the resulting electron distributions as charge densities in the $\mathbb{R}^3$ are obtained by a linear combination of atomic orbitals to molecular orbitals, resulting in non spherical charge distributions around the nuclei. The backaction of the electrons when interacting with an external magnetic field is in analogy to the Lenz-rule, which is, when using its nowadays more generalized form, that any field acting on a moving charge will induce a flux in the charge generating a field opposing the external field. This effect gives rise to the chemical shift, which is orientation dependent in crystalline solids and a scalar quantity in liquids, where fast molecular motion results in a averaging over all orientations. This gives rise to a change of the magnetic field ΔB at the nucleus and the resonance frequency becomes

$$\omega = \gamma_i (B + \Delta B) = \gamma_i B (1 - \sigma) = \gamma_i B (1 - \sigma_P - \sigma_D) \tag{1.78}$$

where σ is the chemical shift with the diamagnetic chemical shift σ_D and the paramagnetic shift σ_P. The contributions to the chemical shift σ_D and σ_P generally have opposing effects and are associated with orbitals with and without angular momentum (σ_D with s-type, σ_P with p,d,f-type orbitals). It is important to note that nuclei which are part of the same molecular group need not have the same chemical shift, because restrictions to free rotation of chemical bonds may still render nuclei magnetically inequivalent.

Molecules in magnetic fields do not only interact with the field, but every nucleus with a spin present in the compound interacts with each other spin. This is typically described by a Heisenberg-ansatz of the form

$$\hat{H}_J = 2\pi J_{IS} \, \vec{I} \cdot \vec{S}, \tag{1.79}$$

where in the following $\vec{I}$ and $\vec{S}$ refer to two unlike spins I and S and not to spin and angular momentum operators. The energy of interaction depends on a scalar coupling constant J, which is also referred to as electron mediated dipole-dipole coupling. The dot product shows that the relative orientation of the two spins in space is important. Just like the force acting between permanent magnets depends on their orientation, the energy of interaction for two spins depends on the relative orientation. Generalization to n-spins in a molecule requires accounting for all possible spin pairs. The J-coupling Hamiltonian of the homonuclear coupling is

generally

$$\hat{H}_J = 2\pi \sum_{i<k}^{k} J_{ik} \vec{I}_i \cdot \vec{I}_k. \tag{1.80}$$

A formal quantum mechanical derivation of the J-coupling is not sensible and the interested reader is referred to literature[59, 1].

As a concluding remark it is appropriate to note that for NMR-spectroscopy in the liquid state J-coupling and chemical shift do not change with orientation in the field, as in the latter case averaging over many particles removes that dependency, where in the former case it is directly a result of quantum mechanics. More explicitly the homonuclear J-coupling is rendered inobservable if all like spins are rotated through the same angle, which is automatically the case in one chemical group that is subject to free rotation, like methylene groups CH_2 in n-alkanes, or molecules with equivalent positions like PF_3. Sometimes unexpected effects occur, e.g. a molecule like PF_5, which differs in number of next neighbors and hence FPF-angles for the two inequivalent F-positions, has no observable homonuclear coupling because Berry-pseudorotation lifts the inequality between equatorial and axial positions[8]. Lastly, due to the dot product in Eq. (1.79), in compounds with restriction to free rotation the J-coupling may depend on the dihedral angle χ as described by the Karplus-relation[38, 37].

$$^3J(\theta) = A\cos^2\chi + B\cos\chi + C. \tag{1.81}$$

As a result of the geometric interpretation of the dot product $|\vec{u}||\vec{v}|\sin\theta$ the J-coupling may get very small for 90° and very large for 0° and 180° dihedral angles. A, B, C are empirical parameters depending on the substitution pattern of the compound. The Karplus-relation is often times to gain information about backbone conformations in complex molecules such as proteins and it often relevant in organic chemistry when compounds with restricted rotation are involved.

1.3.6 Manipulation of spin systems with radiofrequency pulses

As it is generally difficult to detect a small magnetization aligned with the rather large magnetic field, the magnetic moments of nuclei are manipulated by interaction with alternating radiofrequency fields. An electromagnetic wave is not constant in time but will periodically oscillate and only act on the magnetic moment for a specific time τ_p. Treating the effect of pulses classically shall suffice at this point. The Hamiltonian is

$$B_x(t) = B_{x0}\cos\omega t \tag{1.82}$$

usually separated in two counterrotating field components. The result for the inversely rotating component is in full analogy except ω has to be replaced by $-\omega$. It is

$$B_x(t) = B_r = \vec{B}_1(t) = B_1(\vec{e}_x\cos\omega t - \vec{e}_y\sin\omega t), \tag{1.83}$$

where $\vec{e}_x$ and $\vec{e}_y$ are unit vectors and B_1 the amplitude of the field. In most instances the so called pulses, or correctly radiofrequency impulses, are a superposition of several sine-waves resulting in a square shaped pulse. It shall be assumed that the pulse Hamiltonian H_r is the only time dependent factor and the intrinsic Hamiltonian $\hat{H}$ acts on the system. The evolution of the magnetic moment in time is then given by

$$\frac{\mathrm{d}\vec{\mu}}{\mathrm{d}t} = \vec{\mu} \times \gamma_i[\vec{B}_0 + \vec{B}_1(t)] \tag{1.84}$$

This expression can be simplified greatly if a rotating frame, where the coordinate system with coordinates x', y', z' rotates with an angular velocity equal to the precession frequency ω_0 around the z'-axis, is introduced. A vector function $\mathbf{F} = \vec{e}_x F_x + \vec{e}_y F_y + \vec{e}_z F_z$ has fixed unit vector lengths, or norms, and can only be rotated.

This rotation with an angular velocity $\vec{\omega}_z$ is analogous to having an angular momentum so that

$$\frac{\mathrm{d}\vec{e}_x}{\mathrm{d}t} = \vec{\omega} \times \vec{e}_x. \tag{1.85}$$

The time derivative of the vector function describes the rotating system and for the rate of change of the magnetic moment. If the z-axis is chosen as axis of rotation the mean field will be static, and so will $\vec{B}_1$. Then it is

$$\frac{\delta\vec{\mu}}{\delta t} = \vec{\mu} \times \gamma \left[\vec{e'}_z \left(\frac{\omega_z}{\gamma_i} + B_0 \right) + \vec{e'}_x \vec{B}_1 \right] \tag{1.86}$$

and the fields have been expressed in terms of components aligned with the, now rotating, principal axes. The different differentiation symbol serves as a reminder for the change of the coordinate frame. The ω_z is the same ω_z that has been introduced as rotation of the vector function. As radiofrequency-excitation is very near resonance, the precession frequency of the nuclei in an external field B_0, an ω_z may be chosen so that $\omega_z + \gamma_i \vec{B}_0 = \omega_z + \omega_0 = 0$. If $\omega_z = -\omega_0$ is chosen then

$$\frac{\delta\vec{\mu}}{\delta t} = \vec{\mu} \times \gamma \left[\vec{e}_z \left(\gamma B_0 - \frac{\omega_0}{\gamma} \right) + \vec{e}_x B_1 \right] \tag{1.87}$$

and owing to the fact that the unit of γ is $\mathrm{T}^{-1}\mathrm{s}^{-1}$, the entire second term has the unit of a magnetic field called the effective field B_{eff}. This means the magnetic moment will keep precessing around this effective field and may be rotated by any angle. Typical pulses in NMR are 180° and 90° pulses. These pulses rotate the magnetic moment, or the collective magnetization respectively, around an axis, rather than the often colloquially used terminology "flip in a direction". The angle is defined by $\alpha = B_1 \tau_p$. This is immediately evident in the product operator formalism discussed in the next section.

1.3.7 Description of complex NMR experiments - Product Operators

The wavefunction has been commented upon a lot in literature. It is important to note that the wavefunction itself has no physical significance within the Copenhagen interpretation of quantum mechanics. Only the product with its complex conjugate has physical significance and can interpreted as a probability. Owing to this fact the statement made above - the most thorough knowledge one can have about a quantum mechanical system is knowledge of the wavefunction - is true, but knowledge of the wavefunction doesn't immediately convey physical insight.

This is most likely the reason why a more instinctive way of describing NMR experiments, which retains the geometrical feeling from trigonometry, has been developed[60, 65]. The product operator formalism offers a cunning way to perform density matrix calculations and allows for the description of very complex NMR experiments, given that the number of interacting particles is not to large. The dimension of the density matrix still scales as 2^N where N is the number of particles and calculations quickly get numerically expensive. In the following the product operator formalism shall be introduced for a single spin in both mathematical syntax and geometrical picture. In the following it will briefly be shown that product operators are a way of performing density matrix calculations. At this point it is handy to repeat some algebraic rules for complex exponentials and their geometric meaning, as the analogy to the expressions for free precession and action of pulses in the product operator syntax become very obvious.

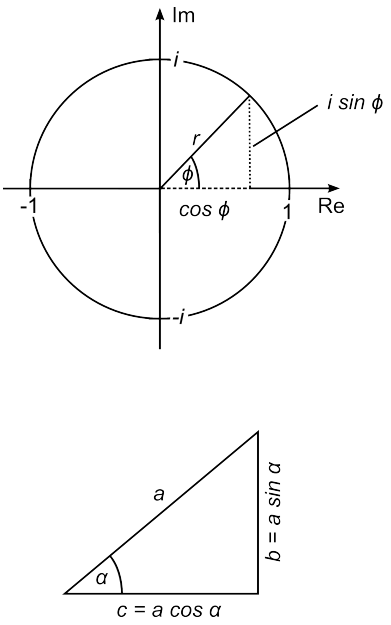

Figure 1.4: The complex exponential as rotation in the Gaussian plane (top) and trignometric relations in right-sided triangles (bottom). Mathematical relations are in full analogy to the product operator approach described below.

For an exponential, with any real or complex k_i, as well as factors r, s

$$re^{k_1 x} se^{k_2 y} = rse^{k_1 x + k_2 y}. \tag{1.88}$$

defines the multiplication. As shown in Fig. 1.4 complex exponentials of the general form

$$re^{i\phi} = r(\cos\phi + i\sin\phi) = r\cos\phi + ir\sin\phi = a + ib \tag{1.89}$$

may be interpreted as rotations in the Gaussian plane and the polar representation (l.h.s of Eq. (1.89)) shows that the algebra is identical to the geometric relations in right sided triangles (l.h.s of Eq. (1.89)). Furthermore, and more importantly for the connection of density matrices, their development and the connection to product operators, an alternative representation is given by

$$a + ib = a\,\mathbb{1} + b\,\mathbb{I} = a\begin{pmatrix}1 & 0\\ 0 & 1\end{pmatrix} + b\begin{pmatrix}0 & -1\\ 1 & 0\end{pmatrix} = a\,\mathbb{1} + b\,\mathbb{I} = \begin{pmatrix}a & -b\\ b & a\end{pmatrix} \tag{1.90}$$

and a complex exponential can be spanned by the symmetric unity matrix $\mathbb{1}$ defining the real and the antisymmetric matrix $\mathbb{I}$, or in a more compact way, by the family of 2x2 matrices on the r.h.s. of Eq. (1.90). Among the Pauli matrices $\hat{\sigma}_y$ constitutes the complex analogue to $\mathbb{I}$ as the antisymmetric matrix.

The Pauli matrices have already been introduced as the operators for spin $^1/_2$ particles and, following the established syntax, they will in the following section be referred to as I_x, I_y, I_z. In accordance with common praxis the operator symbol will be omitted. Firstly, spin manipulations by radiofrequency pulses shall be discussed. As a result of Eq. (1.87) a pulse results in a rotation of the magnetization around the axis corresponding to the phase of the pulse. For a pulse denoted as α with the phase of the pulse in the subscript, we get for an x-pulse

$$\begin{aligned} I_x &\xrightarrow{\alpha_x} I_x \\ I_y &\xrightarrow{\alpha_x} I_y\cos\alpha + I_z\sin\alpha \\ I_x &\xrightarrow{\alpha_x} I_x\cos\alpha - I_z\sin\alpha. \end{aligned} \tag{1.91}$$

where the arrow denotes evolution under the effect of the quantity written over the arrow, in this case the pulse with arbitrary angle α. These examples suffice to generalize the effect of a pulse on a single spin. In the first instance a rotation of a quantity aligned in the x-direction around x yields no effect, the operator is unchanged.

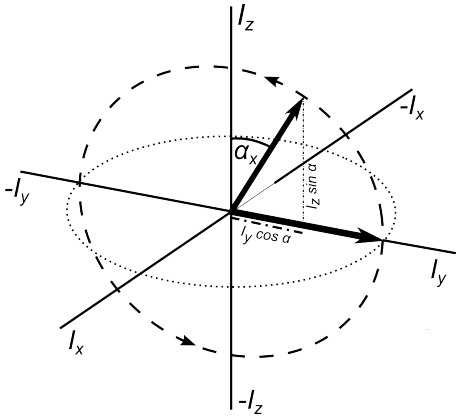

Figure 1.5: The effect of an x-pulse. The right sided triangle and trigonometric functions are shown in the diagram. The figure nicely illustrates the scaling of operators with trigonometric functions found in the product operator description of pulses.

In the second and third instance the pulse will have the effect of rotating by an arbitrary angle α, where evidently, as we rotate around the axis, x-pulses rotate in the y, z-plane and a y-pulse in the x, z-plane. Note the sense of direction for the rotation is visible from the different sign of the sine-term in Eq. (1.91).

Typically NMR experiments also have periods of free precession, where only internal interactions and the interactions with the mean field have to be accounted for. For a single spin free precession for a time t with a resonance frequency offset Ω, which may result from a chemical shift or magnetic field gradients/imhomogenities,

is simply a rotation in the x, y-plane. In product operator formalism free precession is described by

$$\begin{aligned} I_x &\xrightarrow{\Omega t} I_x \cos\Omega t + I_y \sin\Omega t \\ I_y &\xrightarrow{\Omega t} I_y \cos\Omega t - I_x \sin\Omega t \\ I_z &\xrightarrow{\Omega t} I_z. \end{aligned} \tag{1.92}$$

As the magnetic field is aligned along the z-axis it is easy to understand that I_z will remain unaffected if the spin precesses around the z-axis.

If I_x precesses around the z-axis with a frequency offset with respect to the rotation frequency of the coordinate frame it will evidently not stay aligned with the axis for all times. Both the effect of pulses and the free precession are most easily understood from the comprehensive diagrams shown in Figs. 1.5 and 1.6 showing a mixture of a vector model/product operator approach. The analogy to Fig. 1.4 is the reason why the product operator formalism is said to retain a geometric feeling. This can be understood by considering that the Hilbert space has a strict definition of norm and angle (see Eq. (1.31) and Eq. (1.30)) - geometric properties - just like the three dimensional real space $\mathbb{R}^3$ humans know from everyday experience.

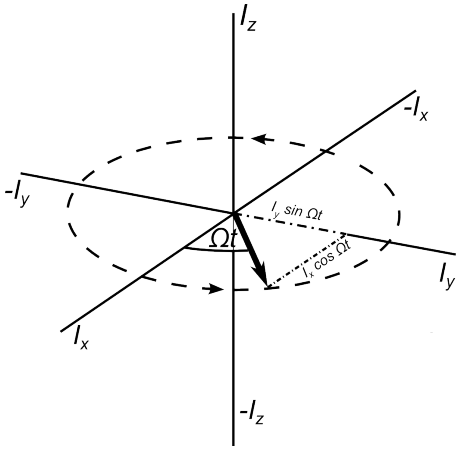

Figure 1.6: Free precession with a frequency offset Ωt. It is easy to see why I_z remains unaffected and why I_x and I_y are functions of the time. The right sided triangle with geometric relations accounts for the product operator expression.

The formalism is also applicable to many spin systems of either like or unlike spins (or both). Usually like spins are denoted by an index e.g. I_{1y}, I_{2y} refers to the I_y operator for nucleus I with spin I, where both will necessarily have a similar Larmor-frequency (Ω is small). Other spin types with different resonance frequency are usually referred to as S_i; $i = x, y, z$. As stated above, the product operator formalism constitutes a means of performing density matrix calculations. In order to show the relationship it is important to clarify how the density matrix evolves under the influence of an operator and then establish the analogy between product operators and density matrix evolution.

From Eq. (1.42) and Eq. (1.43) it is evident that the time evolution is connected to the commutator. The Liouville von-Neumann equation

$$\frac{\mathrm{d}\hat{\rho}}{\mathrm{d}t} = -i\hbar[\hat{H}, \hat{\rho}] \tag{1.93}$$

defines the evolution of the density matrix in time. An alternative way to derive the already encountered Sandwich-formula makes use of Eq. (1.88). Constructive expansion with 1 yields

$$\begin{aligned} -i\hbar[\hat{H}, \hat{\rho}] &= (-i\hbar\hat{\rho}\hat{H} + i\hbar\hat{H}\hat{\rho})1 \\ &= e^{-kt}(-i\hbar\hat{\rho}\hat{H} + i\hbar\hat{H}\hat{\rho})e^{kt} \\ &= -i\hbar\rho(0)e^{-kt}\hat{H}e^{kt} + e^{kt}\rho(0)e^{-kt}i\hbar\hat{H}. \end{aligned} \tag{1.94}$$

$\rho(0)$ is the initial state of the system prior to any evolution. The Hamiltonian is responsible for the evolution, and thus time development of $\rho(0)$ like it was the case for any wavefunction, and by analogy to Eq. (1.37) it is easy to understand that $k = i\hat{H}$. From expression Eq. (1.94) and substituting for k one immediately obtains

the exponential operator, operator exponential or sandwich-formula

$$\hat{\rho}(t) = e^{-i\hat{H}t}\rho(0)e^{i\hat{H}t} \tag{1.95}$$

defining the density matrix at a time t after development under the influence of an operator. It is important to note several details. Firstly, Eq. (1.88) is only strictly valid for commutating operators, that is $[\hat{f}, \hat{H}] = 0$. Secondly the Hamiltonian must be constant. This does, however, often times not pose a large problem as the evolution can be separated into intervals with a constant Hamiltonian for each interval and the density matrix $\hat{\rho}(t)$ after evolution with the first Hamiltonian identifies $\rho(0)$ for the next interval. Regarding the problem of non-zero commutators, like the Liouville von-Neumann equation, where the commutator is the time development, interpretation in analogy to multiplication of exponentials is only valid for small operators, that is operators with small differences between smallest and largest expectation value [42]. One of the most useful relationships makes use of the cyclic permutation relations of the Pauli-matrices defined by Eq. (1.61). For a Hamiltonian of the form $\hat{H} = cI_y$ and any constant c it is

$$\rho(t) = I_x \cos ct - I_z \sin ct \tag{1.96}$$

as

$$\begin{aligned} -ic[I_y, \rho] &= -ic[I_y, (I_x \cos\, ct - I_z \sin\, ct)] \\ &= -ic[B, A] \cos\, ct + ic[B, C] \sin\, ct \\ &= -ic(-iI_z) \cos\, ct + ic(-iI_x) \sin\, ct \\ &= -cI_z \cos\, ct - cI_x \sin\, ct \end{aligned} \tag{1.97}$$

This expression is especially convenient for the evaluation of expressions like

$$\mathrm{Tr}[\rho I_y] = \langle I_y \rangle = -\mathrm{Tr}[I_y^2] \cos\, \omega t + \mathrm{Tr}[I_x I_y] \sin\, \omega t. \tag{1.98}$$

In this example the expectation value of the detectable magnetization after an x-pulse is calculated. The magnetization has been rotated to the y-axis. As a result of Eq. (1.5) the induction of a voltage - the signal - is a result of all spin components in the directions allowing for induction. The expression for multiple spins after an x-pulse resonant with species I is

$$\mathrm{Tr}\{\rho \sum_{i=1}^{n} I_{iy}\} = \langle \sum_{i=1}^{n} I_{iy} \rangle \tag{1.99}$$

the sum of all spins with components aligned in a way that they result in an induced voltage. The density matrix contains only real elements with direct physical significance. As such it has immediate relevance for an experiment, where only real values may be obtained by action of an operator. The operator defining the evolution of the density matrix accounts for the information about a microscopic system, such as one molecule in a sample, and $\rho(t)$ can be readily calculated. The entire system, all molecules in a sample, can often times be understood as a number of non-interacting systems.

Then the evolution of each microscopic system is governed by the same Hamiltonian, as it is the case in a PHIP experiment, and there is no need to treat the systems individually. Instead

$$\hat{\rho}(t) = \hat{\rho}_1 + \hat{\rho}_2 = e^{-i\hat{H}t}\hat{\rho}_1(0)e^{i\hat{H}t} + e^{-i\hat{H}t}\hat{\rho}_2(0)e^{i\hat{H}t} = e^{-i\hat{H}t}[\hat{\rho}_1(0) + \hat{\rho}_2(0)]e^{i\hat{H}t}. \tag{1.100}$$

It is thus possible to deal with an ensemble by means of treating the evolution of a summed density operator. This averaged density matrix is written as $\bar{\rho}$ and unambiguously defines the state of the macroscopic system at a time t. This process is referred to as ensemble averaging. Oscillating matrix elements of random phase distribution average out. Note that the dimension of matrices remains unaffected by summation. Very helpful is a special kind of matrix operation the inner - or dyadic - product. The dyadic product is written as $\otimes$ and has

great relevance in conjunction with product operators, as all products of the form $I_{1x}I_{2x}$ are to be understood as $I_{1x} \otimes I_{2x}$. For example

$$\hat{\sigma}_x \otimes \hat{\sigma}_x = \begin{pmatrix} 0 & 1 \\ 1 & 0 \end{pmatrix} \otimes \begin{pmatrix} 0 & 1 \\ 1 & 0 \end{pmatrix} = \begin{pmatrix} 0\begin{pmatrix} 0 & 1 \\ 1 & 0 \end{pmatrix} & 1\begin{pmatrix} 0 & 1 \\ 1 & 0 \end{pmatrix} \\ 1\begin{pmatrix} 0 & 1 \\ 1 & 0 \end{pmatrix} & 0\begin{pmatrix} 0 & 1 \\ 1 & 0 \end{pmatrix} \end{pmatrix} = \begin{pmatrix} 0 & 0 & 0 & 1 \\ 0 & 0 & 1 & 0 \\ 0 & 1 & 0 & 0 \\ 1 & 0 & 0 & 0 \end{pmatrix} \tag{1.101}$$

the dyadic product of two 2x2 matrices will result in a 4x4 matrix. The identical operation for vectorial quantities allows to express the singlet state as

$$\frac{1}{\sqrt{2}}|\alpha\beta - \beta\alpha\rangle = \frac{1}{\sqrt{2}}\left[\begin{pmatrix} 1 \\ 0 \end{pmatrix} \otimes \begin{pmatrix} 0 \\ 1 \end{pmatrix} - \begin{pmatrix} 0 \\ 1 \end{pmatrix} \otimes \begin{pmatrix} 1 \\ 0 \end{pmatrix}\right] = \begin{pmatrix} 0 \\ 1 \\ -1 \\ 0 \end{pmatrix} \tag{1.102}$$

with the density operator

$$\frac{1}{2}|\alpha\beta - \beta\alpha\rangle\langle\alpha\beta - \beta\alpha| = \frac{1}{2}\begin{pmatrix} 0 \\ 1 \\ -1 \\ 0 \end{pmatrix} \otimes (0\ 1\ -1\ 0) = \frac{1}{2}\begin{pmatrix} 0 & 0 & 0 & 0 \\ 0 & 1 & -1 & 0 \\ 0 & -1 & 1 & 0 \\ 0 & 0 & 0 & 0 \end{pmatrix} = \hat{\rho} \tag{1.103}$$

resulting from the dyadic product of the vector with its adjunct. The resulting singlet state in matrix notation can be expressed by the Pauli-matrices and the unity matrix to yield

$$\hat{\rho} = \frac{1}{4}\mathbb{1} - I_{1x}I_{2x} - I_{1y}I_{2y} - I_{1z}I_{2z}. \tag{1.104}$$

The latter product operators constitute the explicit form of the scalar product $I_1 \cdot I_2$ of the J-coupling Hamiltonian written as product operators.

1.4 Para Hydrogen in NMR spectroscopy

1.4.1 The Para Hydrogen Molecule

The existence of parahydrogen has been predicted by Heisenberg as early as 1927 [30][31]. Bonhoeffer and Harteck adopted the Heisenberg proposal and chose the names ortho- and parahydrogen when they experimentally verified its existence in 1929[9]. After its discovery it was largely used for determination of free reaction enthalpy in chemical reactions, as it differs in thermodynamic properties, such as heat capacity and triple point[40]. Use of parahydrogen has only found widespread use in NMR spectroscopy in the last decade although the effect has been predicted as early as 1986[11]. Parahydrogen is one of the two possible nuclear spin isomers of molecular hydrogen H_2.

As established in the previous sections the state of a molecule is described by its wavefunction. Experimental observations in 1920 showed anomalous band structures[32] for two-atomic molecules. The wavefunction of such a molecule is separable in a product of orthonormalized functions of only one variable.[30]

$$\Psi = \Psi_\mathrm{t}\Psi_\mathrm{r}\Psi_\mathrm{e}\Psi_\mathrm{v}\Psi_\mathrm{n} \tag{1.105}$$

where indices refer to translation of the molecule center of gravity, rotation of the nuclei, electronic wavefunction, and oscillation of the nuclei or vibronic wavefunction, and nuclear wavefunction. The vibronic wavefunction

[31] p. 265
[32] spectral lines

Ψ_v is always symmetric due to the linear diatomic character of H_2 and absence of particle exchange between the nuclei[40], as the only variable would be the nuclear distance. As all elemental particles in molecular dihydrogen are spin 1/2 fermions the overall wave function has to be antisymmetric. Following Heisenbergs example a non-normalized valid wave function corresponding to a value of the rotation quantum number is given by $e^{ij\theta}$, and as this is equivalent to a complex rotation any even value of j will corrrespond to one full rotation in the complex plane, whereas any odd value of j identifies half a rotation and hence exchange of nuclear coordinates, that is symmetric and antisymmetric functions. The translational wavefunctions are always symmetric, as no particle exchange occurs and any translation does not exchange spatial coordinates of the nuclei. Only two possible combinations with an overall antisymmetric function are obtained under the condition of only symmetric vibronic and translational wavefunctions[46, 40].

$$\begin{aligned} \Psi &= \Psi_{\mathrm{r,antisymmetric}}\Psi_{\mathrm{n,symmetric}}\Psi_{\mathrm{v,symmetric}} \\ &\text{or} \\ \Psi &= \Psi_{\mathrm{r,symmetric}}\Psi_{\mathrm{n,antisymmetric}}\Psi_{\mathrm{v,symmetric}} \end{aligned} \tag{1.106}$$

This means either the nuclear or the rotational wavefunctions are antisymmetric. We denote the spin of a nucleus with the small letter s and the overall spin of a composite particle with S, adapt this syntax for all quantum numbers (in multiples of $\hbar$) and denote the rotational quantum number as $j = l + s$ with the angular momentum quantum number l. If we consider the two possible orientations of a spin 1/2 particle we get $S = 1$ or $S = 0$ and we have $S(S+1)$ states for each value of S, corresponding to one state and three states respectively. The corresponding wave functions are symmetric for even j and antisymmetric for odd j and we get the partition function p_{rn} where the index serves as a reminder that nuclear and rotational functions have to be considered. It is

$$p_{rn} = 1 \sum_{j=0,2\ldots} (2j+1)\mathrm{e}^{-j(j+1)\theta_r/T} + 3 \sum_{j=1,3\ldots} (2j+1)\mathrm{e}^{-j(j+1)\theta_r/T} \tag{1.107}$$

with $\theta_r = hcB_r/k$, where B_r is the rotational constant of the molecule. This means there is a degenerate triplet and one singlet state, where at very low temperatures the para, or singlet state, is populated exclusively. In the high temperature limit the ratio of ortho and para-hydrogen is evidently 3:1. In the syntax for the spin functions introduced above the three symmetric triplet wave functions are

$$|T_{-1}\rangle = |\alpha\alpha\rangle, \;\; |T_0\rangle = \frac{1}{\sqrt{2}}|\alpha\beta + \beta\alpha\rangle, \;\; |T_1\rangle = |\beta\beta\rangle \tag{1.108}$$

with the singlet wavefunction

$$|S_0\rangle = \frac{1}{\sqrt{2}}|\alpha\beta - \beta\alpha\rangle \tag{1.109}$$

and define one possible basis for a mathematical description, where it is generally possible to choose a different basis, as all basis sets are connected by unitary rotations, that is $\mathbf{U}^\dagger\mathbf{M}\mathbf{U} = \mathbf{N}$ will connect the bases $\mathbf{M}$ and $\mathbf{N}$.

1.4.2 Para Hydrogen Induced Polarization

As already briefly mentioned in the introduction, spectroscopy making use of photon interaction with electrons is inherently more sensitive than NMR. The greatest drawback of NMR in comparison to other spectroscopic methods is thus the Signal-to-Noise ratio. Equation (1.27) reveals why this problem is more pronounced for spins of low γ, while low natural abundance means less signal simply because there are fewer NMR active nuclei. Therefore polarization transfer from abundant spins, as well as finding efficient polarization sources other than the magnetic field, are among the most important topics in this field.

NMR methods are mainly used in chemistry, structural biology and medicine and in each case poor SNR results its own set of problems. For the chemist concerned with synthesis and evaluation of the developed procedures unambiguous identification of all products and byproducts is very helpful for optimization strategies regarding his synthesis, but if the desired product constitutes an insignificant byproduct the SNR limitations

will often times not allow to find this byproduct in his spectrum thus feigning a completely failed synthesis. The structural biologist is concerned with complex protein structures and will often times not have a large quantity of a sample at his disposal. It will usually be very difficult to isolate large quantities of interesting compounds, say enzymes, and many 2D experiments and spectra of spins with low gyromagnetic ratio are required for structure elucidation. The scientist concerned with medical research might be interested in metabolic intermediates which usually don't accumulate in significant quantities. And lastly, no scientist irrespective of the field wishes to wait a long time for results and, as the increase of SNR scales with the square root of the number of scans, this problem can only be partially alleviated by performing a large number of scans which is still, at the very least, inconvenient and expensive[33].

From an economic viewpoint the cost efficiency of measurement time is an important factor for commercial applications. All problematic factors can be alleviated by making use of polarization transfer routines or hyperpolarization methodology and combinations thereof may result in exceptional results - it is thus clear why development and optimization of hyperpolarization and polarization transfer have always constituted hot topics in NMR. Some methods making use of high polarization levels on a high γ spin are nowadays very commonly used and Hartmann-Hahn Cross-Polarization (CP) and Insensitive Nuclei Enhancement by Polarization Transfer (INEPT) are used in routine applications everyday. However the maximum degree of thermal polarization on nuclear spins remains limited by technically achievable magnetic field strengths, whereas hyperpolarization methods may result in much higher polarization. In the simplest sense, hyperpolarization may result from coupling nuclear spins to an external reservoir serving as a source of high spin order, or polarization, respectively. One of the cheapest sources is the large singlet spin-order of parahydrogen which is made available by Para Hydrogen Induced Polarization (PHIP). PHIP has to be counted among the chemical means of inducing hyperpolarization, as a catalytic step either resulting in a hydrogenation or a reversible reaction with recovery of the educt is involved in the process. Catalysts may generally be heterogeneous or homogeneous. But as already noted in the preceding section, the wavefunction of parahydrogen has an electronic contribution and for heterogeneous catalysts individual hydrogen atoms may diffuse along the surface. If no overlap of electronic wavefunctions of the chemisorbed hydrogen atoms remains any notion of nuclear spin singlet order is automatically removed. For this reason catalysts used in PHIP are mostly homogeneous phase catalysts. Heterogeneous catalyst[34] use extensive surface modification to avoid hydrogen diffusion along the surface[58].

Homogeneous phase catalysts for hydrogenation reactions are a rather well studied class of compounds and generally consist of a transition metal center stabilized by ligands. The challenge is that the metal center is usually not in thermodynamically favorable oxidation state and electronic vacancies at least allowing for coordination by one molecule of hydrogen and one molecule of substrate are required. The advantage of homogeneous phase catalysts is that a correctly tailored system allows to obtain well defined products with high specificity, the disadvantage is the high degree of complexity these systems possess from the point of reaction kinetics. The action of a catalyst within a system is that it allows to split the activation energy ΔE_{A} of a process into several smaller portions with a activation energy $E_{\mathrm{A},i}$, meaning a process occurs in more steps with lower energy of activation while leaving the overall energy of activation unchanged. It should be obvious that conservation of energy and thermodynamics do not allow for changes in net free reaction enthalpy of a reaction. An obvious, but nevertheless important, fact is that a hydrogenation reaction is at least a bimolecular reaction, when uncatalyzed, and involves at least three molecules when catalyzed. A catalyst will not change thermodynamics, the concentrations of educts and products in thermodynamic equilibrium are unaffected by presence of a catalyst. According to the definition a catalyst is a compound which remains structurally unchanged over a reaction while lowering the activation energy required to carry out one specific target reaction in a system - in this case a hydrogenation.

[33] There is even a point where it becomes impossible. One scan can usually be performed after 5 longitudinal relaxation times have passed. Thermal energy deposition from pulses makes it prudent to wait longer, as heating effects will otherwise change a sample if conformation is temperature dependent, as it is the case in macromolecules. As a result it is surprising how fast an experiment can take significant measurement time.

[34] Metal organic framework based catalysts are basically homogeneous phase catalysts with polydentate ligands or linkers connecting reaction centers.

This explains why the PHIP effect was first observed during the investigation of a homogeneous phase hydrogenation reaction. In 1981 Henry Bryndza reported the occurrence of enhanced emission/absorption lines in NMR spectra[46], but the patterns were attributed to a CIDNP (Chemically Induced Dynamic Nuclear Polarization) effect[57]. The same phenomenon was observed by by Eisenberg and Hommeltoft in 1986, but they attributed it to a CIDNP effect in absence of a radical species[32]. In the same year Bowers and Weitekamp had predicted the existence of Para-hydrogen Induced Polarization[11] and were able to prove the effect successfully with their PASADENA (Parahydrogen and Synthesis Allow Dramatically Enhanced Nuclear Alignment) experiment in 1987[11]. The work of Eisenberg attracted the attention of Bowers and Weitekamp and in the course of their correspondence it became clear, that the samples had been stored in liquid nitrogen under a hydrogen atmosphere prior to the investigation and the effect was, indeed, polarization enhancement by para-hydrogen exposure and hydrogenation reaction - they had unknowingly already performed an experiment very similar to PASADENA[11, 10]. In 1988 Pravica and Weitekamp discovered that PHIP enhanced NMR spectra obtained for reactions proceeding outside the magnet (in the Earth's magnetic field) with subsequent transport and detection in the mean field appear vastly different[54]. This approach is labeled Adiabatic Longitudinal Transport After Dissociation Engenders Nuclear Alignment (ALTADENA) and the acronym PHIP (Para Hydrogen Induced Polarization) was created as a means to describe all experiments where signal enhancement is observed as a result of parahydrogen exposure.

A more recent discovery is labeled Signal Amplification By Reversible Exchange (SABRE), or NH-PHIP (Non Hydrogenating PHIP), and has been reported in 2009[2]. The fundamental difference between PHIP and SABRE is in the chemical aspect of the interaction with hydrogen. For the methods classified as PHIP a hydrogenation in the chemists notion of the word takes place - the molecular structure of a compound is irreversibly altered by the hydrogenation reaction and this process may generate a high degree of non-thermal polarization, whereas in SABRE type experiments no change of the chemical structure occurs. More recently studies on fully pyridine-d5 have shown that long time exposure to hydrogen in presence of a catalyst leads to an exchange of deuterium against hydrogen (2% in 24 h). A PHIP catalyst is thus a substance which enables the formation of reversible or irreversible chemical bonds between parahydrogen and another molecule, thereby allowing for order transfer from the singlet state to the nuclei of the other molecule.

1.4.3 A chemical viewpoint of Para Hydrogen Induced Polarization

It is generally impossible to foresee mechanisms of chemical reactions without thorough studies of reaction kinetics and intermediates.[35] Especially for homogeneous phase catalysis it is easy to oversimplify and arrive at wrong conclusions - especially with respect to polarization levels directly calculated from experimentally observed enhancement factors. Firstly, it is important to note that catalyzed reactions have a reaction pathway involving multiple intermediates on the way to the product. Furthermore the empty coordination sites on the metal center of the catalyst allows for multiple molecular species to coexist in a solution. Jack Halpern noted "Mechanistic studies, such as those described in this article, have repeatedly emphasized the essential need for kinetic measurements to define reaction pathways and to establish whether any particular species which may be present in the reaction system under catalytic conditions is an intermediate in the catalytic cycle. That such kinetic measurements are essential for the elucidation of catalytic mechanisms is hardly surprising in view of the fact that catalysis is, by definition, purely a kinetic phenomenon"[27].

Any general reaction

$$aA + bB \cdots \rightleftharpoons sS + tT \ldots \tag{1.110}$$

where $a, b, s, t...$ are numerical values, the stoichiometric coefficients, and $A, B, S, T...$ are reaction partners is described by the law of mass action

$$K = \frac{k_+}{k_-} = \frac{c_S^s c_T^t \cdots}{c_A^a c_B^b \cdots} \tag{1.111}$$

where k_+ and k_- are rate constants of the reaction of A, B to the products S, T, and vice versa, and c_S is the

[35] As well as supporting ab-initio calculations to correlate spectra with geometric parameters

concentration of species S. For any reaction the equilibrium constant K is nonzero and will thus be reached at a specific value for all concentrations c.

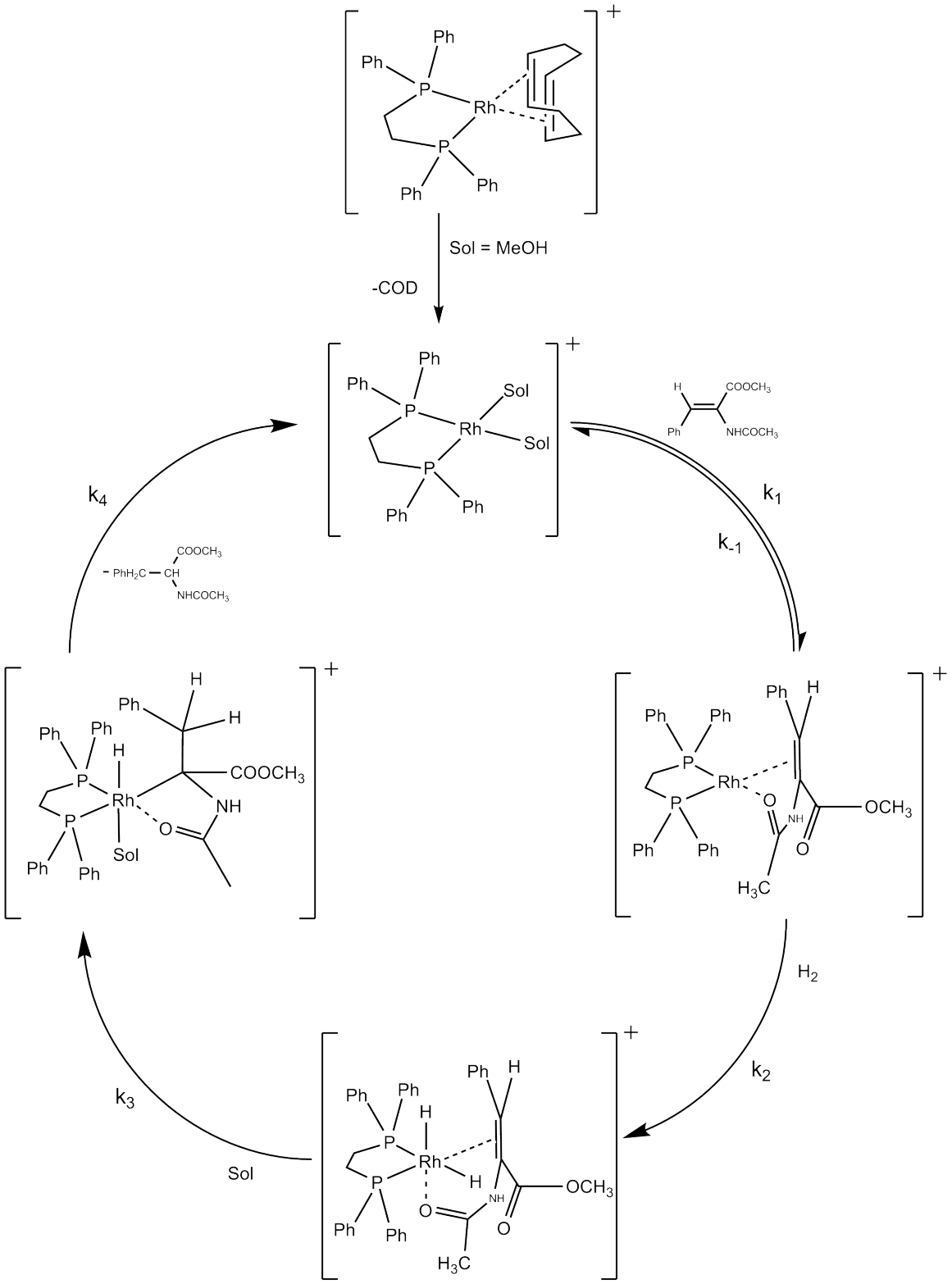

Figure 1.7: Reaction mechanism of the catalytic hydrogenation of methyl-(Z)-α-acetamidocinnamate. The rate constants at 25 ° C are $k_1[M^{-1}s^{-1}] = 1.4 \cdot 10^4$, $k_{-1}[s^{-1}] = 5.2 \cdot 10^1$, $k_2[M^{-1}s^{-1}] = 1.0 \cdot 10^2$, $k_3[s^{-1}] > 1$, $k_4[s^{-1}] = 23$. Mechanism and rate constants taken from ref. [26].

With respect to a catalytic hydrogenation this is true for any of the multiple steps of the process involving discrete hydrido- and organo-metallic intermediates. Furthermore the metal center itself can generally be subject

to ligand exchange processes and one or many species may lead to the product with a generally non-equal rate constant.

It is generally very difficult to fully characterize the action of a catalyst in a system. Elucidation of *all possible* reactions and exchange processes, determination of reaction intermediates on the catalytic cycle and experimental determination of rate constants, as well as their dependencies on extrinsic parameters, is a challenging task that has been undertaken for only a select few systems. A good example is constituted by studies of the action of Wilkinson's catalyst [49] $RhCl(PPh_3)_3$ in the hydrogenation of cyclohexene and styrene, where all rate constants and intermediates have been determined[27]. The article served to illustrate why nowadays polydentate ligands are exclusively used, as bridging μ-ligands render some amount of catalyst inactive. Representative for the action of catalysts in the hydrogenation reactions performed in the later stages of the thesis is the selective hydrogenation of methyl-(Z)-α-acetamidocinnamate (MAC). The reaction mechanism shown in Fig. 1.7, as well as rate constants, are taken from ref.[26].

Up to now no process violating the law of mass action has been identified and, in principle, every PHIP reaction of an alkyne has an admixture of the SABRE mechanism due to equal reaction/back reaction rates in chemical equilibrium. For hydrogenative reactions with modern catalysts, such as [1,4-Bis(diphenylphosphino)butane](1,5-cyclooctadiene)rhodium(I), rate constants of the back reaction are extremely small. The effect is, nevertheless, experimentally observable via hydrogen-deuterium exchange experiments and has been reported in conjunction with both hydrogenative PHIP [28] and SABRE[7].

The NMR scientist is mainly interested in the signal enhancement over thermally polarized spin systems that can possibly be obtained by PHIP. The PHIP signal strength is, however, depending on the number of reactions, and thus hyperpolarized product molecules formed within a time increment $t_0 + \Delta t$. Furthermore it evidently depends on the T_S relaxation time and number of partners to whom polarization is efficiently transferred[36]. For these reasons it is rather difficult to calculate an enhancement factor or a polarization level from the relative signal enhancement or the integrals of the Fourier transformed spectrum. Without knowledge of the net rate constant leading to the reaction product and the reaction order of the catalyzed reaction the number of product molecules formed in a time increment is unknown. This information does, however, constitute the basis for comparison and calculation of a true enhancement factor as well as polarization levels and can not be performed correctly without explicit and thorough knowledge of *all* rate constants, relaxation times of all nuclei and the density matrix, where the density matrix is required to quantify the polarization transfer efficiency from parahydrogen to other nuclei in the molecule.

1.4.4 Analytic description of the PHIP process

An analytic description of the PHIP process requires the formalism developed in section 1.3.7 and the density matrix theory from section 1.3.3. From the chemical viewpoint developed in the preceding section is clear that a number of molecules are hydrogenated within a time interval and become hyperpolarized due to that process. The ensemble consists of like molecules evolving under the same Hamiltonian. Thus description in terms of the averaging process defined by Eq. 1.100 is possible. The density matrix at a time t for an ensemble is then given by the solution of the Liouville von-Neumann equation. For two spin systems $I_1 I_2$, where the notation implies a Larmor-frequency difference between the spins, the analytic solution was derived in 1997 [46]. The product operator formalism is especially easy to use if operators commute and for a two spin system a separation of the Hamiltonian including J-coupling and chemical shift can be written as

$$\hat{H}_0 = \pi(\nu_1 + \nu_2)(I_{1z} + I_{2z}) + 2\pi J I_{1z} I_{2z} \tag{1.112}$$

$$\hat{H}_1 = \pi(\nu_1 - \nu_2)(I_{1z} - I_{2z}) + 2\pi J(I_{1x} I_{2x} + I_{1y} I_{2y}), \tag{1.113}$$

where the latter term is just the explicit form of the J-coupling Hamiltonian separated in the x, y and z-components and the former terms denote the frequency difference between the nuclei as result of e.g. a chemical

[36] The so called singlet relaxation times.

shift. These Hamiltonians are used to express the time development of the spin system according to Eq. (1.95) and Eq. (1.100). As a result of Eq. (1.43) only terms commutating with the Hamiltonian are observable and the *observable* part of the density matrix after evolution $\rho(t)$ is then given by

$$\rho(t) = I_{1z}I_{2z} + a(t)(I_{1y}I_{2y} + I_{1x}I_{2x}) + b(t)(I_{1y}I_{2x} - I_{1x}I_{2y}) + c(t)(I_{1z} - I_{2z}). \tag{1.114}$$

a, b, c are time dependent coefficients. From comparison to the density operator of parahydrogen described by Eq. (1.104) it is evident that with $a(0) = 1, b(0) = 0, c(0) = 0$ the density operator of the singlet is obtained. Equation (1.114) constitutes the general ansatz for the two-spin density matrix after evolution, where different time dependencies have to be expected for different product operators. This ansatz combined with the Liouville von-Neumann equation defines a system of coupled differential equations. The solutions of the system of coupled differential equations will generally consist of an oscillating function of the time and, as a hydrogenation reaction occurs continuously over time, the average density matrix $\bar{\rho}$ describes the state of the macroscopic system. Evaluation of measured spectrum thus relates to the ensemble averaged density matrix. For a general two spin 1/2 system this density matrix is

$$\bar{\rho} = I_{1z}I_{2z} + \frac{1}{x^2+1}(I_{1x}I_{2x} + I_{1y}I_{2y}) + \frac{x}{2(x^2+1)}(I_{1z} - I_{2z}), \tag{1.115}$$

where $x = \nu_1 - \nu_2/J_{12}$ is the Larmor-frequency difference between the nuclei divided by the J-coupling acting between the nuclei I_1 and I_2 that were the parahydrogen molecule prior to the addition reaction. It is important to realize that Eq. (1.115) depends only on quantities characteristic for the molecule - the J-coupling and the chemical shift and constitutes an important point of reference for theoretical investigations.

It is interesting to briefly discuss the appearance of NMR spectra obtained from PHIP experiments. At this point it is prudent to introduce the different addition PHIP experiment types that can be performed in high magnetic fields. The difference between PASADENA (para-hydrogen and synthesis engender nuclear alignment) and ALTADENA (Adiabatic Longitudinal transport and dissociation engenders nuclar alignment) type experiments is where the hydrogenation step is performed. In PASADENA type experiments the hydrogenation proceeds inside the magnet (that is typically at approx. 10 T), in ALTADENA experiments the sample is hydrogenated outside the magnet (that is field strength defined by stray field and Earth's magnetic field). A simple population model can be used to exemplify on the appearance of PHIP spectra encountered at a later stage[46]. If para-hydrogen is added to a system by chemical synthesis a molecule with, at the very least, two hydrogen nuclei will be obtained. In high magnetic fields the frequency separation between two nuclei (in different environments) is typically large, these type of spin systems are labeled AX-spin systems. If a NMR spectrum of a product molecule with thermal polarization is measured the energy differences between the levels will give rise to a small population difference with a small number of transitions. However in para-hydrogen experiment a nuclear spin isomer of the hydrogen molecule has been enriched to high levels. If added to a molecule via a hydrogenation reaction the occupation of states in the product molecule will be defined by the enrichment level of the hydrogen nuclear spin isomer. Schematic NMR spectra resulting from thermal polarization, PASADENA and ALTADENA are depicted in Fig. 1.8. In the PASADENA case the singlet is chemically added to an interaction partner in high field. The result is that both states $|\alpha\beta\rangle$ and $|\beta\alpha\rangle$ become populated. In an ALTADENA case the transfer of the singlet, with symmetry adapted low field singlet state $|S_0\rangle$ and three degenerate triplet states $|T_{1-}\rangle$, $|T_0\rangle$ and $|T_1\rangle$, will identify the state of most similar symmetry in presence of a field, which is either $|\alpha\beta\rangle$ or $|\beta\alpha\rangle$. The transfer is adiabatic in a quantum mechanical sense, that is without population change. With respect to nuclear wave function symmetries the reader is referred to[37][44]. It should be noted that it is very difficult to perform PHIP experiments that are not mixtures of both mechanisms.

[37] In my opinion the most easily accessible publications regarding symmetry are all from the 1950's, as explicit declaration of wave function symmetries is consistently used.

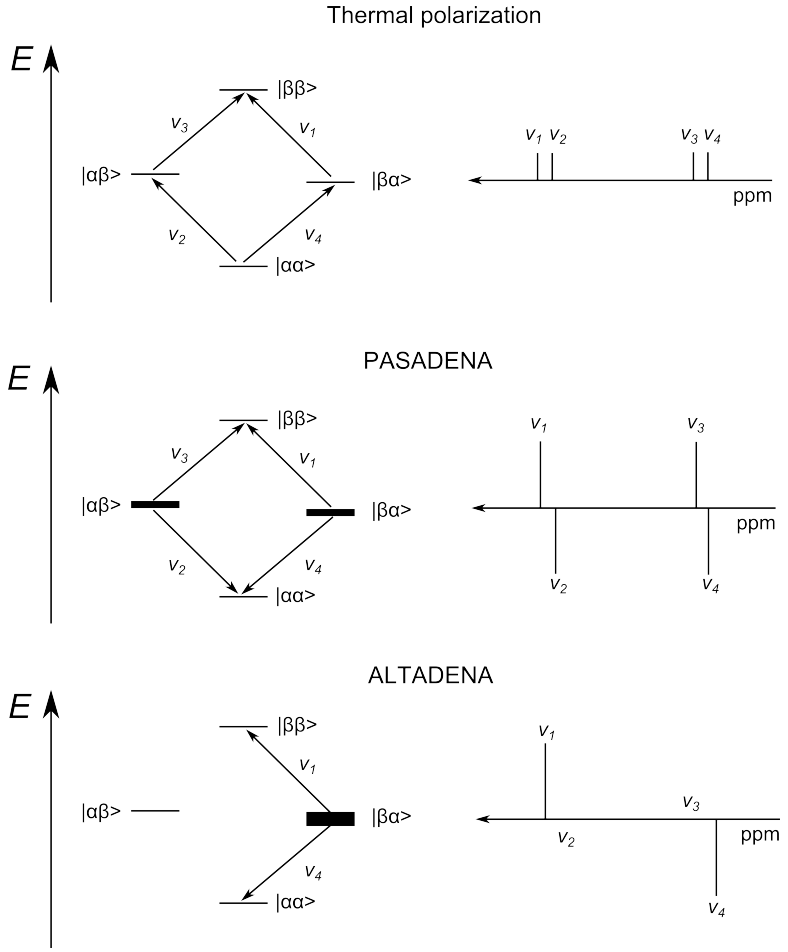

Figure 1.8: Energy levels and schematic stick spectra of top) a thermally polarized spin system middle) the spin system in a PASADENA experiment and bottom)the spin system in an ALTADENA experiment. The population of energy levels is denoted by the width of the level. In a thermally polarized spin system all levels are occupied nearly equally and with $\Delta m = 1$ four transitions are possible. In the PASADENA experiment the singlet state hydrogen is added to a molecule in high field, as a result of conservation of angular momentum both $|\alpha\beta\rangle$ and $|\beta\alpha\rangle$ need to become populated. In an ALTADENA experiment only the wavefunction of most similar symmetry becomes populated, as a result of adiabatic transfer.

Chapter 2

Results

2.1 Construction and Evaluation of a new shimmed Electromagnet system for high-resolution NMR spectroscopy

Developing low field NMR technology is not only motivated by scientific curiosity, but also by necessity. The availability of Helium, required for cryogenic cooling of superconducting magnets, is linked to the availability of natural gases used as energy carriers which are presumed to run scarce within the next 50-100 years. Availability and affordability of Helium is very likely to become a problem in the future. Other sources of Helium are alpha decay of radioactive elements or atomic fission processes. Extraction from the atmosphere is very unfavorable, as Helium does not possess chemical reactivity, has the lowest boiling point of all elements and makes up far less than 1 % of the air. Furthermore no accumulation in the atmosphere occurs as a result of its low mass and high particle velocity - the planet leaks Helium over time. The development of NMR spectroscopy technologies that are not dependent on Helium is thus more significant than one might initially assume, as it is most likely that NMR will remain an important technique for material characterization and medical diagnostics in the future. Currently there are two paths, one based on permanent magnet assemblies and one on electromagnets, for NMR spectroscopy without superconductors. Permanent magnet technology is more similar to the established high field methodology, as systems with a fixed magnetic field of intermediate strength (1 - 2 T) are used. The maximum field strength is limited by advances in solid state chemistry - the state of the art in permanent magnet development.[1] The most notable advantage of these systems is that high field methodology remains applicable and can be utilized without major changes, the disadvantage is the same lack of flexibility arising as a result of fixed magnetic field strength that can be observed for high-field NMR spectrometers.

Electromagnets, on the other hand, allow for a great deal of flexibility due to the direct proportionality of the field to the driving current, and thus theoretically free accessibility of any NMR active nucleus at any frequency, but usually at the expense of field strength and hence Signal-to-Noise ratio[2]. This approach is of special interest for this thesis. This section of the experimental will be concerned with a brief description of the results of the simulation as well as construction details and evaluation of a shimmed electromagnet suitable for high-resolution low-field NMR spectroscopy.

The newly constructed system shown in Fig. 2.1 was used for diverse experiments, such as i) spectroscopy with thermally polarized and thermally prepolarized spin systems ii) hyperpolarization experiments, specifically

[1] It is not actually as easy as that. The maximum surface strength of permanent magnets is currently limited to approx. 0.8 T and an assembly of magnets is required to yield 2 T. The individual magnets field contributions add up/ compensate at a given point in space. Spatial proximity of permanent magnets to each other means that each magnet will be permeated by the fields of other magnets. Hysteresis and spin diffusion over Bloch walls define a notion of magnetically hard materials that are the only usable ones for permanent magnet assemblies for NMR. K. Halbach discusses a lot of practical problems in: Nuclear Instruments and Methods, 169, 1 (1980).

[2] It is evidently possible to obtain significant field strength with very high currents or high number of turns, in both cases requiring cooling and large facilities. The High Magnetic Field Laboratory in Nijmegen (Netherlands) recently reported a 37.5 T field in a non-superconducting magnet. 50 T are possible on short timescales.

PHIP and SPINOE, but also SABRE[3].

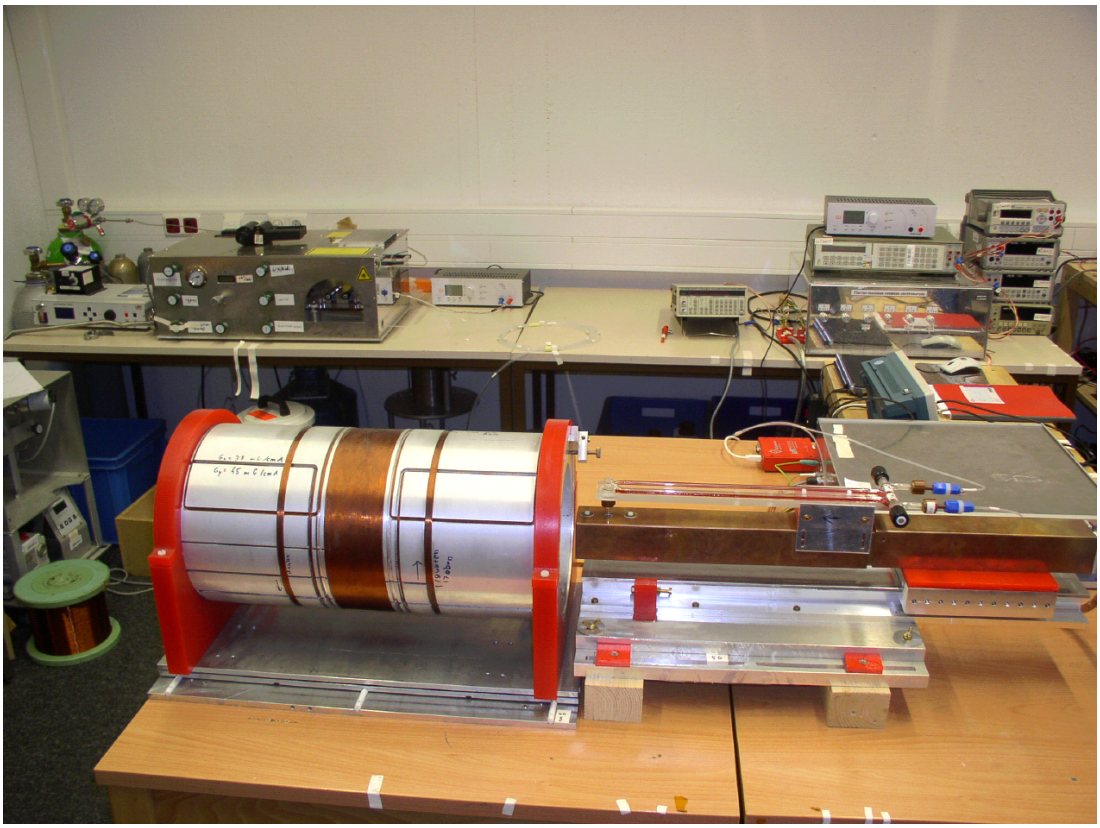

Figure 2.1: The experimental setup. The external cylinder of the magnet with the four shimming coils and the shuttle system with radiofrequency shielded probe are visible in the front. The probe features modular detection coils and an integrated rf-excitation coil. The glas-apparatus allowing for supply of hyperpolarized gases is placed on top of the probe and shows the status of the setup prior to sample transfer in the homogeneous volume as described in the hyperpolarization sections. The Rb-Xe hyperpolarizer (left) and current sources (right) are shown in the back.

2.1.1 Simulation of the magnet

Boundary conditions for the spatial dimensions of all coils are given the length of the supporting material, that had already been manufactured based on rough approximations for suitable dimensions and were available at the beginning of this thesis. The coil supports consist of two duraluminium cylinders[4]. One of those cylinders has a smaller diameter and supports the mean field coil, the second one has larger diameter and supports the shimming system. The internal diameter of the larger cylinder corresponds to the external diameter of the smaller one.

The simulations were carried out with Wolfram Mathematica 4.0[5]. As mentioned in the preceding theory, the fundamental problem of magnetostatics is to calculate the magnetic field at a given point in space resulting from a current density in conductor. The simulation uses a rather simple, yet very realistic model. Every coil is defined by a number of circular, parallel loops characterized by their diameters D_m. The other spacial dimension is given by n-times the wire diameter d_w, where the minimum displacement of an adjacent loop is also d_w. Multiple layers are accounted for by a different loop diameter, where loop diameters also have minimal increments of d_w. It is evident that these parameters immediately relate to the actual construction. The explicit

[3]The results of SABRE experiments have already been reported by S. Glöggler and will not be revisited.

[4]With courtesy of the Zentralabteilung for Technologie, now Zentralinstitut for Technolgie of the Jülich Research Center GmbH.

[5]The source code, written by Prof. Appelt, had already been used to build the first generation magnet unit. The first generation unit is a hybrid of solenoid and Maxwell coil.

solutions of elliptic integrals required for analytic evaluation can be taken from ref. [35].[6]

The magnetic field is calculated as superposition of the fields of all individual loops, where geometrical properties of the shimming coils have immediate effect on the field homogeneity. The simulation was concerned with the problem of how to obtain a field of maximum homogeneity. Restrictions on the choice of wire diameters are imposed by heat dissipation in resistive magnets and an appropriate wire diameter d_w has to be chosen for each coil to allow for long term operation. This problem is closely linked to the driving currents, where it is desirable to use rather small driving currents for each coil of the shimming system.[7] Avoiding deformations in coils as a result of intersecting wires is desirable, as these effects were not accounted for by simulation and the influence on field homogeneity would thus be unknown. As the field homogeneity for spectroscopic application should be one ppm or better it seemed reasonable to avoid unknown factors altogether. The setup should be robust to slight manufacturing errors, such as 10 μm inaccuracies that have to be expected from the mechanical supports as a result of limitations to manufacturing accuracy or deviations of the thickness of wire insulation.

Figure 2.2 shows a schematic drawing of the new experimental setup. The new magnetic field system features a solenoid coil for the mean field (only the milling groove is shown in Fig. 2.2). The external cylinder containing the shimming array can be displaced along the z-coordinate. The four shimming coils fulfill different purposes and thus have different geometries and number of turns. One coil is a solenoid and serves as a means to compensate for the curvature of the mean field. The other three are used to obtain linear gradient fields of constant magnetic field slope over the sample and have a Maxwell-geometry for the $\mathrm{d}B_z/\mathrm{d}z$ gradient and double saddle-coil geometry for the $\mathrm{d}B_z/\mathrm{d}x$ and $\mathrm{d}B_z/\mathrm{d}y$ gradients, respectively. They can be used to compensate for field gradients in the laboratory or positioning inaccuracies between the mechanical parts. This relates to the construction details, where two cylinders were used for the mean field and shimming support. In the following the gradients shall be referred to as G_x, G_y, G_z, and G_{z2} for convenience. Gradient coils were laid out in milling grooves of different depths on the supports surface (8, 6, 4, 2 mm) to avoid wire deformations[8]. The mean field support cylinder has an internal diameter $d_{\mathrm{i,supp}} = 180$ mm, an external diameter $d_{\mathrm{a,supp}} = 259.9$ mm a length $l = 540$ mm and the twine is along a length of $l_t = 500$ mm in a milling groove with a milling depth of 20 mm. The external cylinder has the same length $l = 540$ mm, an internal diameter $d_{\mathrm{i,shimm}} = 260$ mm and an external diameter $d_{a,shimm} = 280.0$ mm. The solenoid coil is laid out in the 2 mm milling groove and has a width w_{Gz2} of 100 mm. Maxwell-coils consist of two parallel coils. The average diameter d_{Helm}, that is the diameter between the geometrical middle of each twine, is identical to the distance of the loops to each other. A linear gradient is obtained by inverting the twine direction in one of the two coils this way inverting the current direction with respect to the other half. Double saddle coils can be used to obtain a linear gradient field when certain geometrical properties and current directions in each of the four parts are fulfilled. For graphical representation of current directions the reader is referred to literature or [14]. Double saddle coils consists of four square coils shaped to the cylinders surface where each coil covers 120° on the surface and is displaced by 60° from the next coil on this half of the cylinder and the sequence 120°, 60°, 60°,120° thus has two planes of symmetry. This condition uniquely characterizes the twine positions along the length coordinate on the surface of the cylinder. The twine positions along the curvature are characterized by ratios of the radius a to the distance between the inner parallel twines of two coils d_1 and the outer parallel twine d_2 and it is $d_1 = 0.38\ a$ and $d_2 = 2.55\ a$. Due to the specificity of current direction in each of the 16 sides of the four squares defining the double saddle coil, of which eight have a curvature, an analytic function describing the geometry and allowing to calculate the field from first principles could not be found. The number of turns and field strength per unit current were thus approximated.[9] The second double saddle coil has the same geometry but is rotated by 90°. Note that due to the dependence of distances between twine parts on the coil radius the different depth of the milling

[6] It is actually easier than that, because Mathematica and Matlab have elliptic integrals implemented as part of their function library.

[7] As explained in the theory, the problem is rather complex. The resistivity of a wire is proportional to the inverse of its cross section where the cross section is proportional to the square of the diameter. The diameter defines the number of turns for a given coil length and also the number of layers. This defines the number of turns and hence field per current. And finally the heat dissipation is proportional to the square of the resistivity and the current.

[8] I would like to thank J. Schmitz from the ZEA-2 for technical assistance.

[9] From experience. We were wrong.

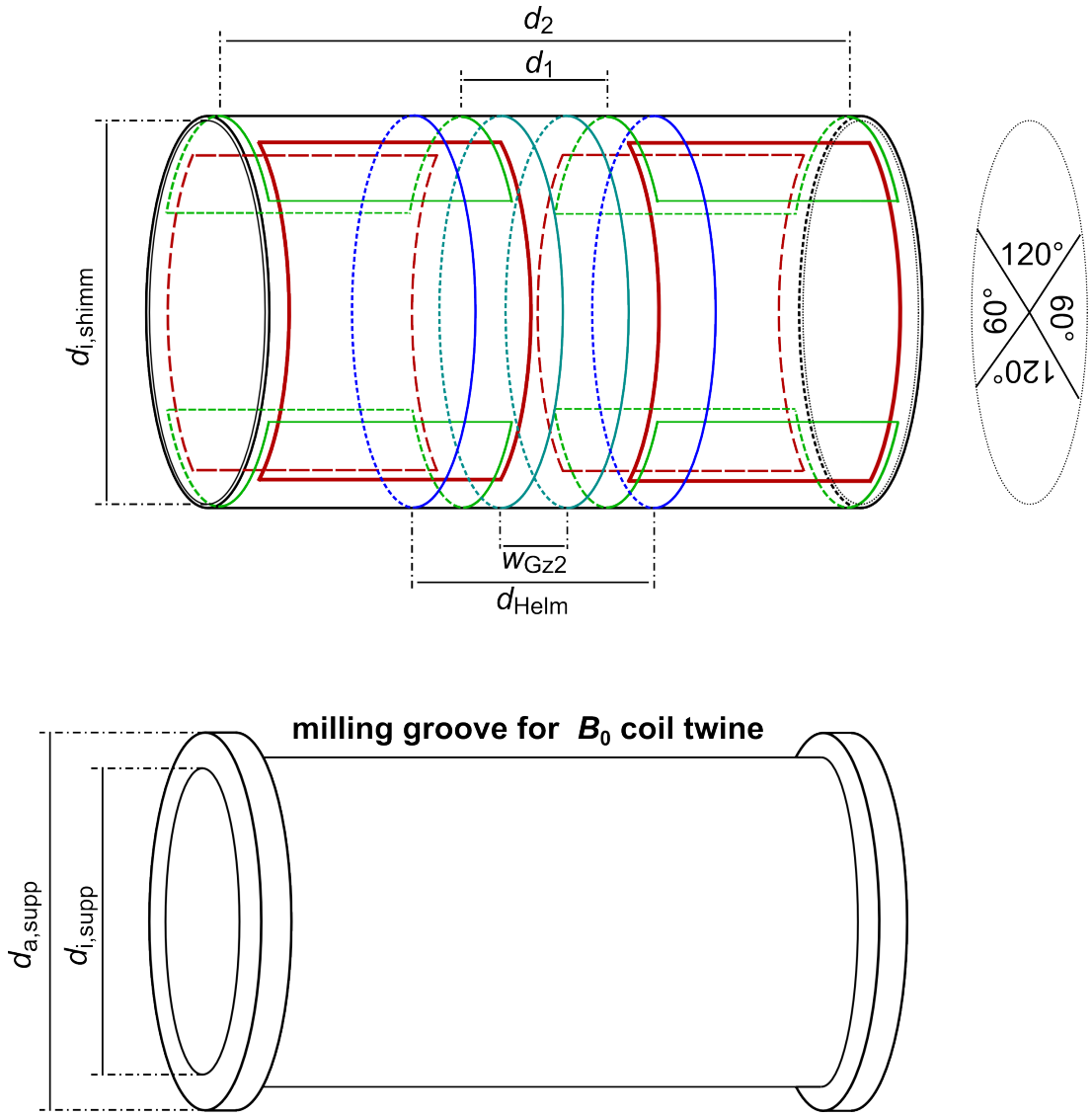

Figure 2.2: Top: A schematic view of the shimming system already shown in Fig. 2.1. The shimming system consists of four coils of different geometries. If a Maxwell coil pair (blue) has different current directions in both halves a field gradient ($\mathrm{d}B_z/\mathrm{d}z$ = const.) of constant slope will be obtained. The double saddle coils (green, red) also result in similar gradients ($\mathrm{d}B_z/\mathrm{d}x$ = const.; $\mathrm{d}B_z/\mathrm{d}y$ = const.). For the solenoid shimming coil (light blue) only the boundaries are shown. Bottom: The main field coil support cylinder with milling groove for the solenoid coil. The mean field coil is not visible in Fig. 2.1, as it is placed inside the shimming system.

grooves leads to a displacement of the entire coil on the surface, thereby allowing to avoid wire deformation if appropriate choices for milling groove depth are made. For a solenoid coil any point in space that has the same value of z and the same value of $\sqrt{x^2+y^2}$ has the same distance to the center of the coil and thus the same magnetic field strength - the magnetic field has the same symmetry as a cylinder. This is accounted for by the ρ coordinate, a plot as a function of x or y would not reveal the necessary information.

The magnetic field of a solenoid without any additional shimms shown in Fig. 2.3 reveals that a significant curvature exists along both length z and the ρ coordinates. Residual gradients are on the order of 10^{-2} G cm^{-1} thus exceeding one ppm by approximately four orders of magnitude.

The effect of shimming the field with the additional solenoid is immediately visible in Fig. 2.4, where the scaling of the ordinate, the magnetic field strength, and increment had to be changed to account for the shimming effect. The magnetic fields axis scaling covers less than 10% of Fig. 2.3, the increment has been reduced by two order of magnitude and is 10^{-4} G. The range of ρ and z has been chosen to show the entire $[2 \times 2]$cm^3 plateau. The homogeneity of the plateau is on a 10^{-5} G cm^{-1} scale as a result of shimming. Note that the overall magnetic field strength is reduced by 1 G as a result of inverted current direction in the shimming coil

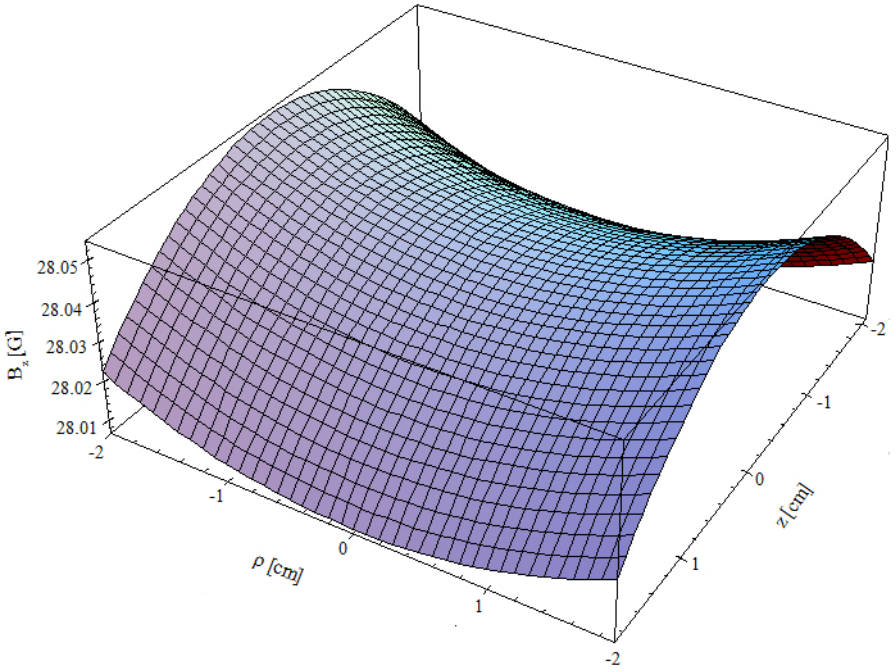

Figure 2.3: 3D-profile of the simulated magnetic field strength of the B_0 coil for 1 A of current without shimming. The z-coordinate is along the length of the cylinder, ρ is the radial coordinate $\sqrt{x^2+y^2}$. Taken from ref. [14].

necessary to obtain the desired curvature compensation.

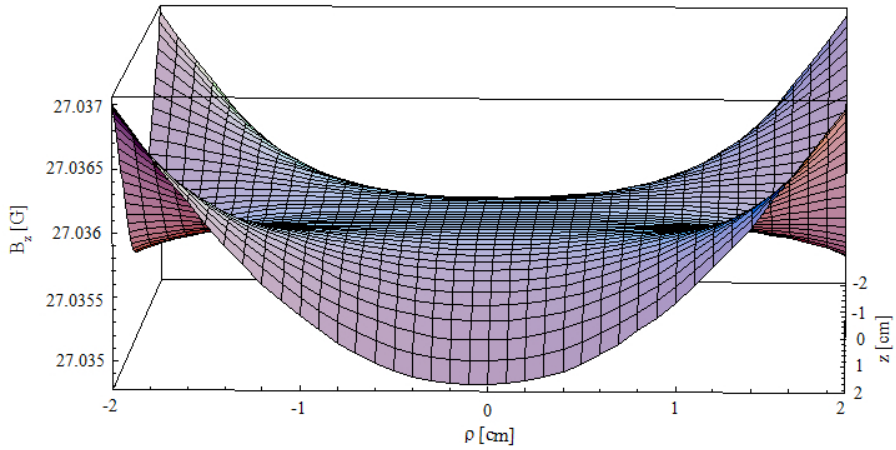

Figure 2.4: Simulated 3D-profile of the shimmed magnetic field at 1 A of current.[14]

It is immediately evident from Fig. 2.4 that, if no material inaccuracies and no laboratory gradients existed, a system of two solenoid coils would already be sufficient for low field NMR spectroscopy. The field homogeneity over a [0.8 x 0.8 x 0.8] cm^3 sample expected as a result of the simulations is 0.3 - 0.5 ppm thus defining the upper boundary for maximum field homogeneity.

2.1.2 Evaluation of the magnet and shimming system

The simulations evidently assumed stationary currents, that is currents not subject to temporal changes. In a real system the magnetic field drift is directly determined by current drifts thus giving rise to a concept unique to nuclear magnetic resonance with electromagnets - the temporal, rather than spatial, magnetic field homogeneity (see Eq. 1.17). As a result of the direct proportionality between current and field strength even an electromagnet system theoretically capable of an infinitely homogeneous field would *never* be applicable for high resolution NMR spectroscopy if current drifts over the measurement time are larger than a ppm. This

problem gets even more pronounced because, as it has been shown in the latter section, at least two currents are required to obtain a homogeneous field and hence drifts can have a cumulative effect. Several generations of current sources[10] are currently available for low-field experiments. A new current source with higher temporal stability and six different current ranges was under construction but was not yet available during initial stages of the performance evaluation.

As a result of laying out each gradient coils twine in a milling groove of different depth the succession of coil manufacturing is not arbitrary, as evidently the lowest layer has to be constructed first due to the arising accessibility restrictions on lower coil layers. The deepest milling grooves were designated for G_x and G_y. As no analytic information regarding number of turns necessary for shimming and expected field gradient values existed a priori for the G_x and G_y because of the complex geometry it was necessary to evaluate field gradient uniformity and determine the gradient per unit current in relation to the number of turns n_t for each coil prior to starting the twine on a new gradient. Too high or too low gradients per unit current would have required adaption of either turn number of current source construction parameters. Immediate evaluation allowed to eliminate technical difficulties, like field offsets in the geometrical middle.[11] This is obviously inacceptable, as a field offset caused by a shimming coil shifts the resonance frequency of the investigated nucleus, which would make shimming practically impossible.

Coils were evaluated by fixing the aluminum support with the newly manufactured shimming coil on a x,y-table and positioning the probe of a Hall-sensor (D.W. Bell, Type 7010 Gauss/Teslameter) carefully in the exact geometrical middle of the cylinder where the sample would be located in later applications. The shimming coils were supplied with 1.00 A of DC-current and several values of the magnetic field measured along the axis of interest. This meant moving the x,y-table, and thus the coils, rather than the probe, as it was rather difficult to maintain probe alignment with the axis and determine its exact position after moving the probe on the inside of a metal cylinder. Surprisingly, the magnetic field of the Earth in the laboratory has slight changes even over very small length scales resulting in an offset upon moving the probe which constituted an additional problem that could be eliminated by moving the magnet rather than the probe. Measurements were carried out with the old current source thus temporal current stability was limited. Short term fluctuations and long term drifts required taking several measurements per data point, while careful readjustment of currents was necessary between the measurements to obtain a time averaged value. Joule heating of the conductor increases the resistivity and, as $U = RI$ wich a constant voltage the current is always a function of the conductor temperature. This problem is evidently more pronounced for coils with a high number of turns, as both current drifts and fluctuations have a larger effect.

The G_x and G_y coils were constructed first and a turn number $n_t = 8$ was chosen, as residual laboratory gradients along those coordinates are expected to be rather small. It should be noted, that the x,y-table was used to change the x- and z-coordinates. Regarding the choice of coordinates, z is along the axis of rotational symmetry, the length l, of both shimming and mean field magnet support cylinders. In order to change to the y-coordinate the shimm support was rotated around the z-axis by 90° prior to measuring a field profile.

Figure 2.5 shows plots of the magnetic field gradients generated by G_x and G_y for 1.000 A of current. Note that for low field strengths per unit current, or low n_t respectively, field fluctuations resulting from the direct proportionality of magnetic field to fluctuations of the driving current could be resolved by the Hall-probe. The gradient per unit current and cm was obtained from linear regression to the measurement data. The agreement of fit function and data is excellent for both coils and it is $G_y = 38.0(1)$ mG $A^{-1}cm^{-1}$ and $G_x = 45.0(2)$ mG $A^{-1}cm^{-1}$.

It was fortunate that these gradient coils did not have to be constructed again (with a lower number of turns) as a current source able to supply several mA with high stability was under construction. The typical range for the required shimming currents on G_x and G_y is 0-10 mA corresponding to maximal gradients of 450 μG $A^{-1}cm^{-1}$. In future designs, where it will be attempted to reduce the mass and size of the electromagnet

[10] Manufactured in house by Prof. S. Appelt.

[11] This occurred several times. The cause are most likely unavoidable inaccuracies in wire insulation thickness. In this case the coil had to be removed and redone prior to starting the twine on a new coil.

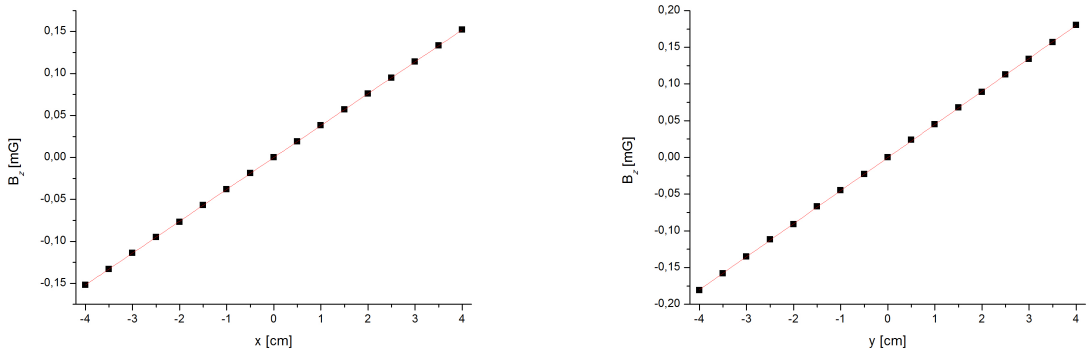

(a) G_x (b) G_y

Figure 2.5: a) Magnetic field profiles of the G_x and b) G_y gradient coils for 1.000 A of current. Note that no field offset in the center is caused by either of the gradients. The gradients are $G_y = 38$ mG $A^{-1}cm^{-1}$ and $G_x = 45$ mG $A^{-1}cm^{-1}$.

and shimm system, the number of turns will be reduced as results indicate that linear contributions to the laboratory gradients only constitute only several μG. Reducing the number of turns becomes a necessity for smaller setups, because bringing the coil closer to the sample increases the field gradient per unit current.

According to the simulation higher magnetic field gradients would be required for G_z with $n_t = 35$ and G_{z2} with $n_t = 298$. As a result of the different coil geometries field gradients and strengths are not only a function of n_t and cannot be directly compared between the different geometries. Gradient and intercept are obtained

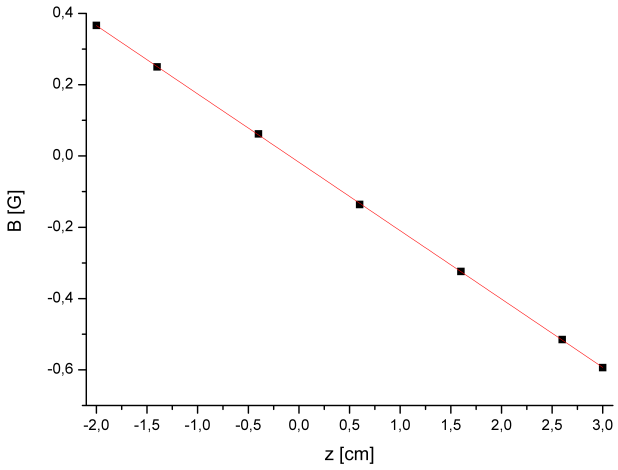

Figure 2.6: Magnetic field profile of the G_z gradient coil along the symmetry axis of the cylinder for 1.000 A of current. Each data point was obtained as an average over several measurements due to current drifts and readjustments. Note the higher gradient per unit current $G_z = 191.8\,\mathrm{mGA^{-1}cm^{-1}}$ compared to G_x and G_y.

from linear regression and it is $G_z = 191.(8)$ mG $A^{-1}cm^{-1}$ with an intercept of 17.(6) mG. It turned out at this stage that the sensor in the hall probe is located approximately 3 mm from its tip thus resulting in the rather arbitrary choice of individual points on the z-coordinate.[12] As a result of this realization and to rule out effects caused by slight inaccuracies in sensor positioning all prior measurements were repeated and 3D-profiles were measured. The results are, however, identical. The G_x and G_y gradients are uniform an homogeneous over an interval of [-2 cm; 2 cm] along the axis of rotational symmetry and no magnetic field could be detected

[12] Considering the gradient the offset corresponds to a positioning inaccuracy of the sensor of below 0.8 mm. Although the exact sensor position in the probe was determined in this measurement it is still experimentally difficult to position the sensor accurately. Note that is has to be exactly 27.00 cm inside a cylinder.

within the measurement precision along the central symmetry axis of the cylinder with either of the gradients active. Therefore both x- and y-gradients will not cause any offset in B_0, and thus the resonance frequency, which is of imperative importance for the application of coils as shimming systems. A residual offset in the exact geometrical middle of the magnet, and hence the sample position, is immediately visible as a resonance frequency shift, which is to be avoided as it renders a gradient coil useless for shimming. With respect to the gradient G_z, measurements indicated that the field gradient is uniform and homogeneous over [-1 cm; 1 cm]. The gradient remains of constant strength when the sensor is displaced along x or y over the sample diameters used in the experiments ($\pm$ 5 mm). Figure 2.6 shows the gradient obtained from the G_z shimming coil. Note the different axis-scaling ob the ordinate as a result of the different coil geometry and higher turn number.

The gradient coil manufactured last was the G_{z2} coil. Figure 2.7 shows the field profile of the G_{z2} coil along the axis of rotational symmetry of the cylinder supporting the shimming coils. The field profile has the expected parabolic shape.

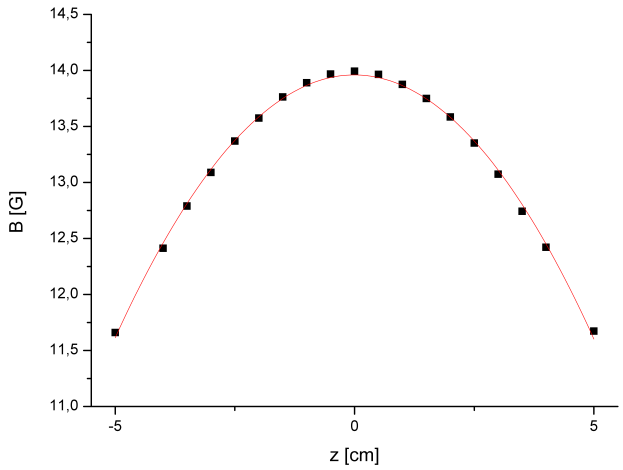

Figure 2.7: Magnetic field profile of the G_{z2} coil along the symmetry axis of the cylinder for 1.000 A of current. Data points are averaged over several measurements in order to compensate for current drift induced errors.

After the gradient coils had been evaluated the externally manufactured B_0 field coil[13] had to be evaluated, especially with respect to interaction of shimms and mean field. The procedural details are similar to evaluation of the gradient coils, but for evaluation the B_0-field was set to approximately 100 G (3.64 A) in the geometrical middle, as it was planned to operate the magnet around this field strength. Data was acquired over an interval of 110 mm along the length coordinate of the magnet and evaluated by non-linear least-square fitting.

[13] I would like to thank R. Thelen and K. Kupferschäger.

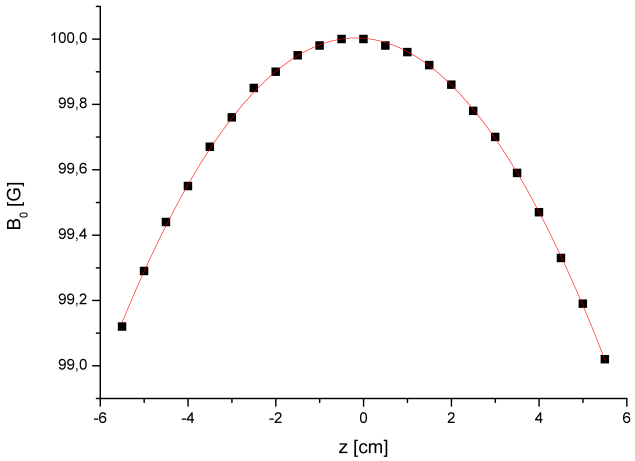

Figure 2.8: Magnetic field profile of the mean field coil along the length coordinate z. Plotted is the magnetic field upon displacement of the coil with respect to the probe. The zero of the abscissa has been chosen as the center of the solenoid. The red line corresponds to the expression $B(z) = 100,00368 - 0,01047\ z - 0.003069\ z^2$.

The overall length of the cylinder is 540 mm, while the twine is along 500 mm of the cylinder. It is evident from the fit function $B(z) = 100,00368 - 0,01047\ z - 0.003069\ z^2$ using the exact current of 3.6427 A[14] that the flux density per unit current is 27.453 G/A. Furthermore it is immediately evident, form the term linear in z, that the maximum value of the magnetic field is shifted from geometric middle of the cylinder. The maximum can be calculated easily from the first derivative of $B(z)$ and is displaced by 1.7 mm. This information was relevant in finding a first approximate position of the external shimming array in relation to the mean field cylinder. The correct shift direction was determined experimentally. Fig. 2.9 shows the magnetic field as a function of z when the B_0 and the G_{z2} shimming coil are supplied with currents required for a homogeneous field predicted by the Mathematica simulation.

[14]Exact means that current and magnetic field were recorded. The current was readjusted to 3.6427 A prior to repetition of a measurement. Data tupels allow to determine the field per current per point in space, which can then be used to calculate the value at exactly 3.6427 A. Evidently, due to the limited number of significant digits, an average is required for a reasonable confidence level.

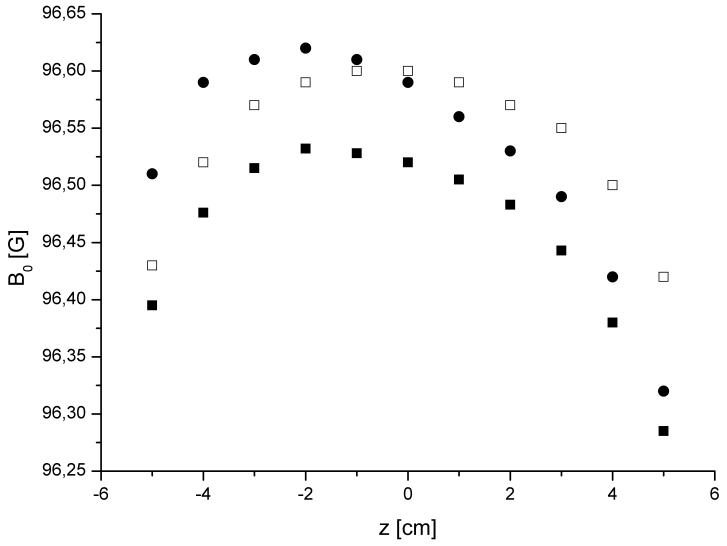

Figure 2.9: Magnetic field profiles of the B_0 field (I = 3,655 A) with G_{z2} shimming (I = 256,1 mA) measured along the z-axis. The zero of the abscissa has been chosen as the center of the solenoid. Black squares: unshifted shimming array, white squares: 1.7 mm to $-z$; black circles: 1.7 mm to $+z$.

It is immediately evident from direct comparison of black circles and black squares, corresponding to displacements of approximately ± 1.7 mm, that the asymmetry becomes more pronounced when displacing the coils in the wrong direction. Furthermore, note that in the region [-2 cm; 2 cm] around the center of the coil the field has a remaining, almost linear, gradient.

It turned out at this stage that this mechanical shimming is extremely sensitive to slightest deviations, hence making it necessary to construct a means of moving the internal cylinder by micrometer calipers (see Fig. 2.1, attached to the shimming array on the top right). Although 1.7 mm is approximately correct, the residual gradient needs to be suppressed by carefully shifting the shimming array several micrometers. If a residual gradient remains, it may be compensated by operating G_z at very low currents to obtain optimal field homogeneity, this has, however, never been necessary so far. It is likely that the gradient per unit current for G_z is too high and a lower number of turns would have been sufficient. Lastly an evaluation of the shimming efficiency was attempted by performing 3D measurements. The unshimmed field is shown in Fig. 2.10.

Attempts to acquire a 3D-profile of the field with shimming currents were unsuccessful[15]. The Hall Sensor used to derive the field profile only has five significant digits, which corresponds to an inherent measurement precision two orders of magnitude below one ppm if the mean field is operated at 100.00(0) G. Direct field measurements were thus not suitable to obtain sufficiently accurate information to judge field homogeneity on a ppm scale. It should, however, be noted that a quick an dirty measurement of the shimmed field indicates the existence of a plateau of approximately $(2 \times 2 \times 2)\text{cm}^3$, where the change of the magnetic field is within the boundaries of measurement precision and the restrictions imposed by the necessity for current readjustment.

2.1.3 The new current source - improvement of temporal homogeneity

The effects of changing the current source were immediately visible upon performing field measurements. It was very rewarding experience, as of now the full number of digits of the Hall-sensor could be considered significant and only slow long term drifts were recorded upon change of the resistivity of the coil due to heat dissipation in the resistive copper wire. But as sub-ppm homogeneity is not directly observable the next logical step was an evaluation of the performance of the new setup with a real experiment and comparison to old results. In

[15]With the old current source. Its likely that it would be possible with the new current source. However, the measurement inaccuracy is insufficient on a ppm scale. The actual performance must be tested by means of NMR experiments.

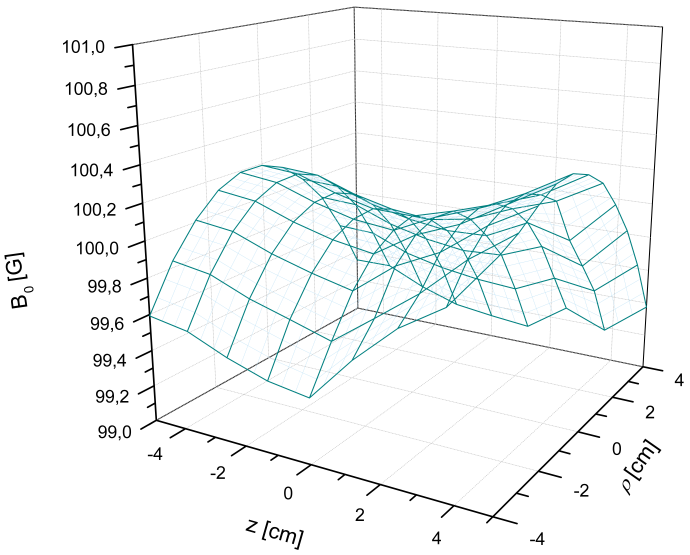

Figure 2.10: 3D field profile of the magnetic field obtained with the old current source. The corner of each large square corresponds to one measurement point. The zero of the abscissa has been set to the middle of the solenoid. Note the strong deviations from the expected smooth double saddle as a result of current drifts over the measurement time. Recalibration was not possible, as the exact geometrical middle is the reference point and current drifts upon probe repositioning limit the accuracy. Note the analogy to the double saddle in Fig. 2.3.

prior applications current fluctuations led to severe restrictions on line resolution by giving rise to artifacts close to the Larmor-frequency and line broadening as a result of both slow drifts changing the resonance frequency during data acquisition and fast fluctuations. This effect is especially pronounced for nuclei with large relaxation time constants such as e.g. ^{129}Xe[4]. In order to directly compare the improvement obtained by changing the current source a reference sample of degassed Milli-Q water stored under Argon atmosphere was prepared. The sample tube diameter is 1.0 cm, has an internal diameter of 7.4 mm and a sample volume of 360 μL. Water has the advantage of a rather high spin density and is nearly 100 % naturally abundant while having the highest γ, and thus sensitivity, among the NMR-active nuclei. As a result the SNR was sufficient at a Larmor-frequency of 500 kHz to perform the measurements without thermal prepolarization at $B_p = 2\,\mathrm{T}$ thus suppressing effects caused by transfer time differences and T_1 relaxation effects. The B_0- and G_{z2}-coils were supplied with the old and new current sources. Currents were set to the values predicting a homogeneous magnetic field obtained from the Mathematica simulations $I(B_0) = 4.4568$ A; $I(G_{z2}) = 325.5$ mA in both experiments. It should be noted that fluctuations of currents monitored by the multimeters were much slower for the new current supply system. Data was recorded for 7.0 seconds after the pulse with a sampling rate of 300 μs. No further data manipulation (apodization) was performed prior to Fourier-transform and Lorentz-fitting. Figure 2.11 shows examples of water-spectra obtained while using the old current source. As the sample is water with only one proton type one sharply resolved line would be expected.

In contrast to the spectra obtained with the old current source use of the new current source led to significant improvement in linewidth and pseudo-line suppression. Figure 2.12 shows the spectrum of the same sample with the new current source. Differences in the off-resonance frequency are caused by the difficulty to adjust currents of several A to yield exactly the same value with a different current source. The linewidth corresponds to an overall field homogeneity of 3.2 ppm in a first experiment, where no efforts had been made to optimize shimming currents obtained directly from the Mathematica simulation. Furthermore only G_{z2} had been used, no additional shimming with other gradient systems was applied in these experiments.

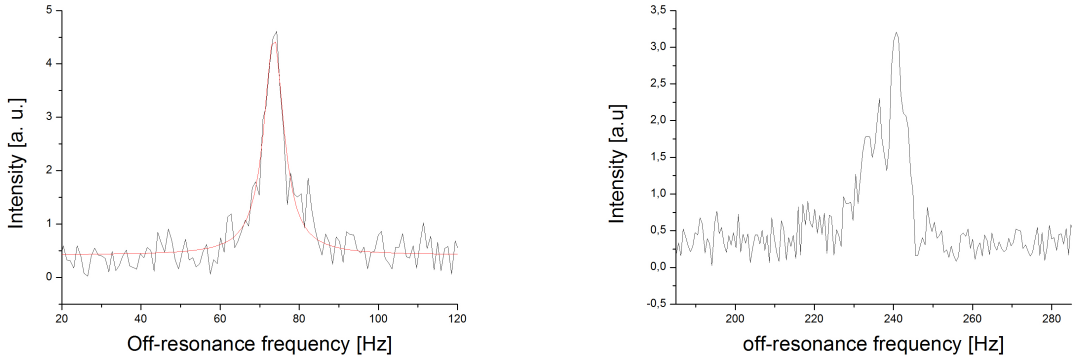

(a) (b)

Figure 2.11: ^{1}H spectra of 0,4 mL of thermally polarized Milli-Q Water obtained while supplying the B_0 and G_{z2} coils with the old current source. The resonance frequency is 500 kHz and the spectra constitute a) one less extreme and b) one very extreme example of effects caused purely by current drifts and the concomitant problem of temporal field homogeneity. Spectra are obtained within a timeframe of five minutes without current readjustment in that timeframe. Note the drifts of the off-resonance frequency from 73.5 to 240 Hz and the pseudo line structures on either side of the peaks. The linewidth in a) is 6.4 Hz, Lorentzian fitting was waived for b).

2.1.4 Experimental Homogeneity limits

Field homogeneity evaluation poses a challenge, as laboratory gradients in the μGcm^{-1} regime are easily caused as a result of moving any object with magnetic parts like chairs, tools and other laboratory equipment. Furthermore these gradients are too small to be directly observable in the presence of the earth's magnetic field, even if other sensor types with extremely high measurements accuracy for DC magnetic fields were used.[16] As a result the field homogeneity can only be evaluated indirectly by means of spectroscopy. Shimming has to be performed prior to the first measurement of each day. Current values have to be readjusted after long breaks, as laboratory gradients are very weak and subject to fluctuations.

Figure 2.13 shows two spectra of C_6F_6 at 500 kHz resonance frequency but with different shimming currents on the G_x and G_y gradients. It is immediately evident that the shimming has a large impact on the obtained spectra and bad shimming may give rise to artifact lines.

It is rather difficult to obtain a definite value for the effective spin-spin relaxation time T_2^* from the FID by curve fitting, as it is evident that residual laboratory gradients cause deviations from the expected exponential hull curve. Note that the line-shapes are no exact Lorentzians thus limiting accurate determination of the FWHM linewidth. This is most likely a result of long data acquisition times, which is several seconds irrespective of the investigated nucleus. In this rather large timeframe each individual molecule has sufficient time for diffusion throughout the sample and samples two different chemical environments - the wall and the bulk. The limit at a field strength of 120 G (^{1}H Larmor-frequency of 500 kHz) has been 0.7 ppm, corresponding to FWHM linewidths of 0.11 Hz, irrespective of the investigated compound. Due to the construction of the setup spectra of the same nucleus at other frequencies can be obtained with relative simplicity. The next logical step was to evaluate whether the field homogeneity is comparable at different Larmor-frequencies. Shimming experiments were performed with different samples but for brevity only the best and most recent results are shown. Figure 2.14 shows the FID and ^{19}F spectrum of C_6F_6 at a Larmor-frequency of 166 kHz. The experiments were rather surprising, as the apparent T_2^* seems to be rather long which is rather unusual for an abundant nucleus with large gyromagnetic ratio, such as Fluorine. The apparent T_2^* is 7.5 s and thus longer than the FWHM linewidth obtained from the spectra suggests. According to these results the homogeneity limit is 0.7 - 0.8 ppm at 166 kHz ^{19}F Larmor-frequency and results obtained at 500 kHz indicate that the homogeneity is largely independent of

[16] SERF atomic magnetometers would have sufficient resolution in zero-field but can't be used at 0.5 G, superconducting parts in SQUIDs strongly interact with magnetic fields, Hall sensors have to poor resolution. Albeit not impossible it would, at the very least, be extremely difficult.

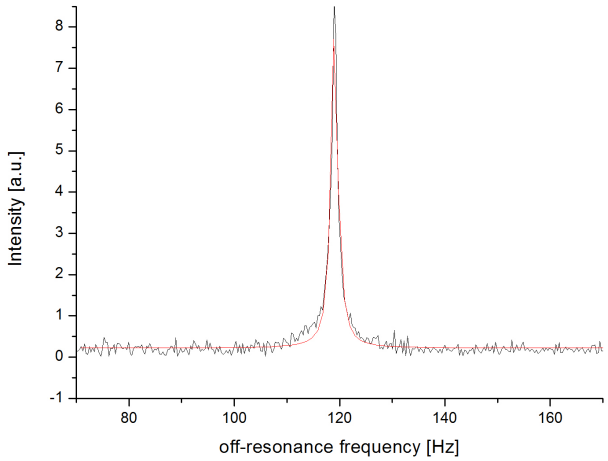

Figure 2.12: ^{1}H spectrum of 0,4 ccm of thermally polarized Milli-Q Water obtained while supplying the B_0 and G_{z2} coils with the new current source at a resonance frequency of 500 kHz. Note the significant improvements with a linewidth 1.6 Hz and the absence of pseudo line structures. The off-resonance frequency is 119 Hz.

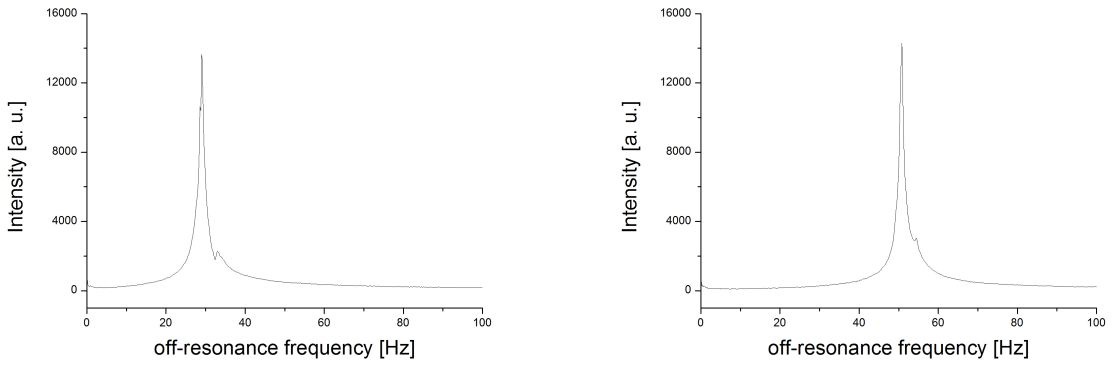

(a) (b)

Figure 2.13: Two ^{19}F spectra of 360 μL thermally prepolarized Hexafluorobenzene at a Larmor-frequency of 500 kHz. Prepolarization time at 2 T is 10 s, transfer time is 3 s. Note the more pronounced sidebands in a) as a result of different shimming currents. The FWHM linewidth of the large line is a) 2 Hz b) 1 Hz.

the frequency.

In order to further evaluate the homogeneity limits detection coils with half the internal diameter of the coils were manufactured. If residual gradients from parabolic field shapes of the solenoid coils determine the homogeneity limit, reducing the coil radius by a factor two should improve the homogeneity by roughly a factor four. Figure 2.15 shows spectra obtained from 0.1 mL samples of benzene[17] and water in a standard high-field NMR sample tube with 5 mm diameter and 0.3 mm wall thickness. Especially when considering that no thermal prepolarization has been used the signal to noise ratio obtained for water is surprisingly similar to the spectrum Fig. 2.12, where the SNR is roughly two times worse. Several factors can be held responsible. Firstly the filling factor of the coil is higher when regular high field NMR tubes are used, as less volume of the detection coil is filled by glass. With the 10 mm sample tubes the glass strength of 0.8 mm results in an internal sample diameter of 8.4 mm corresponding to a filling factor of 80% if the base of the vessel is considered, whereas the filling factor for smaller vessels is approximately 94%. Secondly, although the rms-noise is determined by

[17] Note that benzene distilled over sodium had been used as a sample. It is likely that the incomparability in the Signal-to-Noise ratios of water and benzene results from traces of the quadrupole nucleus sodium in the benzene sample leading to fast spin-lattice relaxation. Benzene samples are always a source of concern, unless it is bought in highest available purity with analysis certificate. This is the reason why my standard sample was changed to hexafluorobenzene, where no such problems occur.

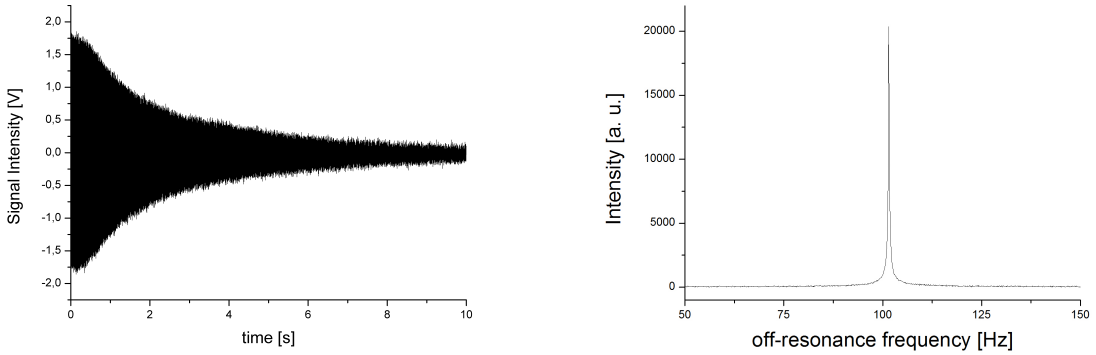

(a) (b)

Figure 2.14: a) FID and b) ^{19}F spectrum of 360 μL thermally prepolarized Hexafluorobenzene at a Larmor-frequency of 166 kHz. Prepolarization time at 2 T is 10 s, transfer time is 3 s. Note the timescale of the FID in a). The range of the frequency axis in b) has been chosen to be identical with the spectra in Fig. 2.13 for better comparability. The FWHM linewidth is 0.118 Hz and corresponds to a field homogeneity of 0.7 ppm.

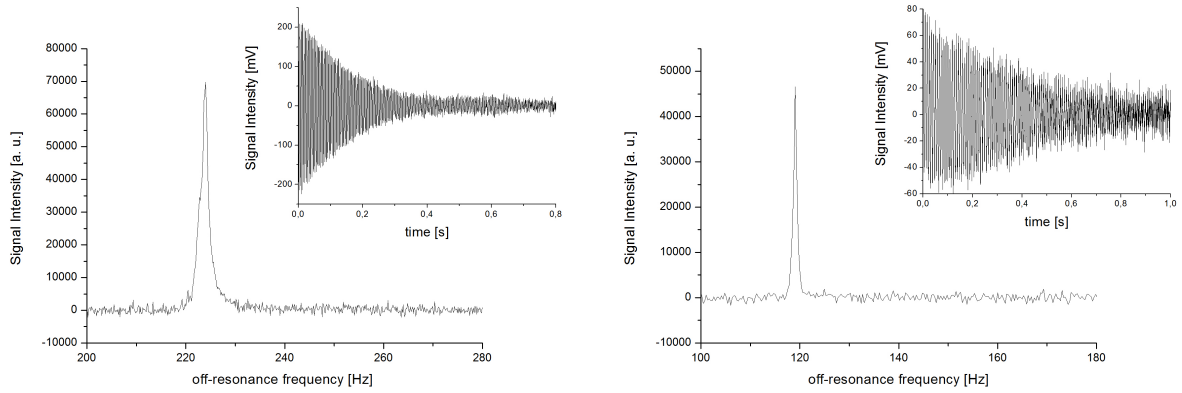

(a) (b)

Figure 2.15: FID (inset) and ^{1}H spectrum at a Larmor frequencies of 500 kHz. a) 0.1 mL of Benzene thermally prepolarized at 2T and b) spectrum of 0.1 mL water not thermally prepolarized.

all noise sources in the periphery electronics, one important factor - the resistivity of the pickup coil - scales favorably with reduction of the sample diameter as the DC resistivity $R \approx n_t \pi d A \rho_{Cu}$ with number of turns n_t, average coil diameter d, conductor cross section A and specific resistivity of the copper wire ρ_{Cu}.

Explicitly the rms-noise determined in the latter experiments is only 8 mV whereas larger coils have noise levels of 20 mV if other parameters (wire diameter) are unchanged. And lastly NMR signal detection based on induction scales favorably with reducing sample, and thus coil, diameters[18]. Efforts to obtain field homogeneity better than 0.7 - 0.8 ppm have been unsuccessful even with small samples. This result indicates that the difference between experimentally determined limit of 0.8 ppm and predictions from simulation of 0.3 ppm must be attributed to other factors. The most obvious ones are variations in wiring insulation thickness of mean field and shimming coils, limited accuracy of manually laying out twines, machine precision while cutting milling grooves and thermal expansion of inner and outer cylinders as a result of heat due to power dissipation.

As a concluding remark it should be noted, that the shimming system has several degrees of freedom (5 currents, one mechanical parameter) that can all only be regulated within certain boundaries of precision. Especially the mechanical displacement of the external shimming array with respect to the mean field coil shows that the magnetic field homogeneity is extremely sensitive to slightest shifts. Therefore a second micrometer caliper was attached to the other side of the mean field coil to maintain the relative positions of the coils.

[18] This avenue of research has been carried on by my colleague Alexander Liebisch. Recently a sample of 0.001 mL Benzene was investigated using a detection coil of 1 mm internal diameter.

A unresolved problem remains for the assembly presented here. Although the use of two separate support cylinders for B_0-coil and shimming array worked out favorably, as it allowed for the displacement of the cylinders to correct for the mean field solenoid imperfections, there is a drawback. The internal diameter $d_{\mathrm{i,shimm}}$ of the shimm support cylinder may not exactly correspond to the external diameter $d_{\mathrm{a,supp}}$ of the mean field support cylinder, because a small gap is required for assembly. But as the inner radius of the external cylinder will evidently be larger than the outer radius of the nested cylinder by exactly the gap size chosen for assembly gravity will displace the inner cylinder by the gap size (see Fig. 2.16).

Considering the incredible sensitivity to the smallest of shifts along the z-axis[19], it must be expected that displacement along the y-coordinate leads to a similarly large effect[20]. Given the small size of the assembly gap[21] a solution to the displacement problem could not be found[22]. It can thus not be guaranteed, and is unlikely that, the theoretical performance limit of the setup has been reached in any application. However due to thermal expansion of coil support materials and rather large currents of several Ampere on the mean field coil assembly gaps remain a necessity.

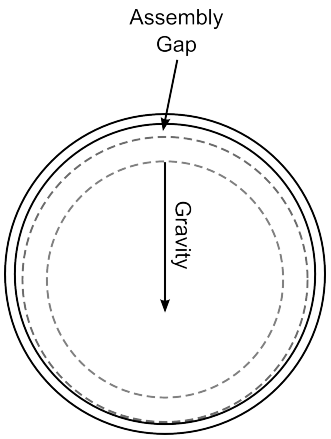

Figure 2.16: The outer (black) and inner support material cylinder (gray) for coil assembly have different inner radius $d_{\mathrm{i,shimm}}$ and $d_{\mathrm{a,supp}}$. Gravity will displace the centers of both cylinders, and thus all coils, by the difference of the diameters.

[19] No exemplary spectra are shown. Albeit nice for demonstration i never recorded a spectrum that is deliberately bad.

[20] It is likely that this is the reason why typical sets of shimming currents have smaller currents on the x-gradient than on the y-gradient.

[21] According to information from the mechanics workshop of the ZEA-2 of the Jülich Research Center gap sizes are typically set to 0.1 mm.

[22] The problem is a little annoying. The inner cylinder with 5994 turn solenoid coil has a mass of easily 20 kg. It needs to be movable for mechanical shimming so one can't simply place paper in between the two cylinders. The result is that required shimming currents on the y-gradient are usually slightly larger than on the x-gradient.

2.2 Spin Polarization induced Nuclear Overhauser Effect

Hyperpolarization of ions is experimentally challenging and has so far only been realized in a few instances. The working horse is Dynamic Nuclear Polarization as the oldest [13] and best established method. DNP has been successfully used for hyperpolarization of ^{6}Li-salts, which can be applied as contrast agents in medical applications[29]. The power of DNP lies in its versatility and reliability but affordability of the required experimental hardware, such as cryotechnology to achieve ultra-low sample temperatures of 1-2 K[23] and microwave sources, and its need for organic radicals as polarization source restrict use of DNP-based methods to ex-vivo applications or academic research. Similarly, the currently emerging idea of using para-hydrogen polarized substrates, which could in theory be specifically tailored to act as diagnostic tools, requires transition metal catalysts for the hydrogenation step. Both organic radicals and heavy metal catalysts have significant toxic impact on organisms and would have to be quantitatively separated from a contrast agent before application in medical or biological applications.

An alternative method of hyperpolarization is constituted by the Spin Polarization Induced Nuclear Overhauser Effect (SPINOE) method. The intrinsic advantage here is that the primary polarization step, which involves optical excitation of alkali metal valence electrons in the gas phase with subsequent transfer of electron spin order to a noble gas nucleus (Spin Exchange Optical Pumping SEOP), is spatially removed from the NMR sample. Highly polarized spin 1/2 noble gas nuclei, such as ^{129}Xe, are obtained as a mixture with chemically inert gases N_2 and He.[24] SPINOE is the process of exposing a sample to a high number of ^{129}Xe nuclei and the unusually high degree of nuclear polarization $P_{\mathrm{Xe}} = 0.3 - 0.4$ allows it to act as a polarization source for other nuclei in the sample. The advantage of hyperpolarized Xenon lies in affordability of the experimental setup and non-toxicity (as well as non-reactivity) of the gas mixture which, in principle, makes SPINOE the least problematic hyperpolarization methodology with respect to applicability. However, SPINOE has, so far, only been successfully used for organic molecules [47]. Extension of SPINOE to, for example, ionic compounds would be desirable.

2.2.1 SPINOE-Equations

Important facts about SPINOE are most conveniently introduced by briefly discussing the equations governing the process[56].

$$\rho_S = \frac{1}{10}\rho_{0S}\left(\frac{1}{1+(\omega_{0I}-\omega_{0S})^2\tau_C^2} + \frac{3}{1+(\omega_{0S}^2\tau_C^2)} + \frac{6}{1+(\omega_{0I}+\omega_{0S})^2\tau_C^2}\right) \tag{2.1}$$

with ρ_{0S} given by

$$\rho_{0S} = \frac{4}{3}I(I+1)\hbar^2\gamma_I^2\gamma_S^2\tau_C\sum_i r_i^{-6} \tag{2.2}$$

are the two fundamental equations describing the polarization transfer from a nucleus I, the ^{129}Xe, to a nucleus S. Equation 2.1 describes the relaxation rate ρ_S of the S spins caused by contact with the relaxation channel defined by the modulated dipole-dipole interaction of spins I and S, where I subsequently gets polarized itself. Equation 2.2 reveals that the polarization transfer is dipolar in origin due to the inverse dependency on the 6^{th} power of the averaged internuclear distance r_i. The other relevant parameters, the spin quantum number I and the gyromagnetic ratios γ_I, γ_S, immediately relate to the magnetic moment of the nuclei $\hbar\gamma I$ and quantify the local field strength around a nucleus. The efficiency of the transfer will decrease with increasing difference of the Larmor-frequencies $\omega_{I,S}$ and increasing intermolecular distance between the spin pair I, S. Greatest enhancements are expected for high γ nuclei such as fluorine or protons. Dynamics are described by the Solomon equation

$$\frac{I_z(t)-I_0}{I_0} = -\frac{\sigma_{IS}}{\rho_I}\frac{\gamma_S}{\gamma_I}\frac{S(S+1)}{I(I+1)}\frac{S_z(t)-S_0}{S_0}, \tag{2.3}$$

[23] Room temperature DNP is also applicable, but challenging.
[24] Another possible nucleus for SEOP is ^{3}He but its availability is, due to its origin from nuclear reactions, too limited.

accounting for the cross-relaxation rate σ_{IS} between the nuclei I and S. It states that the polarization of a nucleus I at a time t, denoted $I_z(t)$, is inversely proportional to the polarization of the nucleus S to which the polarization is transferred. The parameters I_0 and S_0 are the thermal polarization levels of nuclei I and S at the strength of the measurement field - the equilibrium Boltzmann polarization - as it will generally be impossible for nuclei to have their polarization levels drop under the value characteristic for the field strength. The additional scaling factor σ_{IS}/ρ_I is the quotient of cross-relaxation rate σ_{IS} and self-relaxation rate ρ_I, quantifying the ratio of polarization transferred from I to the nucleus S and lost due to other relaxation pathways. The term γ_S/γ_I is a direct measure of the strength of dipolar fields of the nuclei involved. Conservation of energy requires this factor in the transfer equation, as the cross-relaxation process can also be understood as spin lattice relaxation, where the polarization target is the lattice. The correlation time τ_C is defined in analogy to the Arrhenius-equation for the equilibrium constant k of a chemical process

$$\tau_C = \tau_0 e^{-\frac{E_A}{k_B T}}. \tag{2.4}$$

As usual E_A is the activation energy of the process and τ_0 the correlation time at $T = 0$ K.

2.2.2 Experimental procedure

Several factors are important when using hyperpolarized Xenon in a NMR experiment. In order to avoid relaxation of hyperpolarized Xenon due to exposure to traces of paramagnetic oxygen, which negatively influences Xenon relaxation times, NMR-solvents and liquid sample compounds must be degassed prior to use. Samples in the solid state were transferred to a Schlenk-tube, and repeatedly evacuated to 10^{-3} mbar and flushed with argon. In order to obtain a sample of defined concentration a Schlenk-tube with an argon atmosphere is tared, an amount of substance added to the tube and the tube weighed again to determine the sample mass. Known mass and molar mass of the compound allow dissolution in a defined amount of anhydrous solvent to obtain the desired concentration. In order to obtain a NMR sample 0.4 mL of the solution are transferred to a NMR tube which is sealed under a dry argon atmosphere. The gas supply of the NMR setup is flushed with dry nitrogen in order to remove parts of the residual oxygen from the tubing and the sample connected while a low flow rate of nitrogen is maintained.[25] If applicable, samples are frozen in liquid nitrogen and repeatedly evacuated and flushed with dry nitrogen to remove residual oxygen traces from the connection process and saturate the solution with nitrogen.

If possible[26] ^{129}Xe was measured at the Larmor-frequency of the target nucleus prior to each experiment. Sample tubes had an internal diameter of 8.0 mm, the height of the solenoid pickup coil was 10 mm, the internal diameter 10 mm and the sensitive volume is 0.40 cm^3. The composition of the gas mixture used in the experiments was 4% Xe (26.4% ^{129}Xe), 10% N_2 and 86% He. Assuming the gas mixture behaves like an ideal gas at a pressure of 5 bar and an ambient temperature of 22°C the number of ^{129}Xe-isotope atoms in the pickup coil is $n_{\mathrm{Xe}} = 5.18 \cdot 10^{17} = 0.86$ μmol.

Experiments with liquid samples are carried out by subjecting a sample to the hyperpolarized Xenon atmosphere. The spin density of Xenon in solution is due to diffusion of Xenon into the liquid and thus limited by the solubility. n_S can be approximated by taking the ratio of the gas peak integral in the reference experiment in relation to the solution peak. For SPINOE experiments high molar amounts of Xe are beneficial in order to resolve even small effects. In order to yield high Xenon amounts in contact with the solution samples are placed in a 1 T Halbach-magnet, frozen in liquid Nitrogen and exposed to a continuous flow of hyperpolarized Xenon at 400 cm^3/min. With its melting point of 161.4 K, well above the boiling point of liquid nitrogen (77,15 K) and long T_1 a solid Xenon phase may be accumulated on the sample surface. Liquid Xenon can be obtained by carefully heating the sample. Typically Xe(s) is collected for 60-240 seconds, as longer accumulation times are unreasonable due to spin lattice relaxation.

[25] Schlenk-technique.
[26] similar gyromagnetic ratio allows to use the same pickup coil.

It should be noted that the liquid Xenon phase may generally be miscible or immiscible with the sample. Furthermore liquid Xenon has a high density $\rho = 3.1\text{g/cm}^3$ compared to standard organic solvents, which usually results in liquid Xenon accumulating as a second phase on the bottom of the sample tube.

2.2.3 SPINOE Hyperpolarization of organic molecules

Although there are only $5.18 \cdot 10^{17}$ ^{129}Xe nuclei it is nevertheless possible to obtain a very clearly defined FID from single transient down to the Earth's magnetic field [3]. A ^{129}Xe FID and reference spectrum at 83 kHz is shown are shown in Fig. 2.17.

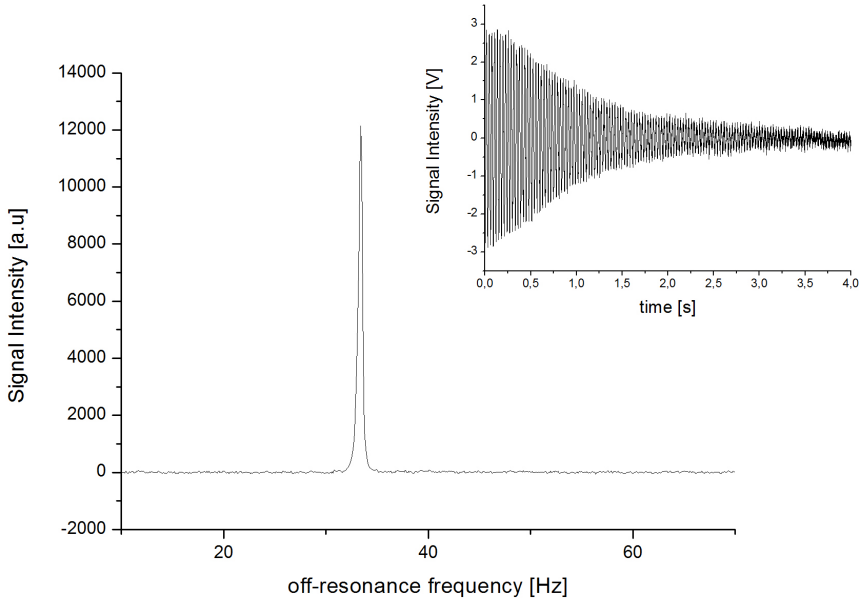

Figure 2.17: FID (inset) and spectrum of ^{129}Xe at a Larmor-frequency of 83 kHz. The FWHM linewidth is 0.45 Hz.

As greatest enhancements from SPINOE enhancements are expected for high γ nuclei it was interesting to investigate a substrate containing both ^{1}H to ^{19}F, the nuclei with the largest value of γ and extremely high natural abundance (100% ^{19}F, 99,985% ^{1}H). From study of literature [52, 51, 53] it was evident that aliphatic organic compounds with low dipole moments allow for high Xenon solubility and 3,3,4,4,5,5,6,6,6-nonafluorohex-1-ene was identified as a suitable test compound.

A sample containing 50 μL 3,3,4,4,5,5,6,6,6-Nonafluorohex-1-ene in 350 μL methanol-d4 was placed in a 2 T magnet for 20 seconds and transferred to the sensitive volume of the NMR. The structure of the compound and ^{1}H FID and spectrum at a proton resonance frequency of 83 kHz are shown in Fig. 2.18 a) and b). The FWHM linewidth of more than 5 Hz is not a result of bad shimming but is rather caused by the presence of many different heteronuclear J-couplings. Throughout the remainder of the text the established $^{\text{Distance}}J_{\text{AB}}$ convention is consistently used for identifying J-couplings. In the 3,3,4,4,5,5,6,6,6-nonafluorohex-1-ene heteronuclear J-couplings range from $^3J_{\text{HF}}$ $-^7$ J_{HF}. Using the general procedure outlined above the spectra and FIDs shown in Fig. 2.19 were obtained in a single transient. Both ^{19}F in the perfluorobutyl-moiety and ^{1}H in the ethylene moiety of the nonafluorohexene can evidently be polarized using SPINOE. The integral ratio of SPINOE polarized ^{1}H to ^{19}F is 1.75:1, the SPINOE polarized ^{1}H spectrum has a 3.4 times enhanced SNR over the same sample thermally prepolarized at 2 T. As transfer time from the 1 T Halbach magnet used in the SPINOE experiment and the 2 T Halbach magnet used in the thermal prepolarization experiment are very similar [27] the obtained signal enhancement immediately translates to ^{1}H polarization levels. Note that these experiments did not require accumulation of a high amount of Xenon by freezing the sample in liquid nitrogen and accumulating Xenon in

[27] within the boundaries imposed by human reaction time.

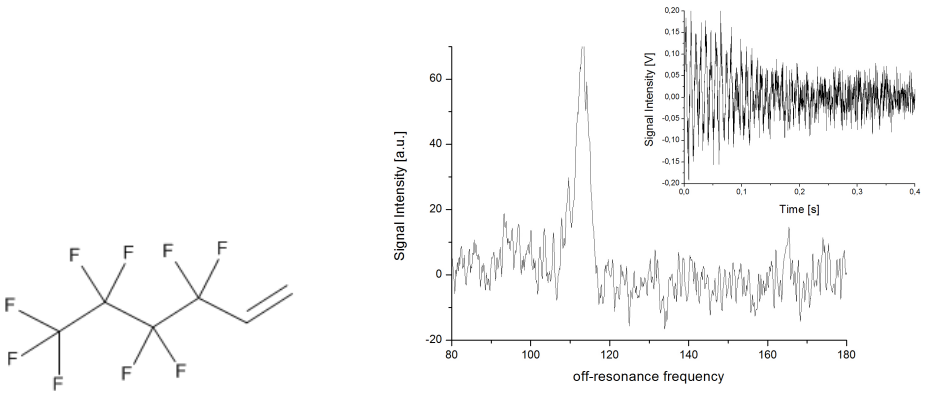

(a) (b)

Figure 2.18: a) Structure of 3,3,4,4,5,5,6,6,6-nonafluorohex-1-ene and ^{1}H spectrum of a 50 μL sample dissolved in 360 μL methanol-d4 and prepolarized at 2 T.

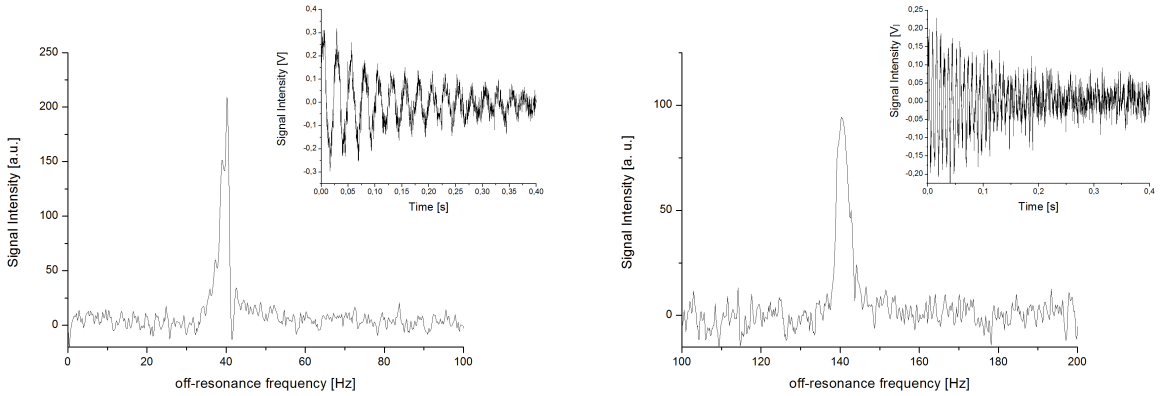

(a) (b)

Figure 2.19: a) FID (inset) and ^{1}H SPINOE spectrum of 3,3,4,4,5,5,6,6,6-Nonafluorohex-1-ene and b)FID (inset) and ^{19}F SPINOE spectrum at a Larmor-frequency of 83 kHz. Line broadening is a result of the many different homonuclear and long range heteronuclear couplings.

its solid state.

SPINOE has also been successfully demonstrated in conjunction with aromatic organic compounds. Navon et al. used a 3:1 mixture of benzene-d6 and benzene-d5 to demonstrate the effect[47]. It is unsurprising that SPINOE could be successfully demonstrated for Benzene, as the existence of Argon-Benzene and Xenon-Benzene van der Waals clusters is known from literature. They constitute a convenient model system for non-covalent bonding[66]. Heterocyclic organic compounds exhibit more interesting reactivities and azabenzenes have interesting functions in natural processes[28]. With respect to hyperpolarization of cations heterocycles are potentially interesting SPINOE targets. Action of aromatic systems and multiple bonds as haptic[29] η^x ligands and many transition metals, including catalysts and precatalysts, have structure elements similar to xenon-benzene van der Waals molecules. Heterocycles may also act as ligands with a given denticity, where Crabtree's catalyst is a good example for a compound with both ligand types. In was interesting to investigate whether a heterocyclic system behaves in analogy to benzene when subjected to the SPINOE procedure. To that end a sample containing 72 mg of pyrazine (1,4-Diazabenzene)[30] in 0.4 mL of methanol-d4 was prepared with the outlined procedure. The ^{1}H of pyrazine thermally prepolarized at 2 T could be recorded in a single transient and FID and spectrum are shown in Fig. 2.20 a). Fig 2.20 b) shows the FID and spectrum of ^{129}Xe for the same sample.

[28] I personally like the biochemistry of pyridoxalphosphate as an example.
[29] hapticity refers to a sequence of analogous and contiguous atoms.
[30] low toxicity, solid state compound. Other heterocycles are often suspected to be carcinogenic or hazardous. The NMR

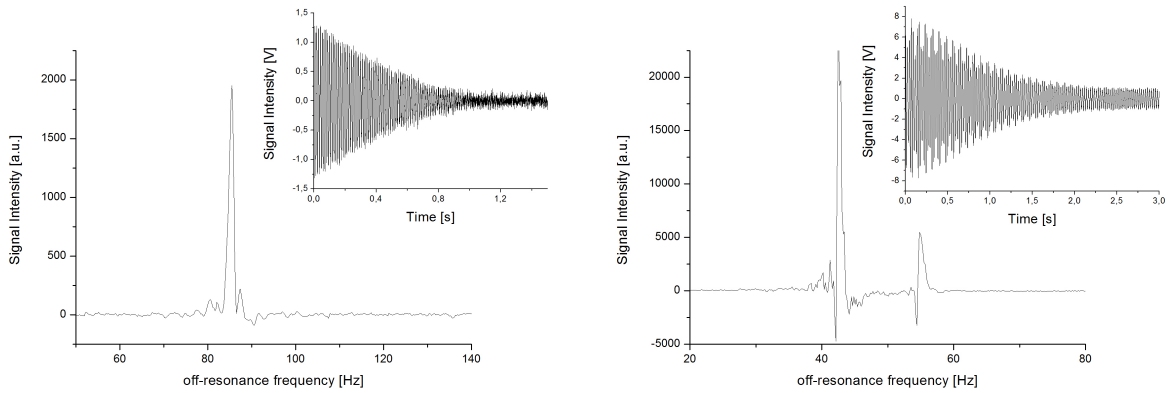

(a) (b)

Figure 2.20: a) ^{1}H FID (inset) and spectrum of 72 mg of pyrazine prepolarized at 2 T. The resonance frequency is 83 kHz. b) ^{129}Xe FID (inset) and spectrum. Two separate lines identify free Xenon gas and Xenon in solution. The separation between the lines is 12.5 Hz $\pm$ 0.5 Hz corresponding to a chemical shift difference of 150 $\pm$ 6 ppm, consistent with the literature value of 148 ppm.

The spectra obtained for pyrazine are rather badly resolved, as a technical defect made it necessary to use to old current source for these experiments. This limited the accuracy of line frequency determination significantly, as sidebands from current drifts limit the spectral resolution. The value for the chemical shift difference of 150 $\pm$ 6 ppm does nevertheless agree with the value reported in ref. [45].

Efforts to obtain a SPINOE polarized ^{1}H spectrum of pyrazine remained unsuccessful in methanol-d4. Typical values for the chemical shift of Xenon in aromatic environments, such as toluene, benzene and pyridine range from 190-197 ppm [45] and the observed chemical shift of approximately 150 ppm is indicative of xenon predominately sampling methanol-d4 environments. Rapid exchange between the coordination environments would have resulted in observation of an average weighted by spin densities (0.9 mmol for pyrazine and 8.4 mmolfor methanol), slow exchange would result in two lines indicative of coordination environments and, most likely, an observable polarization transfer to pyrazine via SPINOE. As a result of exchange averaging of characteristic chemical shifts it is, unfortunately, not possible to make a definitive statement whether the ^{129}Xe chemical shift is influenced by the pyrazine content of the sample[31]. Note that chemical shifts of Xenon in water and common aromatic compounds, such as benzene and pyridine, are virtually identical (Benzene 195 ppm, water 196 ppm, pyridine 197 ppm)[45].

2.2.4 SPINOE Hyperpolarization of Ionic compounds

From the SPINOE equations it is evident that spatial proximity between the hyperpolarized Xenon nucleus and the target nucleus is one of the necessities for a polarization transfer to occur. In the solid state an extremely small grain size on the scale of several ionic radii would be required to yield an appreciably high ratio of surface to bulk nuclei. In order to allow for direct contact between Xenon and Ion it does at first glance seem reasonable to work with solutions of ions in solvents with comparably high Xenon solubility. From references [52, 51, 53] it is evident that water is a poor solvent for xenon thus requiring use of organic solvents. The choice of organic solvents is evidently limited to compounds that allow for salt dissolution and polar solvents are required. High Ion concentrations would seem to be beneficial, as they increase the ratio of ions to solvent molecules and the Xenon-Ion collisions should become more likely. From this simple model it seems reasonable that experiments should start from a highly concentrated solution of a salt in an organic solvent.

Lithiumchloride has a very high solubility in aqueous solutions (22 mol/L) and showed good solubility in methanol-d4. A concentrated solution of isotopically enriched ^{6}LiCl in methanol-d4 contains approximately 50

laboratory does not have an exhaust and exposure to hazardous compounds should be kept low.

[31] methanol is never anhydrous and residual water content imposes an error on the reported 148 ppm. The authors do, however, not elaborate on exact sample composition for alcohols.

wt% of LiCl (4 mmol/0.4 mL standard sample volume). A spectrum of ^{6}Li in solution at a resonance frequency of 83 kHz could be easily acquired by thermally prepolarizing the sample at 2 T followed by transfer to the sensitive volume of the NMR magnet (spectrum not shown)[32]. Exposing the sample to hyperpolarized Xenon at 5 bar and room temperature resulted in a Xenon spectrum showing only a free gas line. Although xenon is soluble in pure methanol the increase in average solvent polarity upon salt dissolution seems to inhibit xenon solubility. Similarly the SPINOE procedure did not allow for detection of dissolved Xenon even for long Xenon accumulation times. Liquid Xenon forms a clearly separated phase in these experiments. An additional problem was constituted by the temperature dependency of solubility and precipitation of LiCl(s) from the solution upon cooling the sample with liquid nitrogen. As a result Lithium concentrations in solution are unknown and the sample was not suitable for further investigation. The logical approach is to reduce the concentration of Lithium in solution to both avoid precipitation of solid LiCl from the solution and increase Xenon solubility. A standard NMR sample of 400 μL sample volume containing 83.9 mg, corresponding to 2.00 mmol of ^{6}Li per sample, was prepared. At this concentration precipitation upon cooling could be largely avoided. The average solvent polarity does indeed affect the solubility and in this experiment it was possible to observe Xenon in solution. To that end solid Xenon had to be accumulated for several minutes and melted. A solution signal was observable after approximately two minutes. The rather long time period before a signal for Xenon in solution could be observed indicates that liquid phase Xenon isn't sufficiently miscible in any composition with methanolic Lithiumchloride solution. It is more likely that the solution-Xenon line originates from unavoidable contact between xenon evaporating from the high density phase on the bottom of the sample and the low density methanol phase on top. The spectrum is shown in Fig. 2.21. The results obtained in this experiments are

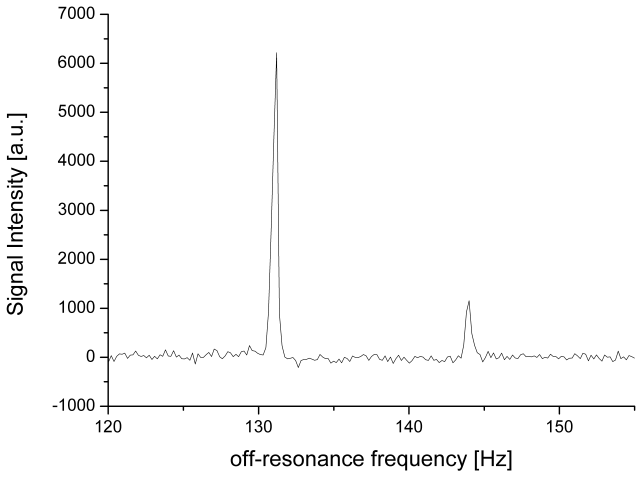

Figure 2.21: Spectrum of ^{129}Xe at a Larmor-frequency of 83 kHz showing two well resolved lines with a separation of 150 ppm, indicative of Xenon sampling only methanol environments in a halfconcentrated methanolic LiCl solution.

identical to the results obtained for a pyrazine sample. The chemical shift difference between free Xenon line (131.2 Hz) and Xenon in solution (143.9 Hz) is 153 ppm, which is indicative of Xenon in solution predominantly sampling methanol environments. It is likely that the dissolved xenon signal mainly results from evaporation of xenon from its high density liquid phase in the bottom layer of the sample requiring Xenon to pass through the solution. Repetition of the SPINOE procedure after current and pulse readjustment to Lithium did not yield an observable ^{6}Li signal, consistent with the observation that the chemical shift seems largely unaffected by the presence of LiCl in the sample. The SNR without thermal prepolarization at 2 T or successful SPINOE is insufficient, hence no signal could be detected. Decreasing the Lithium concentration seemed to increase Xenon solubility, as a line for xenon in solution could be more easily obtained, but Lithium remained inobservable.

[32]The spectrum shows a single line is not very interesting.

In order to gain more information a number of different compounds have been subjected to the same procedure as Lithiumchloride. Lithiumcations are among the smallest cations with respect to their ionic radii[17]- it is a hard ion in terms of the definitions made by the hard soft acid base (HSAB) principle, which allows to make non-quantitative predictions about particle interactions. Xenon, on the other hand, is an atom that could be considered soft[33]. Its main interaction mechanism with other particles are van der Waals type interactions and correlation times and internuclear distances with larger particles with lower point charge density might be more favorable experimental conditions. Obviously solubility and availability of pure samples, as well as natural abundance of the NMR active isotope, remain important factors and the following compounds were investigated in methanol-d4 as solvent CsF, Cs_2CO_3, K_2CO_3, $K_2\ ^{13}CO_3$, LiCl. Changing concentrations, Xenon exposure time and pressure did not result in an observable SPINOE effect irrespective of the sample. Hyperpolarizing inorganic salts in solution by SPINOE thus constitutes an experimental challenge. The naive assumption that a high enough Xenon and target nucleus number in a given volume should result in an observable SPINOE effect had to be reevaluated in the context of the implications gathered from experimental evidence. The signal enhancement obtained in an experiment seems to be dependent on several other parameters only indirectly accounted for by the SPINOE equations. Thermodynamic and chemical properties of the system evidently play an important role and the correlation time τ_C does not offer a means of optimization for an experiment[34]. Inspecting the problem on a molecular scale does, however, allow for some more insight and even without explicit quantitative analysis several general statements relating to the problem can me made. One thing is immediately evident: Xenon in a solution of a salt is at least a quaternary mixture of anions, cations, solvent, and Xenon. It is known that dissolution processes generally require the free Gibbs energy of hydration to exceed the lattice energy of the salt at the given thermodynamic temperature. Dissolution involves formation of a ligand shell around both ions and the complex ions may have one or several layers of coordinated solvent molecules. Xenon in solution will also have a coordination sphere, but van-der-Waals type interactions usually have small interaction energies the hydration sphere should be considered less stable. As a result of coordination the intermolecular distance r_i, one of the most important parameters, is larger than the sum of ion and xenon radius. The true value of r_i is evidently related to the interaction energy between Xenon and ion, ion and solvent and Xenon and solvent. If Xenon acts as a polarization source a good solubility in the quaternary mixture is required. A low solvent viscosity should be desirable, as viscosity indirectly accounts for solvent-solvent interactions. The solvent used should have a lower melting point than Xenon at 5 bars pressure, because it does not seem reasonable to evaporate the polarization source before it can contact the sample. Finally, xenon is mainly subject to van-der Waals type interactions so an "unpolar salt" should allow to observe a SPINOE effect.

2.2.5 Ion SPINOE and strongly coupled systems

Spectra presented in this section are strongly coupled and it shall be briefly elaborated on strong coupling to avoid confusion about appearance of the spectra. Historically there have been several reasons why NMR spectroscopy at low magnetic fields seemed unreasonable. Firstly, the chemical shift of a group i is $\delta_i \propto \gamma B_0$, that is its value in Hz is proportional to the magnetic field. Secondly, the SNR is better for higher polarization levels that once again scale with the field.

Another very important reason is often not considered further, as it is unique to magnetic fields in the μG-G regime. NMR spectroscopy has been carried out in high magnetic fields, because of the high complexity of spectra in the strong coupling limit present at aforementioned low magnetic fields, where neither the Zeemann-interaction nor the J-coupling can be treated as dominant interaction in terms of a perturbation calculation. The strong coupling limit is entered when $1 < |\nu_I - \nu_S|/J_{IS} < 100$, that is the difference of precession frequencies of two types of nuclei becomes similar to their heteronuclear coupling. Stated differently, the interaction with an external factor (the magnetic field) and the internal interaction (the J-coupling) become equally important.

Restricting the discussion to spin 1/2 nuclei, the spectral pattern identifying a nucleus of a given type in

[33] although the HSAB principle does not account for noble gases

[34] Apart from decreasing the temperature to increase the correlation time.

high magnetic fields is usually either a line or a fully symmetric multiplet of lines separated by the J-coupling constant when coupling partners are present. Intensity ratios of multiplets are defined by Pascals triangle and multiplicities given by $(1+p)$, where p is the number of coupling partners. For one nucleus with spin 1/2 coupled to two spin 1/2 nuclei (with a different chemical shift) a triplet with relative line intensities 1:2:1 is the result. The lines with intensity 1 are found at the highest and lowest frequency of the triplet and correspond to the $|\alpha\alpha\rangle$ and $|\beta\beta\rangle$ states, whereas the $|\alpha\beta\rangle$ and $|\beta\alpha\rangle$ states are degenerate in high fields and thus give rise to a line with intensity 2, as there are two states. This makes evaluation of spectra and peak assignment straightforward, at least for small molecules[35].

The degeneracy of states is lifted in the strong coupling regime and, given the necessary resolution, every transition between spin states is identified by its own characteristic frequency[5]. In high fields the spectrum of a general group denoted by SI_N, for example a methylene group $^{13}CH_2$ with $N = 2$, would be a doublet spaced by the heteronuclear coupling constant $^1J_{CH}$, typically around 100 Hz. In low magnetic fields the SI_N group can be identified by each of the two lines of the doublet splitting into K-lines, where K is a natural number given by

$$K = \sum_{n=1,\ n\in U}^{N} 2(N-n)\frac{1}{2} + 1 = \sum_{n=1,\ n\in U}^{N} N - n + 1. \quad (2.5)$$

In this expression U is a set of odd numbers, n is a natural number and N is the number of equivalent nuclei per group. The meaning of this expression will become clearer in the following. It should, however, be noted that an inorganic molecule, like PF_6, is considered one group with $N = 6$ and there doesn't necessarily have to be another molecular group.

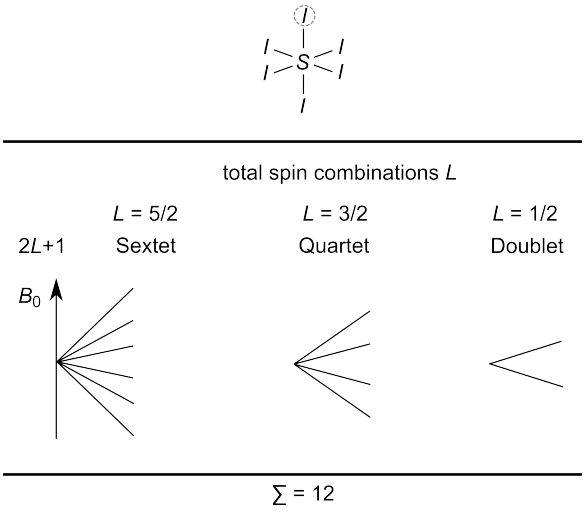

Figure 2.22: Top: The compound SI_N with $N = 6$. Both I and S are spin 1/2 nuclei. One spin I is arbitrarily chosen as the observed spin (dotted circle). Bottom: Other spins may combine to several different total spins L with $2L+1$ levels. The number of lines maximally observed for this group is the sum from Eq. (2.5).

The spectra presented in the following may be understood in terms of a vector model (see Fig. 2.22). If out of the N spins one spin is said to be observed there will be $N-1$ unobserved spins. These unobserved spins, with magnetic moment μ, may combine theirs spins as defined by the summation of like vectors to $L = (N-1)(1/2)$; $(N-3)(1/2)$...., where the first term accounts for the observed nucleus and the second for two like spins with antiparallel alignment. The limit will evidently be $L = 0$ for odd N or $L = 1$ for even N, as one spin is chosen as the observed one and one spin will always remain uncompensated for an even number of nuclei.

Each of the spin combinations with total spin L will have $2L + 1$ allowed orientation with respect to the magnetic field. The odd number n always contains the one observed spin, where two more like spins are required for vector summation yielding zero. As any odd number plus any even number is odd it must be $n \in U$. The total spin L may be identified to be $L = (N-n)(1/2)$ and results in the sum over all odd n from Eq. (2.5). In weak magnetic fields these levels are not spaced equally[5, 4] and as a result each transition has its own characteristic frequency, as transverse components for all allowed L cannot be neglected.

The strong coupling limit is typically connected with very low magnetic fields, as a spin system is strongly coupled when the frequency difference between two nuclei of different gyromagnetic ratios becomes close to the J-coupling. This is completely correct for hydrocarbon samples with ^1H homonuclear J-couplings ranging

[35] Actually free rotation of the groups is required. And the ratio of chemical shift difference of the groups to the J-coupling needs to be larger than 10, otherwise the roof-effect influences spectral appearance. For simplicities sake, and as it is the scenario encountered in most instances if proton Larmor-frequencies are sufficiently high, the text has been restricted to the facts important to understand the argument historically made for favoring high fields.

from 0-20 Hz and heteronuclear ^{1}H ^{13}C couplings of roughly 100 Hz, but the J-coupling constant is strongly dependent on the nuclei and the number of bonds between the coupled nuclei and the J-coupling becomes larger with increasing atomic number of one (or both) of the partners, given that they have a nuclear spin. As a result very large J-coupling constants are observed mainly in inorganic compounds, e.g. $^{31}P^{19}F_3$ has a J-coupling of more than 1000 Hz. Hence strongly coupled spin systems exist not only at magnetic field strengths of several μG- the typical range for hydrocarbons- but also at higher magnetic field strengths. Additionally, organic compounds ($S = {}^{13}$C) never allow for $N > 4$ as a result of the octet rule, that is carbon may only have a maximum of eight electrons in its valence.

It is noteworthy, that the vector model presented in ref. [5] is insufficient to account for all spectral features observable in extremely low magnetic fields (μG -mG for hydrocarbons). An extension of the theory included multiple quantum transitions and predicts a maximum for the number of lines observable for a strongly coupled spin system. The maximum is reached at $(N+1)^2$ lines that should be observable in a spectrum[4]. Although this has been experimentally demonstrated for hydrocarbons[41], both the existence of strongly coupled spin systems at elevated fields and the line number for compounds not restricted by the octet rule has not been investigated so far. The SNR obtained in the experiments using either thermal prepolarization of samples at 2 T or SPINOE was, however, insufficient to resolve the full number of lines and the situation depicted in Fig. 2.22, where 12 lines are expected, is sufficient to account for all observed spectral features at a ^{19}F resonance frequency of 83 kHz (20 G).

Locating a suitable test compound turned out to be less easy than expected, as toxicity, solubility, reactivity, natural abundance of NMR active isotopes and low sensitivity as a result of small γ are problematic factors prone to occur in inorganic compounds. The above mentioned PF_3, as well as PF_5, for example, are highly reactive and may not be stored in glass vessels as it reacts with the glass walls to form SiF_4 and phosphorous oxides. Most metallic compounds have a rather low γ and ligands may not be considered firmly attached to the metal center. A suitable compound was finally found in the hexafluorophosphate anion $[^{31}P^{19}F_6]^-$, where a J-coupling of 700 Hz, 100% natural abundance and stability under neutral conditions enable the planned experiments.[36] As a result of the large J-coupling of 712 Hz the intensities of line patterns are already influenced by the filter bandwidth. Figure 2.23 a) shows the full range of the spectrum with negative and positive frequency axis[37]. Note that the intensities of high frequency lines are affected by the filter bandwidth. The frequency separation between the centers of the groups, the high negative frequency peak and the low frequency positive peak (or vice versa) is the heteronuclear J-coupling. In the following the reflection will be used and the J-coupling is thus the sum, not the difference, between the peaks (no splitting due to strong coupling), or peak group centers (splitting due to strong coupling), respectively (vide infra). Figure 2.23 b) shows the magnification of one peak group, where a dip exceeding the noise level is clearly visible. Spectra obtained at lower Larmor-frequencies of 166 and 83 kHz will have pronounced line splittings into distinct groups.

Ionic solutions of high concentration often result in a residual offset in the FID. At higher frequencies (500 kHz) this offset can be described by a first order exponential decay and removed by fitting an exponential to the FID followed by correction according to the fit function[38]. Following the general procedure outlined above samples containing PF_6^- were investigated. It is sometimes considered a lipophilic ion because the salts are often soluble in organic solvents without decomposition. Different cations have been investigated, but the best spectra were obtained with saturated KPF_6 solutions. Executing the SPINOE procedure with the KPF_6 sample in methanol-d4 did not yield any observable effect with respect to SPINOE polarization of ^{19}F irrespective of the concentration of the hexafluorophosphate anion in solution.

As ions, concentrations, xenon exposure times, pressure and flow rates had been changed the only remaining parameter is solvent interaction. Solvent interactions have to expected to play a significant role for any process in condensed phase reactions, as they usually account for a major part of the system composition, be it in an NMR experiment or chemical synthesis. Locating suitable solvent for SPINOE experiments requires to consider

[36] This might seem like a trivial task but its not as straightforward as one might expect. There is always some kind of problem.
[37] This is a result of the detection method used in the NMR spectrometer. Waiving quadrature detection has its disadvantages.
[38] Consistent with a residual charge in a capacitor. At low frequencies, with correspondingly softer pulses, a linear correction is sufficient.

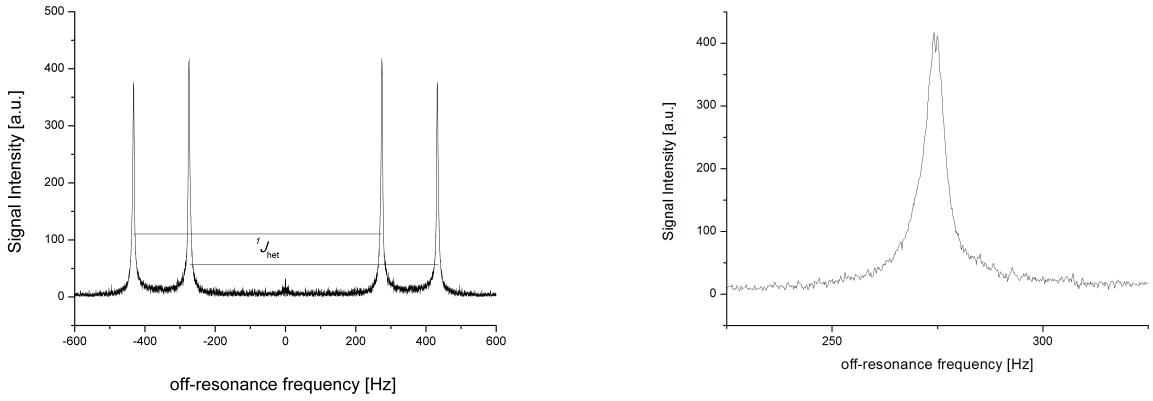

Figure 2.23: a) positive and negative axis of the ^{19}F spectrum of a saturated KPF_6 solution. Different line intensities are a result of filter bandwidth. Due to single channel signal detection and the large value of the heteronuclear J-coupling constant of over 700 Hz one line is reflected to the positive, or negative, half axis. b) One peak group magnified shows line splitting at 500 kHz ^{19}F frequency.

several properties of the solvent. Firstly the melting point of the solvent should be below the melting point of Xenon at the internal pressure of the system. Second, the solvent viscosity and surface tension should be low to allow for rapid diffusion of the xenon into the liquid phase. Third, and most importantly, the solvent molecules should have low correlation times with the ions. The last requirement ensures that the ion will have an empty coordination site allowing for interaction with Xenon, thus reducing the nucleus nucleus distance r_i. Among the commercially available NMR solvents acetone-d6 has a very low viscosity ($\eta = 0.36$) and its melting point is well below the melting point of Xenon at pressures from 3-5 bar. It is thus another solvent suitable to explore Ion-SPINOE. A solution of 53,4 mg (0.3 mmol) KPF_6 in 400 μL acetone-d6 was subjected to the same procedure as the methanol solutions. The spectra at 166 kHz and 83 kHz are shown in Figs. 2.24 and 2.25.

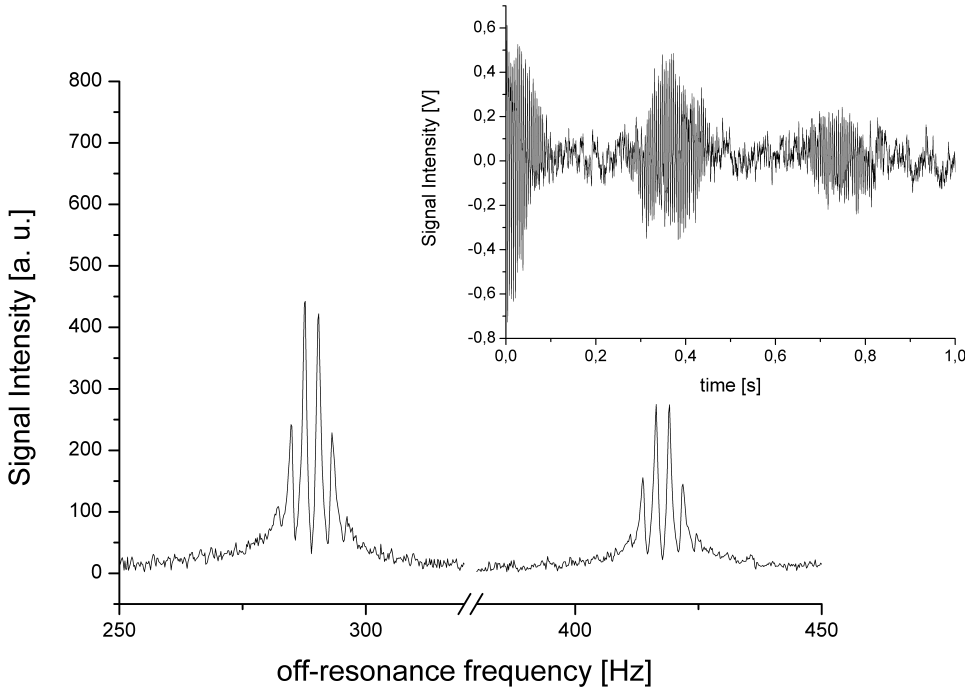

Figure 2.24: FID (inset) and spectrum of the ^{19}F at 166 kHz. The sample is KPF_6 in acetone-d6 prepolarized at 2 T. Note that the doublet shown in Fig. 2.23 b) has split into 6 lines.

At 166 kHz ^{19}F Larmor frequency the spectral complexity increases significantly over the spectrum of the

same sample at 500 kHz. Each peak is now split into a well resolved sextet, as for one observed and five identical spin 1/2 particles the spin S of the ensemble is $L = 5/2$ and line multiplicity is given by $2L + 1$.

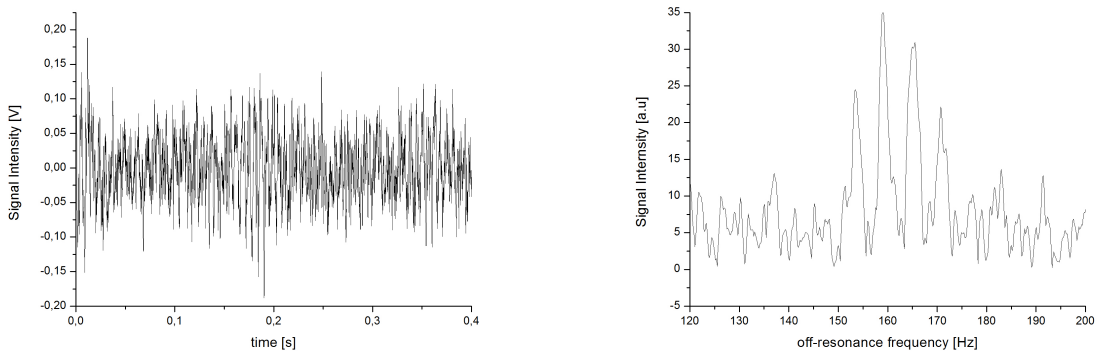

(a) (b)

Figure 2.25: a) FID and b) spectrum of the ^{19}F SPINOE. The sample is KPF_6 in acetone-d6, the resonance frequency 83 kHz. Due to poor SNR only 4 lines could be resolved.

The SNR at 83 kHz was unfortunately too low to observe further splitting using SPINOE. Attempting an averaging procedure over 16 scans did not yield sufficient improvement to resolve any further fine structure. Attempts to observe further line splitting at lower resonance frequencies up to the predicted maximum of of $(N+1)^2$ lines were hence not successful so far. The experimental setup is currently being optimized to allow for better SNR at lower frequencies. With respect to enhancements observed for SPINOE, great care needs to be taken, because the procedure involves storage of the sample at a field of 1 T. It must be taken care whether the observed enhancement is simply a result of thermal prepolarization at 1 T, as the sensitivity of the experimental setup is high enough to observe even non-prepolarized samples given a high enough spin density. In order to rule out that observed enhancements were wrongly attributed to interaction with hyperpolarized Xenon a direct comparison of SPINOE at 500 kHz and a sample of the same composition thermally prepolarized at 1 T was performed to rule out that the observed polarization is wrongly attributed to SPINOE. It is important to note here that SPINOE samples cannot be assumed to have reached thermal equilibrium with the room. The sample was thus briefly cooled with liquid nitrogen and melted inside the 1 T magnet to confirm that the observed SPINOE is indeed a real effect and not a result of decreased spin-temperature and thermal prepolarization. It is

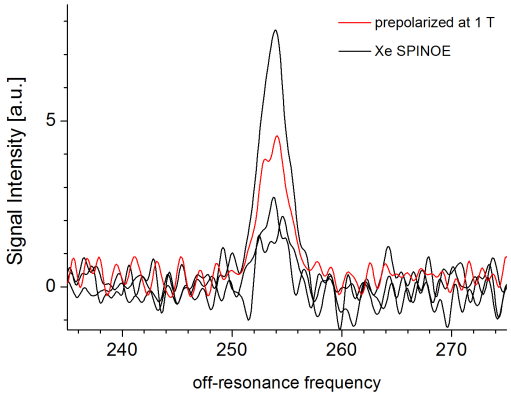

Figure 2.26: Comparison of several ^{19}F SPINOE experiments performed in succession with a repetition time of 20 seconds (black lines) and thermal prepolarization at 1 T (red line) at a resonance frequency of 500 kHz. Note that the first SPINOE experiment yields a higher signal intensity than the reference experiment with thermal prepolarization.

reassuring that SPINOE-enhancement remains observable in an experiment involving accumulation of Xenon,

waiting for a time exceeding 5 T_1 for ^{19}F, shaking liquid Xenon into solution and transferring the sample to the homogeneous volume of the magnet. The experiments performed in this section constitute successful proof of principle experiments demonstrating the feasibility of SPINOE with ionic targets. The experiments performed in this section show how important the choices made for the composition of a system are with respect to successful hyperpolarization. Although the physical aspects of SPINOE are theoretically well investigated and allow for quantitative calculations this statement does not hold for investigations regarding the applicability of hyperpolarized Xenon and the future potential the methodology bears. An interesting perspective involves use of hyperpolarized Xenon as a solvent for photochemically induced chemical reactions or processes requiring very low energies of activation e.g the dimerization of cyclopentadiene. The suitability of liquid xenon as a solvent for several organic molecules constitutes an interesting perspective and has been sucessfully demonstrated by Rentzepis and Douglass[55]. Furthermore the gas mixtures used in the experiments use naturally abundant Xenon with only 26% natural abundance and greater SPINOE efficiency will result from using isotopically enriched Xenon. The effect of isotopomers in chemical processes is usually small, as chemistry is dominated by electronic effects rather than nuclear mass[39].

[39]with the exception of hydrogen bonding, where effects are rather significant as the mass difference hydrogen/deuterium is roughly a factor two.

2.3 Para Hydrogen Induced Polarization

2.3.1 Introductory remarks

Parahydrogen Induced Polarization was a new research topic for our group at the early stages of this thesis. As the PHIP process is a rather involved application of homogeneous phase catalysis in NMR it was important to develop an understanding of the parameters influencing the signal enhancement. As laid out in the introduction PHIP requires careful consideration of the purely synthetic aspect involved in the hyperpolarization process. With respect to hydrogenative PHIP it is evident that the hydrogenation process, the addition of singlet state hydrogen to a molecule, is responsible for the *selective* hyperpolarization of hydrogenation product nuclei and in some instances catalyst ligands. The polarization of substrate molecules is defined by the Boltzmann limit thus rendering minute quantities of educt inobservable in low magnetic fields of several Gauss due to insufficient SNR. For a homogeneous phase hydrogenation reaction in presence of a catalyst it is evident that one molecule of catalyst will be required to either sequentially or simultaneously collide with at least one molecule of substrate and one molecule of hydrogen in order for a hydrogenation reaction to proceed. In a zeroth order model one would thus expect the PHIP signal enhancement to increase with the catalyst amount of substance. Due to the difficulties involved in a thorough investigation of a catalytic process the investigation was restricted to evaluating the NMR signal intensity at different catalyst amounts of substance. In order to clarify other limiting factors for reaction rates the molar fraction of dissolved hydrogen in the solvents acetone-d6 and methanol-d4 as a function of hydrogen pressure is an interesting quantity. The molar fraction χ_i of a component is defined as

$$\chi_i = \frac{n_i}{\sum_{j=1}^{m} n_j} \tag{2.6}$$

and the data in ref. [12] shows that hydrogen solubility is linearly dependent on the pressure. For pressures in [bar] the solubility of hydrogen in acetone at a temperature of 298.15 K is defined by

$$\chi_{H_2}(p_{H_2})_T = 2.8 \cdot 10^{-4} p_{H_2} = a p_{H_2}, \tag{2.7}$$

where at a hydrogen pressure of zero bar there will be obviously be no dissolved hydrogen. In analogy, the data from ref. [16] allows to obtain

$$\chi_{H_2}(p_{H_2})_T = 1.5 \cdot 10^{-4} p_{H_2} \tag{2.8}$$

for the solubility in methanol at a temperature of 291.2 K. If the amount of substance of hydrogen is neglected, meaning $n_1 + n_2 = n_2$, an approximation justifiable at low hydrogen pressures because of the small slopes in Eqs. (2.7, 2.8), the molar amount of dissolved hydrogen at a given pressure can be calculated by

$$n_{H2} = \frac{a\, p_{H_2} n_{Solvent}}{1 - a\, p_{H_2}} \tag{2.9}$$

where a is the slope of Eqs. (2.7) or (2.8), respectively, depending on the solvent. This means that for constant solvent volume the concentration of hydrogen in solution has is a function linear in the pressure. As a result of the law of mass action the rate constant of hydrogenation reactions must be expected to show a linear dependency on the pressure[40].

In order to obtain maximum SNR in a PHIP experiment an optimization experiment was conducted. To this end samples with different catalyst amounts were prepared.

Signal enhancements and spectral appearance are strongly influenced by the exact choice of the development field, that is the field used in a simulation for the time development of the density matrix to the equilibrium density matrix that is experimentally observed. It is the common scenario in every PHIP experiment to have not only ALTADENA or PASADENA but a mixture of both, as not all substrate will instantaneously react to

[40] If catalyst concentrations are much lower than substrate and hydrogen concentration. Under these conditions a pseudo-zeroth order kinetics is observed.

the product and not all dissolved hydrogen, or hydrogen in the gas phase, is instantaneously depleted.

Several factors influence the observed enhancement. These include amplifier settings, resonance frequency, substrate amount, hydrogen pressure, sample temperature, solvent and catalyst purity, which are hardware or procedural details and can be controlled with ease. Potential error sources are differences in transfer time from the development field to the magnet, and the exact field in which the ALTADENA part of the experiment was performed[41]

The ^{1}H NMR experiments were conducted at a resonance frequency of 500 kHz using 20 μL of phenylacetylene (Sigma-Aldrich) in 340 μL of freshly opened anhydrous acetone-d6 and commercially available Bis(diphenylphosphino)butane](1,5-cycloocta-diene)rhodium(I)tetrafluoroborate) (Sigma-Aldrich). Figure 2.27 shows the SNR in sucessive experiments and the averaged SNR for different catalyst concentrations for identical amplifier settings and an identical probe. The rms noise voltage level is 17-22 mV.

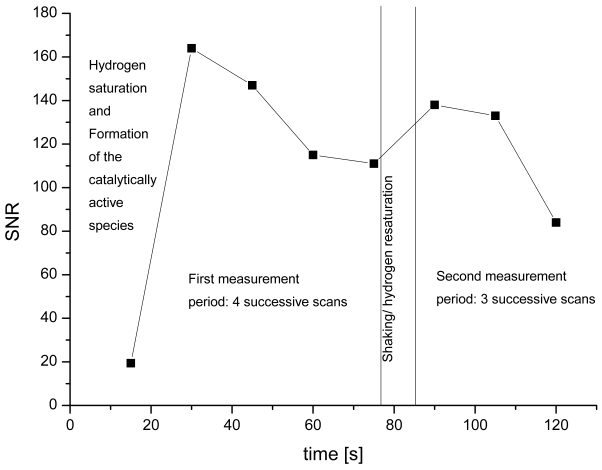

Figure 2.27: NMR signal intensity in terms of a Signal-to-Noise ratio in an addition PHIP experiment with a very low amount of catalyst (0.3 mg). Initially low SNR can be attributed to hydrogen saturation period and the catalyst activation step (exchange of COD). Maximum SNR is observed for the initial scan of the experiment (low substrate depletion). Four measurements were performed in the first shake-measure period. Removing the sample from the magnet, shaking and transfer to the homogeneous volume leads to an increase in SNR.

Figure 2.27 shows that the obtained signal intensity is, as expected, not independent of the available hydrogen in solution. The exemplary curve shown for a low catalyst amount of 0.3 mg shows that the PHIP signal intensity is very dynamic. Initially a sample is supplied with a given pressure of para-hydrogen leading to an exchange of COD against a substrate or solvent molecule - not all catalyst is available for hydrogenation of the substrate. Due to the rather large internal diameter of sample tubes shaking the sample actually has a pronounced effect[42]. After saturation of the solution with hydrogen the SNR is high, the reaction is not diffusion limited. Several experiments performed in succession, four per shake-measure cycle in the example in Fig. 2.27, show that the SNR immediately after saturation of the solution with hydrogen is comparably high. For higher catalyst amounts the higher number of hydrogenations per time, given by the molar amount of substance times the turn over number of a catalyst[43], makes it more difficult to observe oscillation of the signal intensity due to faster depletion of hydrogen in solution. An average of the SNR at different catalyst amounts (0.3, 0.6 2.0 mg) over two shake-measure cycles with an equal number of point does, however, allow to state that the SNR is a function of the catalyst amount and thus the number of conversions (chemical reactions). The average SNR is 135 (0.3 mg), 158 (0.6 mg) and 209 (2.0 mg), with a maximum SNR of 164, 219 and 245 at the respective

[41] Every experiment was conducted by shaking the sample outside the magnet at the 5 G stray field line for 15 s. Shuttling to the magnet takes 2-3 s. Shuttling out of the magnet and resupply with hydrogen take 20 s.

[42] High field samples tubes with their small diameters often make it difficult to get hydrogen in solution, as the surface tension of the liquid often makes it difficult to saturate solution in a short time.

[43] The turn over number, of turn over frequency, is a measure of catalyst efficiency in a chemical synthesis. It defines how many reactions are preformed on one molecule of catalyst per second.

catalyst amounts, which means both average and maximum signal-to-noise ratio scale with the catalyst amount and hydrogen availability.

It is noteworthy, that a linear dependency of the NMR signal on the hydrogen pressure over a wide range of substrate concentrations is a phenomenon already observed in conjunction with SABRE type experiments[22]. SABRE experiments have the advantage that no substrate depletion occurs thus eliminating the dependency of the NMR signal on the amount of substance available at a given time.

No claim to a thorough investigation of addition PHIP signal intensity with respect to chemical kinetics can or will be made based on these results. However, due to the observed dependency of the NMR signal on the catalyst concentration and hydrogen availability it is not prudent to calculate an enhancement factor directly from comparison of a thermally polarized sample and a PHIP spectrum.

The reasoning is as follows. The occurrence of the term $V_s N_s$ in the Signal-to-Noise equations, which is equivalent to nx, where n is the molar amount of substance and x the natural abundance of the NMR active nucleus, shows that the NMR signal is directly proportional to the number of nuclei. Without knowledge of the number of hydrogenated molecules present in the sample at a given time, that is thorough knowledge of kinetics, the spin density is unknown. The molar amount of substrate in the sample is not suitable as a basis for comparison, as experimental evidence shows that it is applicable to perform several PHIP experiments with nearly identical signal intensity using one sample (the measurements taken immediately after shaking in Fig. 2.27). This is equivalent to stating that $\mathrm{d}c/\mathrm{d}t = const.$, as expected from a process with a zeroth order kinetics, and to stating that only a fraction $\Delta n < n_0$ of the molar amount of substance can be held responsible for the observed increase in signal intensity. A true enhancement factor would require knowledge of this fraction of molecules and an experiment with thermal polarization with only this molar amount of substance n in the sample.

However, an additional problem arises making a disentanglement of all factors difficult. Experimental observations in conjunction with SABRE and PHIP type experiments show [7, 15] that polarization does not spread *evenly* over all nuclei in a molecule. Furthermore, similar to the definition made by the Solomon-equation in conjunction with SPINOE, the hyperpolarized molecules present in sample will be subject to T_1-relaxation until the thermodynamic equilibrium defined by the magentic field strength is reached. But, as the hydrogenation reaction will continue until the educt and product concentrations defined by the law of mass action are reached, not all product molecules in the sample are in the same quantum state. As a result, an enhancement factor in PHIP is a characteristic number for one specific way to perform an experiment - if any parameter changes the enhancement will be different.

2.3.2 Experimental verification of the heteronuclear three spin density matrix

It is of special interest to determine the exact form of the symmetry breaking process in terms of a density matrix description. Especially interesting is the density matrix for systems of the type $I_1 I_2 S$, because the hydrogenation reaction introduces two like spins with similar resonance frequencies $I_1 I_2$ into a molecule. At least for small molecules the low natural abundance of rare spins will often times result in only one NMR active heteronucleus in vicinity to the hydrogenation site which will have a significantly different Larmor-frequency and is usually referred to as S. The $I_1 I_2 S$ system is of special significance, as it constitutes the zeroth order model for all heteronuclear PHIP effects.

A catalyst/substrate system with a high product specificity is necessary to avoid unwanted complexity for mathematical modeling. Secondly, one needs to consider what makes hydrogen positions nonequivalent and the parameters used in NMR to express this inequality. As noted above the chemical shift is a measure of the interaction strength of a nucleus in a given environment with the external magnetic field, hence different chemical shifts of the chemically added hydrogen nuclei in the product constitute a symmetry breaking pathway. This can be understood as an extrinsic interaction parameter. The value of the chemical shift (in Hz) is proportional to the external field strength, hence at low field strengths of several mT a rather large chemical shift is required to have an appreciable effect. J-coupling may act as a symmetry breaking pathway if the chemically added hydrogen

nuclei formerly in the para-state couple with a different value of J to an existing third nucleus, which may be a heteronucleus or a third hydrogen. This effect was first observed for hydrogenation of acetylenedicarboxylic dimethyl ester to maleic acid dimethyl ester[6]. The J-coupling is an intrinsic parameter, independent of the field while depending on the molecular structure, meaning the sequence, type and orientation of nuclei.
The performance characteristics of the experimental setup are known from the preceding section and define boundaries which frequency differences are distinguishable[44]. However, as sample positions after field cycling, currents on all coils/ shimm quality and linewidths were not expected to be perfectly reproducible between the experiments the test compound should allow for a certain margin of error.[45] Empirical data, which may be taken from the literature [20] shows certain tendencies how chemical shifts may be manipulated. If we have the sequence $^{29}Si{-}C{-}^{1}H$ in a molecule, the hydrogen atom will have a small chemical shift, typically 0-1 ppm. Tetramethylsilane $Si(CH_3)_4$ is the standard added to most NMR solvents and is the reference for a 1 H chemical shift of 0 ppm. It is convenient that most of naturally abundant Silicium is ^{28}Si(95.3 %) which does not have a nuclear spin, thus not introducing NMR active heteronuclei, or S spins, in most molecules. On the other hand the vicinity of electronegative substituents, such as oxygen, will increase the chemical shift of protons, while homonuclear coupling constants over heteronuclei is often not observable because of rapid rotation around single bonds occurring at room temperature. In order to obtain a largely undisturbed two-spin system I_1I_2 the most straightforward approach is selective hydrogenation of a triple to a double bond. An aliphatic chain sequence of the form $R_1R_2R_3Si{-}H_1C{=}CH_2{-}O{-}R_4$ is thus expected to result in a rather large chemical shift difference between the hydrogen positions while at the same time the heteronuclei (Si, O) render all homonuclear J-couplings other than between the chemically added pair inobservably small. Thereby all undesired symmetry breaking pathways, except for the desirable heteronuclear coupling with naturally abundant ^{13}C (1%) and ^{29}Si (4.7 %), are eliminated. The undefined groups R_1 - R_4 need to constitute inert rests under the hydrogenation conditions. The meaning of inert in this context is that undesirable effects such as catalyst deactivation, fragmentation or chemical reaction under reduction conditions, oxidation, steric effect leading to low reactivity and thus low reaction rate and signal, have to be avoided. Furthermore no protic hydrogen atoms should be contained in either of the groups, as these are subject to rapid exchange in polar solvents, such as CD_3OD. Furthermore one wishes to increase the number of bonds between chemically added and present hydrogen atoms to decrease the value of the homonuclear J-coupling constants, and thereby the level of system distortion. A short chained saturated aliphatic group is very suitable and synthetically simple for R_4. Silicium, on the other hand, naturally only occurs in the form of its oxides (Silicates). While the oxidation problem is less pronounced as for phosphorus it is still prudent to use bulky substituent groups to avoid having to use an air sensitive reagent. Lastly commercial availability and affordability of reagents and a synthesis pathway requiring very few steps is desirable. Concerning the hydrogenation reaction stereoselectivity and the single/double hydrogenation problem need to be considered. The hydrogenation product needs to be either the E- or the Z-product, but not a mixture of both. The stereoselectivity aspect is rather easy to fulfill, as several years of catalyst development allow to simply purchase catalysts with high product specificity. Most heterogeneous catalysts will selectively form Z-products due to the nature of the adsorption process, which is necessarily single sided for both hydrogen and substrate. A similar argument holds for several catalysts with bidentate ligands, such as dppb (1,4-Bis(diphenylphosphino)butane). These ligand types have a fixed phosphorus-phosphorus distance, the chelate effect ensures a higher stabilty of the catalyst complex than monodentate ligands and thus the hydrogen substrate adduct, whose formation is the most relevant step in the hydrogenation reaction, has a given geometry defined a priori by coordination sites, or empty orbitals, available at the metal center. The following hydrogenation can thus only occur from that geometry and a specific product is obtained if the correct system and conditions (catalyst, solvent, substrate, pressure, temperature) are chosen. multiple hydrogenation to the saturated products can sometimes be avoided by catalyst poisoning. The most prominent example of a poisoned catalyst is constituted by the heterogeneous Lindlar-catalyst system ($Pd/CaCO_3$ /Quinoline/$Pb(CH_3CO_2)_2$),

[44] as the magnet homogeneity is 0.8 ppm the boundary is 0.4 ppm for uncoupled lines

[45] The magnet system uses four current sources that are each subject to individual drifts. Albeit the drifts are extremely small a homogeneity loss of 0.2 ppm is normal in 20 minutes, especially when the sample is repeatedly pulled out of the resonator, shaken and transferred back to the homogeneous volume.

which allows to obtain *Z*-alkenes from alkynes in high yields. It was thus necessary to find a catalyst which can be easily poisoned, yields a specific product, has a high turn-over frequency at room temperature and reasonable hydrogen pressures and which should be either commercially available or easy to synthesize. Furthermore poisoning should not require a synthetic step, but should be possible in-situ prior to hydrogen exposure. Based on these general considerations a system resulting in a heteronuclear *J*-coupled three spin system, while constituting a good approximation to an undisturbed two-spin system, was designed and used to elucidate the exact form of the three spin density matrix. This three spin density matrix will allow to shed some light on the empirical knowledge gained in the early years of PHIP, especially with respect to the polarization transfer to heteronuclei observed under ALTADENA conditions.

2.3.3 The model system

Based upon the above mentioned considerations 1-*tert*-butyl(diphenyl)silylethoxyethyne (**1**) was identified to be a suitable substrate. The synthesis of the model compound was carried out in analogy to [43], except that the base hexamethylphosphoric triamide (HMPA) was replaced with 1,3-Dimethyl-3,4,5,6-tetrahydro-2(1H)-pyrimidinone (DMPU) and *n*-hexane, when possible, was substituted by either cyclohexane or *n*-heptane due to safety considerations. For the synthesis *n*-butyllithium solution (0.70 mL, 2.50 mol/L in n-hexane, 1.75 mmol, 1.05 equiv.) was added dropwise and under constant stirring to a solution of ethoxyacetylene (40 wt% in hexanes, 0.40 mL, 1,67 mmol, 1 equiv.) in anhydrous THF (5 mL) at 0 ° C over a period of 10 min under inert conditions. After stirring for 1.5 h 0.25 mL DMPU (approx 1.15 equiv.) and *tert*-butyldiphenylsilylchloride (0.43 mL, 1,67 mmol, 1 Eq.) were carefully added. The cooling bath was removed and the mixture was stirred for 8 h at room temperature. The reaction mixture was poured on ice (3 g) in cyclohexane (6 mL). The organic layer was separated and the aqueous layer was extracted twice with cyclohexane (4 mL). Organic layers were combined, washed with saturated NaCl solution (4 mL), dried over$MgSO_4$, and solvents removed in vacuo. The crude product was purified by chromatography (SiO_2 (63 micrometer, Sigma Aldrich) using cyclohexane/ ethylacetate/ triethylamine 100:10:1 as eluent. The purified product was obtained as a colorless liquid of high viscosity in 89 % yield[46]

The first step of the synthesis involves using the irreversible base *n*-BuLi removing the proton of highest acidity under formation of an organometallic Lithium compound. The reaction is selective at low temperatures, at higher temperatures the proton C-H acidic proton in alpha position to the oxygen may also be abstracted resulting in a loss of specificity. Subsequent addition of *tert*-butyldiphenylsilylchloride immediately yields the

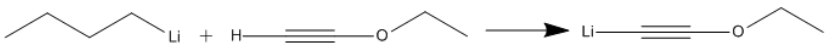

Figure 2.28

product 1-(tert-butyldiphenylsilyl)-2-(ethoxy)ethyne.

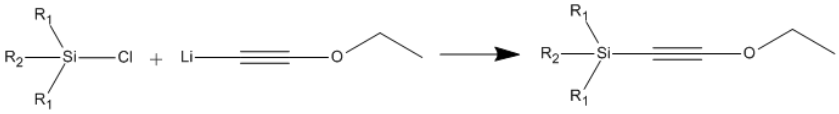

Figure 2.29: R_1 = Phenyl, R_2 = *tert*-butyl.

Analytic high field NMR data is reported as: Nucleus (Larmor frequency, solvent): chemical shift in ppm (multiplicity, number of protons, *J*-coupling). 13 C spectra were recorded as proton decoupled APT spectra hence only containing chemical shift information. ^{1}H-NMR (400 MHz, $CDCl_3$): δ: 8.09 (m, 4H), 7.58 (m, 6H),

[46] As we didn't have a chemistry laboratory at this point, i had to to this somewhere else. I would like to thank P. Schleker and J. Klankermayer for supplying laboratory space and help.

4.38 (q, 2H, J = 7.3 Hz), 1.60 (t, 3H, J = 7.3 Hz), 1.36 (s, 9H) ^{13}C-NMR (400 MHz, $CDCl_3$): 138, 136, 129.6, 128, 11, 75.6, 33, 28, 19, 14.7. The obtained NMR data is identical with [43]. The sample contained trace amounts of water as impurity (^{1}H-NMR: 1.56 ppm (s)), most likely from the use of NMR solvent not stored under inert conditions[23, 21].

The ethoxyethylene derivate resulting from the hydrogenation of 1-(tert-butyldiphenylsilyl)-2-(ethoxy)ethyne (see Fig. 2.30) constitutes a good approximation to an undisturbed two spin system. The rapid rotation of the C-O single bonds suppresses J-coupling between H_b and protons in the ethylene group. The shortest range homonuclear J-coupling available for H_a, other than the desirable $^3J_{HaHb}$ is a ^5J coupling to protons on the phenyl and *tert*-butyl moieties. These J-coupling constants are well below the resolution of the experimental setup. The molecule will be an example of either a nearly perfectly isolated homonuclear J-coupled two spin system I_1I_2 with a large chemical shift difference between I_1 and I_2 or, when containing naturally abundant heteronuclei, one of three possible isotopomers of the type I_1I_2S with S either ^{29}Si or $^{13}C_a$ or $^{13}C_b$.

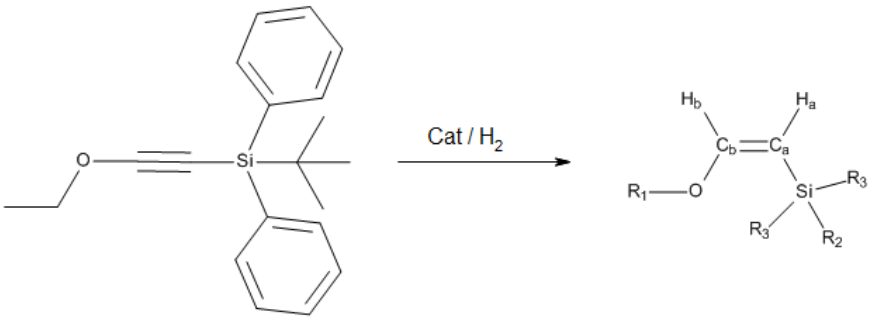

Figure 2.30: Catalytic hydrogenation of 1-(*tert*-butyldiphenylsilyl)-2-(ethoxy)ethyne to 1-(*tert*-butyldiphenylsilyl-2-(ethoxy)ethylen. The reaction product will in the following be referred to only as ethoxyethylen for convenience.

The set of J-coupling constants introduced in Fig. 2.31 along with position identifiers used in the remainder of the discussion should be sufficient to account for all experimentally observable spectral features.

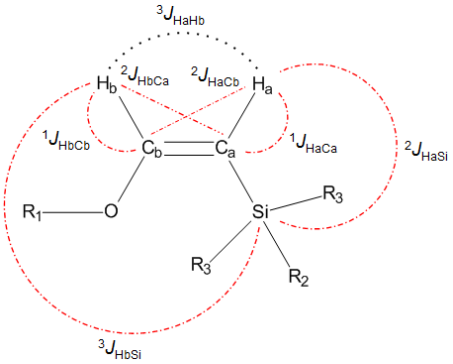

Figure 2.31: Relevant J-coupling constants and position identifiers in the reactions product.

2.3.4 Experimental procedure for ^{1}H experiments

For the reasons discussed in the introductory remarks of this section it is of essential importance to define an exact procedure for para-hydrogen experiments that is to be followed strictly in every experiment. The parahydrogen used in the following section was generated using a commercially available BPHG090 system (Fa. Bruker Biospin, 92.8 % parahydrogen enrichment, 32 K conversion temperature)[47]. Samples for PHIP experiments were obtained by preparing a solution of the homogeneous phase hydrogenation catalyst [1,4-Bis(diphenylphosphino)butane](1,5-cycloocta-diene)rhodium(I)tetrafluoroborate) in 340 μL anhydrous acetone-

[47] At this point i would like to thank Bruker Biospin for support of the generator

d6 and adding 25 μL of the ethoxyacetylene. The samples are repeatedly frozen and degased in vacuo prior to the experiment to avoid catalyst inactivation. The solution is subjected to 5 bar parahydrogen and the chemical reaction commences shortly after the parahydrogen has been supplied[48]. In order to avoid diffusion limited hydrogen supply the solution is shaken for 5 - 10 seconds to saturate with hydrogen. This shaking period is identical to the evolution period τ_{evo} of the density matrix used in the theoretical description (vide infra). As already mentioned ALTADENA and PASADENA experiments are defined by the evolution field strength. However, in low magnetic fields of several Gauss, these terms are not really applicable. For ^{1}H experiments the evolution field was the 5 Gauss stray field outside the NMR magnet. After shaking for the designated time the hydrogen flow was stopped and the sample transferred to the homogeneous field in the center of the shimmed electromagnet. The free induction decay is detected with a coil tuned to the resonance frequency after excitation with a θ-pulse. A preamplifier stage[49] amplifies the signal before a second amplification with a lock-in amplifier operating close to the Larmor-frequency. Data was recorded with a sampling rate of $1 \cdot 10^{-4}$s.

2.3.5 Field-dependent Ethoxyethylene spectra

Spectra of the ethoxyethylene were recorded at different Larmor frequencies of 666 kHz, 500 kHz, 336 kHz, 166 kHz and 83.3 kHz. As mentioned in the introductory comments, substrate depletion in an addition reaction makes every sample usable for a limited number of experiments. The hydrogenation product ethoxyethylene has four possible isotopomers, namely the two-spin system H_aH_b (93.3 %) as well as three heteronuclear three spin systems $H_aH_b^{29}Si$ (4.7%), $H_aH_b\,^{13}C_a$ (1%) and $H_aH_b\,^{13}C_b$ (1%). The J-coupling constants in the product molecule are $^3J_{H_aH_b}$ = 8.5 Hz, $^1J_{H_aC_a}$ = 140.7 Hz, $^1J_{H_bC_b}$ = 177.9 Hz, $^3J_{H_bSi}$ = 11.0 Hz, $^2J_{H_aSi}$ = -0.5 Hz and the chemical shift difference between H_a and H_b is $\delta_2 - \delta_1$ = 2.46 ppm. Given high enough signal intensities these parameters, with exception of $^2J_{H_aSi}$ = -0.5 Hz, could be encoded by the spectra.

Spectral features are most conveniently discussed by showing an exemplary spectrum of the para-hydrogen polarized ethoxyacetylen. The compound itself was designed to be a model for a two spin and a three spin system. In the syntax proposed by Pople the compound is an AB spinsystem I_1I_2 or an ABX spinsystem I_1I_2S[24, 34]. In Pople's synthax, letters close to each other in the alphabet, e.g. AB, denote strong coupling, or small $x = \delta\nu/J$ for a spin pair, and it is an advantageous property of this syntax that it intrinsically defines a value of x[24]. In the exemplary spectrum shown in Fig. 2.32 an overall of twelve lines (including the small peak at 116,76 Hz) are consistent with the four lines expected for an AB spin system (all four lines resolved) and an ABX spinsystem (all eight lines resolved), where superposition of isotopomer spectra would result in 12 lines. This spectrum exhibits an unusual amount of complexity, considering that the Larmor-frequency is only

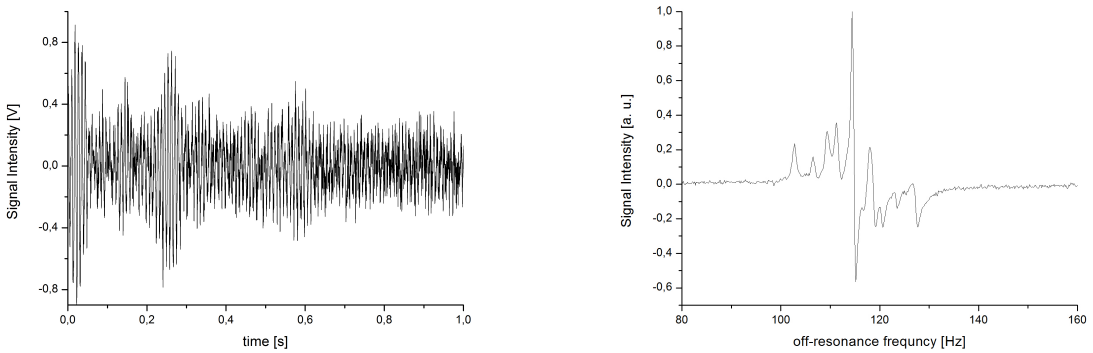

Figure 2.32: a) FID and b) ^{1}H spectrum of parahydrogen polarized ethoxyethylen at a Larmor frequency of 166 kHz with 90° pulse excitation.

[48]Once the hydrogen diffusion has happened or the solution has been saturated by shaking. Presence of cyclooctadiene at the catalyst allows to work carefully, as measurements indicate that a significant NMR signal is only obtained after 15 s.

[49]The choice of Operation Amplifiers and other elements is very important. The voltage and current noise characteristics of each chip are essential. In order to maximize SNR at given frequencies the trade off between low voltage noise and high current noise needs to be considered for every chip depending on whether a currents or voltages are high in this part of the circuitry.

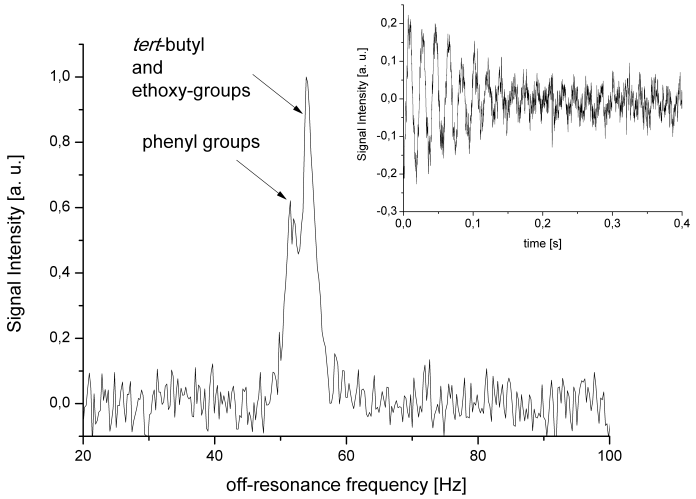

Figure 2.33: FID and ^{1}H-spectrum of 20 μL ethoxyacetylen in d6-acetone thermally prepolarized at 2 T. No fine structure arising from homonuclear J-coupling can be resolved (e.g. the ethoxy-group ($J = 7.3$ Hz)) at a ^{1}H Larmor-frequency of 500 kHz. Two broad lines result from superposition of protons in aromatic and aliphatic environments with similar chemical shifts.

166 kHz. At this Larmor frequency the chemical shift induced frequency difference between proton H_a and H_b is only 0.4 Hz. With a J-coupling of 8.48 Hz it is $x = 0.047$ and typically, that is with thermally polarized spin systems, no fine structure arising from homonuclear J-coupling should be observable. This very fact is observed in the educt spectrum in Fig. 2.33, where thermal prepolarization at 2 T has been applied to increase the SNR.

The spectrum observed in the para-hydrogen experiment does however, exhibit an antisymmetric structure with respect to its center frequency, where the term center frequency refers to the zero transition at an off-resonance frequency of 115 Hz between the highest amplitude lines in Fig. 2.32.

The spectral complexity observed here warranted the question of how the spectrum would appear at other resonance frequencies, which could be done with relative ease by making use of the flexibility of the new experimental setup. Using the outlaid general procedure for PHIP hyperpolarization, additional spectra at resonance frequencies of 83 kHz, 334 kHz and 500 kHz were recorded. A comparison of the spectra is shown in Fig. 2.34.[50]

The comparison of the spectra at 83 kHz and higher Larmor-frequencies in Fig. 2.34 reveals, that the number of spectral lines changes with the frequency. The spectrum in the top panel, at the lowest resonance frequency and thus lowest value of $x = 0.02$, does not show characteristic lines at 141.5 and 158.5 Hz. The line separation of approximately 17 Hz, that is $2^3 J_{H_a H_b} = 2 \cdot 8.5\,\text{Hz}$, indicates that these lines are associated with the two-spin system AB, the former para-hydrogen molecule. The rationale here is the roof effect. In an AB system with a vanishing chemical shift difference the inner lines of the doublet of doublets merge, whereas the outerl lines drop in intensity until they become inobservable due to insufficient SNR. The low and high frequency peaks of such a doublet of doublets would then be spaced by $^2J_{AB}$ rather than ^1J.

[50] Note that off resonance frequencies were corrected to allow for better comparability, as it is not possible to match the off-resonance frequencies accurately in an experiment.

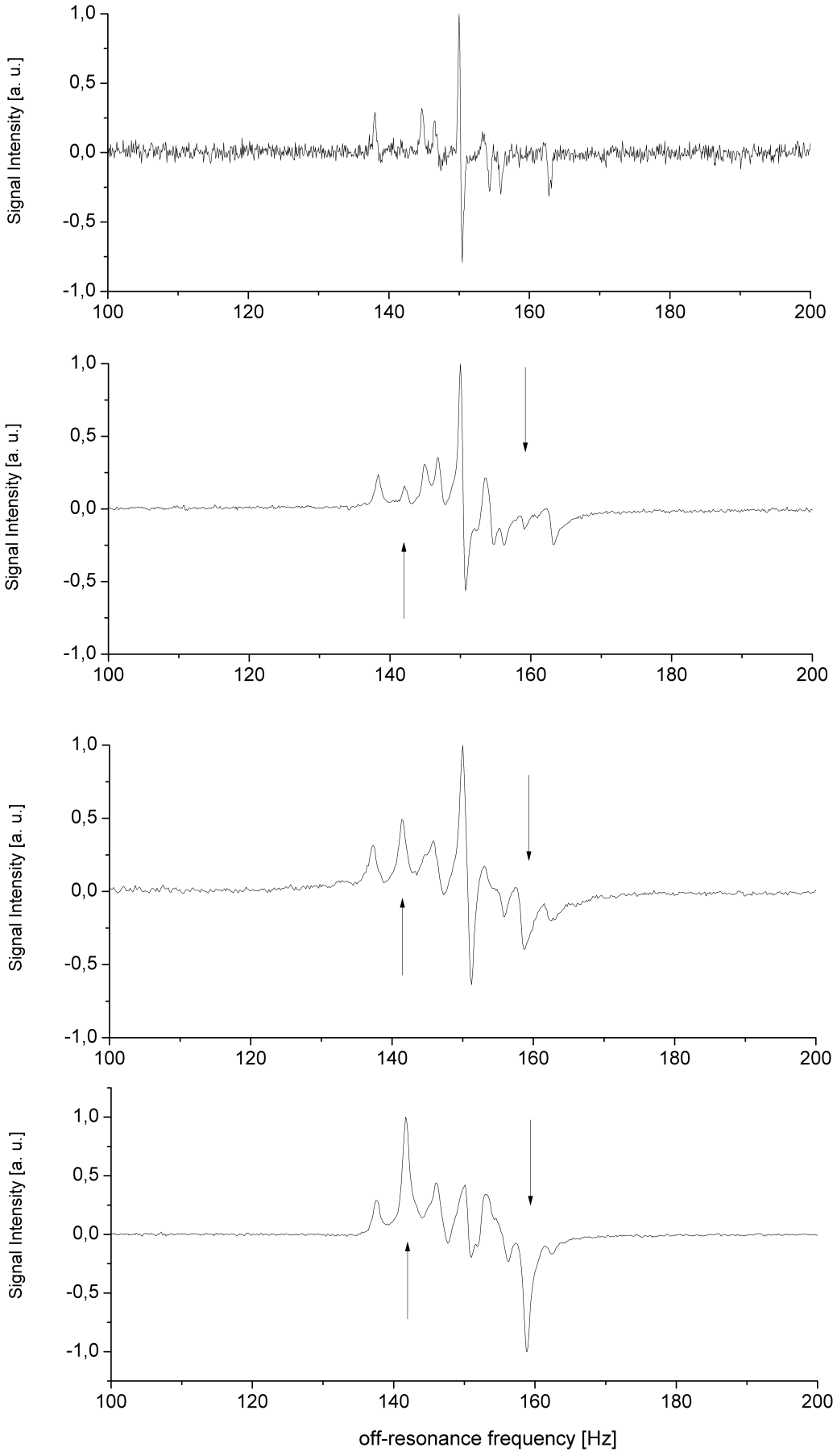

Figure 2.34: ^{1}H-spectra of parahydrogen polarized ethoxyethylen at four different resonance frequencies (top to bottom: 83.3, 166, 334, 500 Khz). Spectra have been normalized. The off-resonance of the center frequency has been set to 150 Hz. The values of $x = \delta\nu/J$ for the AB two-spin system at the resonance frequencies are $x = 0.02, 0.047, 0.094, 0.141$. Arrows denote lines associated with the two-spin system AB, the nuclei stemming from para-hydrogen.

It is noteworthy that an exact analysis of the two-spin density matrix gives rise to a non linearity in the line separation of the peaks associated with the AB-spin system shown in Fig. 2.34[15, 63]. Introducing the strict definition of the center frequency $\nu_0^\delta = \nu_0(1 + (\delta_1 + \delta_2)/2)$, that is the frequency of the central line for thermally polarized spins, allows to write the energy levels of a two spin system conveniently as

$$
\begin{aligned}
E_1 &= -h\left(\nu_0^\delta - \frac{J_{HaHb}}{4}\right)) \\
E_2 &= h\left(-\frac{1}{2}\sqrt{J_{HaHb}^2 + (\delta\nu)^2} - \frac{J_{HaHb}}{4}\right) \\
E_3 &= h\left(\frac{1}{2}\sqrt{J_{HaHb}^2 + (\delta\nu)^2} - \frac{J_{HaHb}}{4}\right) \\
E_4 &= h\left(\nu_0^\delta + \frac{J_{HaHb}}{4}\right).
\end{aligned}
\tag{2.10}
$$

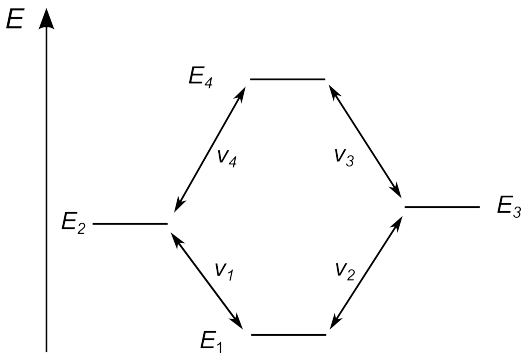

Figure 2.35: Energy levels and allowed transitions (arrows) in the two-spin system AB.

The frequencies of allowed transitions (see Fig. fig:EnergyLevelsTransitionsFreqs2sp) are given by the corresponding energy differences. It is interesting to note that, if the expression $\sqrt{J_{HaHb}^2 + (\delta\nu)^2}$ is expanded as a Taylor-series and truncated after the fourth order

$$
\begin{aligned}
\nu_1 &= \frac{E_2 - E_1}{h} = \nu_0^\delta - J_{HaHb}\left(1 + \frac{1}{4}x^2 - \frac{1}{16}x^4\right) \\
\nu_4 &= \frac{E_4 - E_2}{h} = \nu_0^\delta + J_{HaHb}\left(1 + \frac{1}{4}x^2 - \frac{1}{16}x^4\right)
\end{aligned}
\tag{2.11}
$$

the frequency separation between the peaks of the two-spin system AB $\nu_4 - \nu_1$ is not exactly $2J_{HaHb}$, as

$$
\nu_4 - \nu_1 = 2\,J_{\mathrm{HaHb}}\left(1 + \frac{1}{4}x^2 - \frac{1}{16}x^4\right) \tag{2.12}
$$

thus defining a residual non-linearity of the frequency separation. This non-linearity is difficult to prove experimentally, as the linewidth in the spectra shown in Fig. 2.34 and the vicinity of other peaks makes it difficult to define a baseline for Lorentzian-fitting. Using the values of $x = 0.02, 0.141$ at the resonance frequencies 83 and 500 kHz allows to calculate the change in frequency separation to be 0.35 Hz. This is consistent with experimental observations, where the frequency separation at a Larmor-frequency of 500 kHz is 17.1 Hz. At lower Larmor-frequencies the SNR is too limited to determine line splitting directly form experimental results with a sufficient degree of accuracy. However, there are also three different ABX systems, where X is either of, but due to the low natural abundance not all, $^{13}\mathrm{C_a}$, $^{13}\mathrm{C_b}$ or ^{29}Si. Due to the different magnitude of the ^{1}H-^{13}C and ^{1}H-^{29}Si coupling constants the spectrum must be split in three parts - low and high and intermediate frequencies- where the low and high frequency parts are associated with the $^{13}\mathrm{C_a}$ isotopomer subspectra that must be expected to be of very low intensity. The intermediate frequency region in vicinity to the center frequency must contain spectral features only associated with homonuclear J-coupling and ^{1}H-^{29}Si heteronuclear coupling.

Details for the low intensity carbon satellites are more easily accessible from spectra obtained with 45° pulse excitation. Using a different excitation pulse angle changes the pattern of carbon satellite peaks as shown in Fig. 2.36. Using this excitation pulse angle it is possible to resolve additional lines as result of the much larger C-H-couplings $^1J_{HaCa}$, $^1J_{HbCb}$. Correct coupling constants for $^3J_{HaHb}$, as well as determination of the heteronuclear coupling constant, is facilitated by the anti-phase line pattern. The spectral width of $^1J_{\mathrm{H_bC_b}} + ^3J_{\mathrm{H_aH_b}} = 186.4$ Hz leads to the observed phase behavior of the satellite peaks, where low frequency peaks are phase shifted by approximately 90° from high frequency peaks. This can be easily explained as

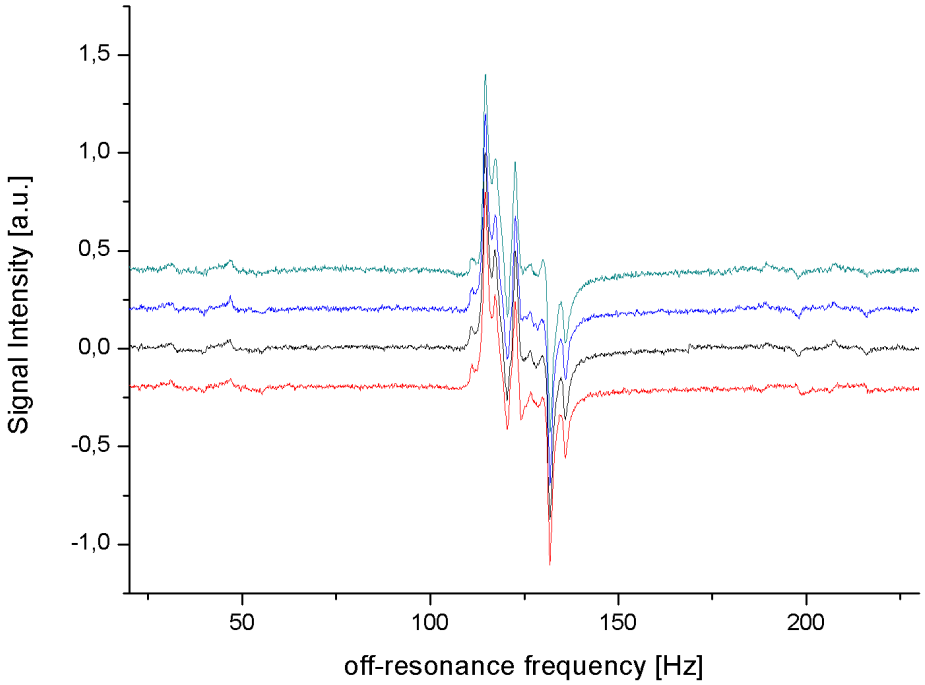

Figure 2.36: Four ^{1}H spectra of parahydrogen polarized ethoxyethylen at a Larmor-frequency of 500 kHz with 45° pulse excitation. Spectra have been corrected to obtain the same off-resonance frequency. Line positions and amplitudes are reproducible but satellite peaks have different phase.

inspection of Fig. 2.37 a) shows that the phase needs to be separated into three intervals as a function of the off-resonance frequency. In both the regime from 0-90 and 200-400 Hz the phase has a different slope. In all experiments the low frequency satellites are in the first of these three intervals and high frequency satellites were located at off-resonance frequencies over 200 Hz. The phase of the Fast Fourier Transform requires different phase corrections for the satellites regimes. The non-linearity originates from the lock-in amplifier stage and is an electronic, rather than a physical, effect.

By means of frequency dependent phase correction averaging is possible and Fig. 2.37 b) shows an average of the spectra shown in Fig. 2.36 with phase correction.[51] It should be noted that it is rather difficult to obtain perfectly phased anti-phase peaks, as anti-phase peaks with very center frequency shifts below the linewidths result look and behave similar to functions with a discontinuity with sign change at this position and spectral appearance is sensitive to even 0.1° phase shifts.

As mentioned above the chemical shift difference between H_a and H_b is $\delta_2 - \delta_1 = 2.46$ ppm. As H_a is ^1J-coupled to C_a and H_b to C_b the difference between the center frequencies of the homonuclear J-coupled doublets should correspond to the chemical shift. As expected the chemical shift can be extracted from the spectrum by means of evaluating the frequency difference between the satellites doublets of doublets center of mass.

[51] Correction works better for the high frequency regime, as the phase is more accurately described as a linear function of the frequency. The peaks are thus more clearly resolved.

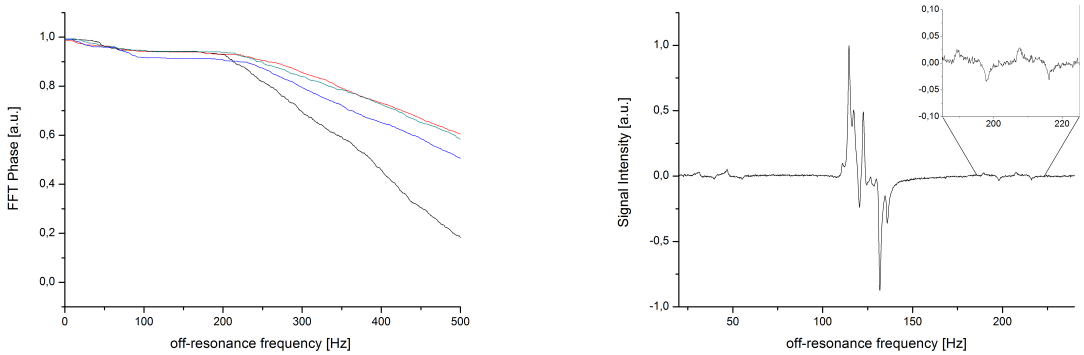

Figure 2.37: a) Fast Fourier transform phase as a function of the frequency. The kinks in the curve at 90 and 200 Hz are reproducible and require frequency dependent phase correction with three correction intervals. The FFT phase has been unwrapped, that is not given as multiples of $2/pi$, and normalized to unity. b) Average of the four spectra shown in Fig. 2.36 using the information gained from a). Two anti-phase doublets of doublets are well resolved. ${}^{3}J_{HaHb}$ and ${}^{1}J_{HaCa}$ and ${}^{1}J_{HbCb}$ can be obtained directly from the frequency separation of the satellite peaks.

2.3.6 Derivation of the three-spin density matrix

The Liouville von-Neumann equation (Eq. 1.93) describes the temporal evolution of the spin state under the influence of a constant Hamiltonian. The intrinsic Hamiltonian responsible for spin system evolution is given by the sum of chemical shift and J-coupling Hamiltonian. The explicit form for a three spin system with one heteronucleus and a sufficiently large Larmor-frequency difference between I and S spins is[15, 63, 64]

$$H_{I_1I_2S} = \hbar(\omega_{I_1}I_{1z} + \omega_{I_2}I_{2z} + \omega_S S_z) + 2\pi(J_{I_1I_2}\ I_1 \cdot I_2 + J_{I_1S}I_{1z}S_z + J_{I_2S}I_{2z}S_z). \tag{2.13}$$

The time dependent density matrix contains all spinoperators generated by action of the Hamiltonian on the initial singlet state. Non-detectable spin states - all those non-commutating with the Hamiltonian, where the time derivative thereof is undefined as a result of Eqs. (1.42) and (1.43) - are neglected the time dependent form of the density matrix is given by

$$\begin{aligned}\rho_{I_1I_2S}(t) = {} & I_{1z}I_{2z} + a(t)(I_{1x}I_{2x} + I_{1y}I_{2y}) \\ & + 2b(t)(I_{1y}I_{2x} - I_{1x}I_{2y})S_z \\ & + c(t)(I_{1z} - I_{2z})S_z \\ & + 2d(t)(I_{1x}I_{2x} + I_{1y}I_{2y})S_z \\ & + e(t)(I_{1y}I_{2x} - I_{1x}I_{2y}) \\ & + 1/2f(t)(I_{1z} - I_{2z}).\end{aligned} \tag{2.14}$$

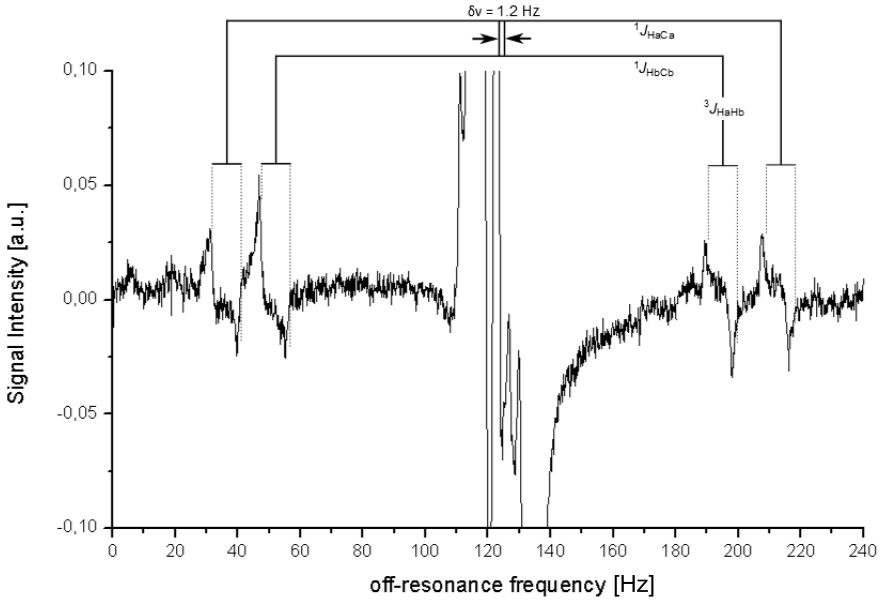

Figure 2.38: Chemical shift encoded as frequency difference between the centers of mass of the heteronuclear J-coupled doublets. The frequency separation of 1.2 Hz corresponds to a chemical shift of 2.4 ppm which is in good agreement with the value obtained from high field measurements.

As usual the time dependency is expressed by the coefficients $a(t).....f(t)$. The system of coupled differential equations

$$\begin{aligned}
\frac{\partial a}{\partial t} &= \pi\Delta J\, b(t) + \Delta\omega\, e(t) \\
\frac{\partial b}{\partial t} &= 2\pi^3 J_{HaHb}\, c(t) - \pi\Delta J\, a(t) - \Delta\omega\, d(t) \\
\frac{\partial c}{\partial t} &= -2\pi^3 J_{HaHb}\, b(t) \\
\frac{\partial d}{\partial t} &= \pi\Delta J\, e(t) + \Delta\omega\, b(t) \\
\frac{\partial e}{\partial t} &= 2\pi^3 J_{HaHb} f(t) - \pi\Delta J\, d(t) - \Delta\omega\, a(t) \\
\frac{\partial f}{\partial t} &= -2\pi^3 J_{HaHb}\, e(t),
\end{aligned} \tag{2.15}$$

where $\Delta\omega = \omega_1 - \omega_2$ and $\Delta J = J_{1S} - J_{2S}$ - the difference of proton Larmor-frequencies and difference of the heteronuclear couplings with respect to a given position of the heteronucleus have been introduced - must be solved under the boundary condition that the initial state of the system at $t = 0$ has be identical to the singlet state of parahydrogen, in singlet basis defined by Eq. (1.103). Note that S can be any, but only one of the heteronuclei defined as C_a, C_b and Si in Fig. 2.31. The real spectrum will be a superposition of isotopomer spectra weighted by their natural abundance. In conjunction with PHIP this observation has, to my knowledge, been reported first by Barkemeyer et al[6]. The coefficients are oscillating functions, which is easy to understand given that time dependent parts of the wave function are complex rotations. The frequencies of the oscillation are given by the J-couplings and chemical shifts characteristic for the system. The oscillation frequencies

$$\begin{aligned}
\nu_{up} &= 2\pi J_{\mathrm{HaHb}} \sqrt{1 + \left(\frac{J_{2S} - J_{2S}}{2J_{\mathrm{HaHb}}} + \frac{\nu_2 - \nu_1}{J_{\mathrm{HaHb}}} \right)^2} = 2\pi J_{\mathrm{HaHb}} \sqrt{1 + (y + x)^2} \\
\nu_{down} &= 2\pi J_{\mathrm{HaHb}} \sqrt{1 + \left(\frac{J_{1S} - J_{2S}}{2J_{\mathrm{HaHb}}} - \frac{\nu_2 - \nu_1}{J_{\mathrm{HaHb}}} \right)^2} = 2\pi J_{\mathrm{HaHb}} \sqrt{1 + (y - x)^2}
\end{aligned} \tag{2.16}$$

are a function of the differences in heteronuclear coupling constants and absolute precession frequency differences, both normalized to the homonuclear coupling between the former singlet state protons. The experimental spectrum is predicted by the time averaged density matrix, the steady state solution, where the ensemble averaging is over the time period τ_{evo} defined in the description of the experimental procedure. Time averaging under the condition $\tau_{evo} >> \nu_{up}$, which is (roughly) equivalent to stating that the evolution time is much larger than the homonuclear J-coupling, results in $\bar{b} = 0$ and $\bar{e} = 0$. The non-zero time averaged coefficients are[52]

$$\begin{aligned}
\bar{a} &= \frac{1}{2}\left(\frac{1}{1+(y+x)^2} + \frac{1}{1+(y-x)^2}\right) \\
\bar{c} &= \frac{1}{2}\left(\frac{y+x}{1+(y+x)^2} + \frac{y-x}{1+(y-x)^2}\right) \\
\bar{d} &= \left(\frac{1}{1+(y+x)^2} - \frac{1}{1+(y-x)^2}\right) \\
\bar{f} &= \frac{1}{4}\left(\frac{y+x}{1+(y+x)^2} - \frac{y-x}{1+(y-x)^2}\right).
\end{aligned} \tag{2.17}$$

The averaged three spin density matrix is very similar to the two-spin density matrix from Eq. (1.115). The density matrix after θ-pulse excitation is immediately obtained by application of Eq. (1.96) and for the I spins it is

$$\begin{aligned}
\overline{\rho^{\theta}_{I_1 I_2}} = &\sin\theta\cos\theta(\bar{a}-1)(I_{1y}I_{2z} + I_{1z}I_{2y}) \\
&+ \sin\theta\ \bar{c}\,(I_{2y} - I_{1y})S_z \\
&+ \sin\theta\ \cos\theta\bar{d}\,(I_{1y}I_{2z} + I_{1z}I_{2y})S_z \\
&+ \sin\theta\ \bar{f}\,(I_{2y} - I_{1y}).
\end{aligned} \tag{2.18}$$

2.4 Styrene

As nuclear magnetic resonance spectrosopy with PHIP polarized molecules in low magnetic fields yielded sufficiently high Signal-to-Noise ratios, that is SNR > 100, in ^{1}H-spectra it was attempted to obtain ^{13}C-spectra for quite many different compounds. Interestingly, ^{13}C-spectra could only be obtained in the hydrogenation of phenylacetylene to styrene.[53] An analysis of this behavior in the context of the three-spin density matrix was attempted. To that end knowledge of spectral parameters is of essential importance, as relevant parameters

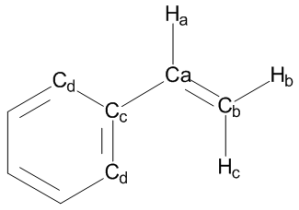

Figure 2.39: Position identifiers used for the description of styrene spectra.

for the spin system are only hetero- and homonuclear coupling constants as well as chemical shift differences. Spectral parameters were either obtained from high field measurements at 400 MHz ^1H Larmor-frequency or, in case of long range coupling constants, taken from ref. [36]. Position labels are explicitly shown in Fig. 2.39. Explicit declaration of the J-coupling constants has been waived for clarity due to the abundance of parameters required. Homonuclear J-coupling constants in the vicinity of the double bond have the following values $^3J_{\mathrm{HaHc}}$

[52] Note that some coefficients are very similar to Eq. (2.1) from the SPINOE section. An equation with lot of similarity to this can be found for every hyperpolarization method. The numerator of the fraction scales the intensity, the denominator contains a frequency difference. This can be a modulation by spin-spin coupling or a resonance frequency difference, if both is present in a compound it will be both.

[53] Note that during the ERS visit of Dr. Theis we also tested isotopically labeled diphenylacetylene and successfully managed to obtain spectra. These are, however, not my results to talk about, albeit significant time was invested from my side.

= 17.6 Hz, $^3J_{\mathrm{HaHb}}$ = 11.0 Hz and $^2J_{\mathrm{HbHc}}$ = 1.0 Hz. The ^{1}H chemical shifts in acetone-d6 are δ_{Ha}= 6.89 ppm, δ_{Hb} = 5.39 ppm, δ_{Hc}= 5.93 ppm. ^{13}C chemical shifts are δ_{Ca}= 137.2 ppm, δ_{Hb}= 113.6 ppm with experimentally determined heteronuclear coupling constants $^1J_{\mathrm{HaCa}}$= 154.0 Hz, $^1J_{\mathrm{HbCb}}$ = 160.0 Hz, $^1J_{\mathrm{HcCb}}$= 154.6 Hz. Taken from ref. [36] were $^2J_{\mathrm{HaCb}}$ = -1.0 Hz, $^2J_{\mathrm{HbCa}}$ = 0 Hz, $^2J_{\mathrm{HcCa}}$ = -4.5 Hz, $^3J_{\mathrm{HbCc}}$ = 11.2 Hz and $^3J_{\mathrm{HcCc}}$ = 6.4 Hz. Low field measurements with thermal prepolarization allowed for the determination of chemical shifts between aromatic protons and the alkyne proton referred to as H_c after hydrogenation to styrene. Thermally prepolarized samples of pure pheylacetylene as well as the sample used for PHIP experiments were taken prior to the experiment. Figure 2.40 shows the spectra obtained from 400 μL pure phenylacetylene and a normal NMR sample with only 20 μL of phenylacetylene.

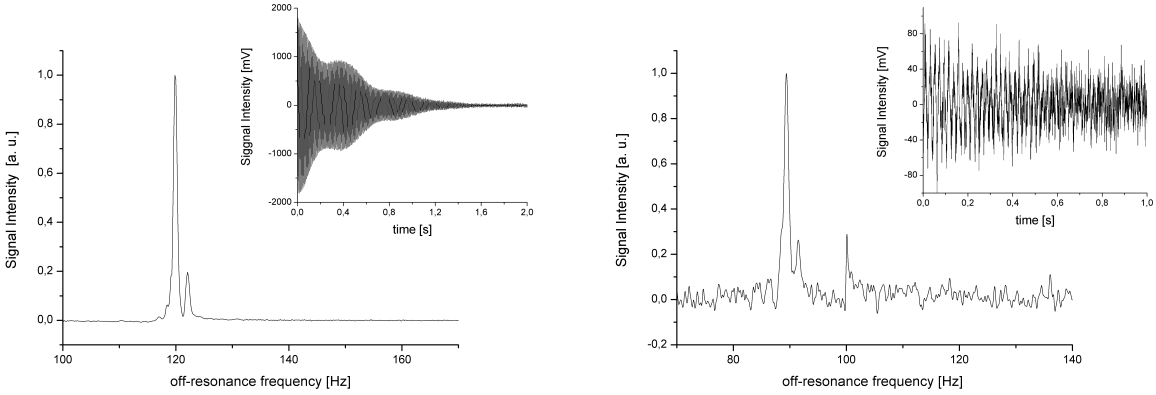

(a) (b)

Figure 2.40: a) FID (inset) and ^{1}H spectrum of 400 μL phenylacetylene thermally prepolarized at 2 T. The Larmor frequency is 500 kHz, the SNR is 400. b) Same as a) but a regular PHIP sample including catalyst and only 20 μL phenylacetylene. The SNR is 8:1. In both spectra the chemical shift difference between the vinyl and aromatic protons is well resolved (2.2 Hz) and corresponds to 4.3 ppm. The origin of the line at 100 Hz in b) is unknown.

If only the vicinity of the hydrogenation site is considered the system can be described as one three spin system $H_aH_bH_c$ and two four spin systems $H_a\,^{13}C_aH_bH_c$ and $H_aH_b\,^{13}C_bH_c$. The FID and spectrum at a ^{1}H resonance frequency of 500 kHz using $\pi/2$ pulse excitation for a parahydrogen experiment are shown in Fig. 2.41.[54]

Similar to the ^1H spectra of the ethoxyethylene the spectrum of styrene has the highest amplitude peak at the center frequency with an anti-phase line structure. The SNR of 285 allowed to resolve carbon satellites with a spectral width of approximately 34 Hz. The carbon satellites centers are shifted from the center frequency into two groups at $\pm$ 78 Hz, half the average heteronuclear $^1J_{CH}$ coupling in the vicinity of the hydrogenation site. The fine structure and spectral width observed in the satellite peaks a result of the homonuclear coupling constants $^3J_{\mathrm{HaHc}}$ and $^3J_{\mathrm{HaHb}}$. The peaks groups are the H_a, H_b and H_c subspectra of the $^{13}C_a$ and $^{13}C_b$ isotopomer subspectra. The C_a isotopomer subspectrum is a doublet of doublets of doublets (*ddd*). The largest frequency separation is caused by $^1J_{\mathrm{HaCa}}$ = 154.0 Hz, corresponding to the average frequency shift of the satellites. Further fine structure arises as a result of homonuclear J-coupling with $^3J_{\mathrm{HaHc}}$ = 17.6 Hz and $^3J_{\mathrm{HaHb}}$ = 11.0 Hz split each line of the heteronuclear doublet into a doublet of doublets resulting in the observed *ddd*-pattern. The anti-symmetric line structure most likely results from a coefficient and a spin order term (product operator) similar to $\bar{c}$ in the three spin density matrix. In the three spin density matrix this coefficient acts on a product operator of the form $+I_{1z} - I_{2z}$, also referred to as Anti-Zeemann spin order. These spin order terms result in an anti-phase signal pattern for the I spins as observed for the structures in the spectrum. The exact density matrix is, however, unknown. The C_b subspectrum is slightly more complicated as two protons are ^1J-coupled to this position. Both H_b and H_c subspectra do, however, have the same *ddd*-pattern as the H_a subspectrum. In this instance the largest frequency separation is caused by the heteronuclear

[54] procedure is exactly identical to the procedure detailed for ethoxyacetylene and will not be repeated.

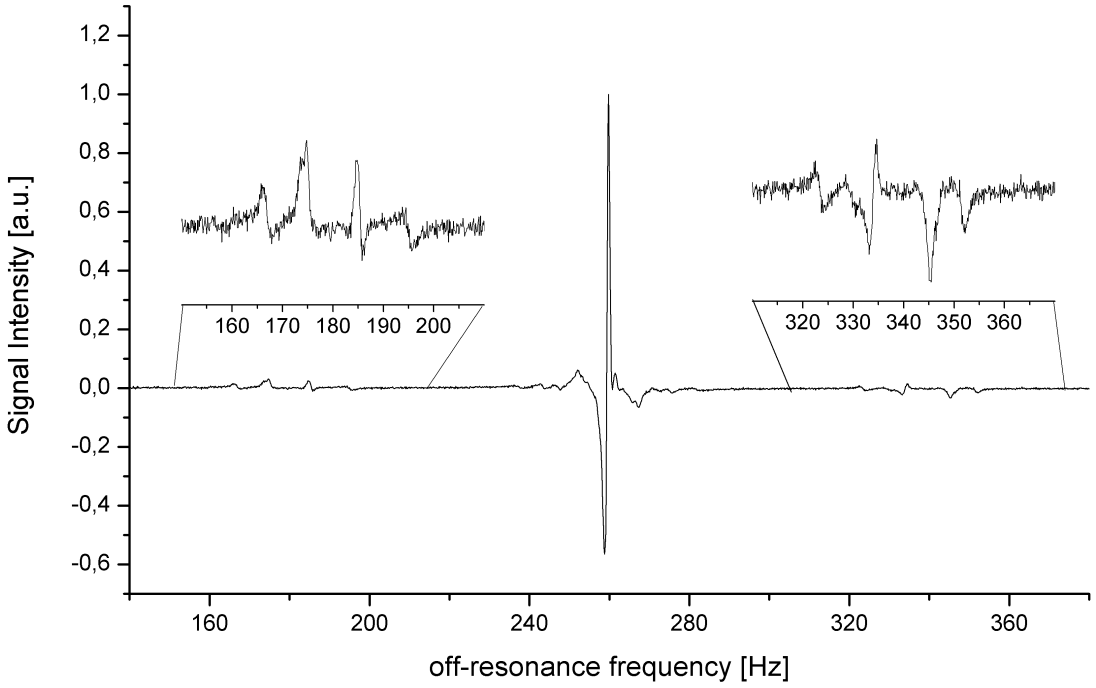

Figure 2.41: Single scan ^{1}H spectrum of styrene with para-hydrogen induced polarization and 90° pulse excitation. The SNR is 200:1. The insets show 10 times magnified ^{13}C satellite peaks.

coupling constants $^{1}J_{\mathrm{HbCb}}$ = 160.0 Hz and $^{1}J_{\mathrm{HcCb}}$ = 154.6 Hz. The doublet of doublets fine structure for $\mathrm{H_c}$ arises as a result of $^{3}J_{\mathrm{HaHc}}$ = 17.6 Hz and $^{2}J_{\mathrm{HbHc}}$ = 1.0 Hz; likewise for $\mathrm{H_b}$ only with $^{3}J_{\mathrm{HaHb}}$ = 11.0 Hz and $^{2}J_{\mathrm{HbHc}}$ = 1.0 Hz. The smallest splitting of 1 Hz is poorly resolved as linewidths are approx. 1 Hz. Another two group of peaks are located in a range of ± 20 Hz around the center frequency. The determination of the exact line positions and assignment of lines is very difficult. Long range heteronuclear coupling constants (that is ^{n}J, $n > 1$) have a similar magnitude as the homonuclear coupling constants. For example $^{2}J_{\mathrm{HcCa}}$ = -4.5 Hz, $^{3}J_{\mathrm{HbCc}}$ = 11.2 Hz, $^{3}J_{\mathrm{HcCc}}$ = 6.4 Hz are similar in magnitude to $^{3}J_{\mathrm{HaHc}}$ = 17.6 Hz and $^{3}J_{\mathrm{HaHb}}$ = 11.0 Hz. The chemical shift induced Larmor-frequency differences between aliphatic protons at a Larmor-frequency of 500 kHz are $\nu_{\mathrm{Ha}} - \nu_{\mathrm{Hc}}$ = 0.48 Hz, $\nu_{\mathrm{Ha}} - \nu_{\mathrm{Hb}}$ = 0.75 Hz and $\nu_{\mathrm{Hc}} - \nu_{\mathrm{Hb}}$ = 0.27 Hz. The chemical shift induced frequency differences are thus much smaller than the homo- and heteronuclear J-coupling and the spectrum of strongly coupled spinsystems of the type ABCX shows asymmetric line splitting in the strong coupling limit.

2.4.1 PHIP-Hyperpolarization of Heteronuclei

Adiabatic Longitudinal Transport After Dissociation Engenders Nuclear Alignment (ALTADENA) is one of the classical PHIP experiments for high field and the name is indicative of the chemical reaction being carried out prior to transfer in the high magnetic field of the experimental setup. As a result of different initial energy level populations the spectra obtained in ALTADENA experiments differ from PASADENA type experiments, but more importantly heteronuclear polarization levels are very different when performing an otherwise identical experiment with both procedures. In the earlier days after discovery of the effect rather of lot of empirical data has been gathered and a lot of the recent activity in the field consists of rediscoveries with concomitant refinement of the theoretical understanding of the processes involved. Among the empirical data gathered was that polarization transfer to heteronuclei is often observed under ALTADENA conditions as an intrinsic property, rather than an effect forced by pulse sequences, of the spin system. This phenomenon has been observed for several different heteronuclei in different compounds, and transfer to nuclei of the ligands of homogeneous phase

catalysts [19, 18] as well as transfer to heteronuclei in hydrogenative PHIP experiments has been reported individually by several groups. A comparison of ^{13}C signal enhancements has been performed by Stephan et al. using different alkynes[62].

It should be noted that, although different molecules were attempted (1-(tert-butyldiphenylsilyl)-2-(ethoxy)ethyne, methylpropiolate, ethylpropiolate, diphenylacetylene) the only instance where a ^{13}C-spectrum could be obtained from a single transient was the hydrogenation of phenylacetylene to styrene. Direct averaging of the FID cannot be performed due to slight resonance frequency drifts and spectra can be averaged only if the SNR is sufficient to assign one peak with a reasonable confidence level[55]. As a result no assessment about enhancement of heteronuclei could be made for other components[56]

Although the exact four spin density matrix for $I_1I_2I_3S$ spinsystems is unknown experimental evidence and evaluation of the three spin density matrix suggested that a qualitative explanation of the observations made by other groups could be preformed by evaluation of the terms in the three spin density matrix associated with S magnetization. Introducing the zero quantum coherence $(I_{1x}I_{2x} + I_{1y}I_{2y}) = ZQ_x$ the density matrix after a theta pulse for the S spins is

$$\overline{\rho_S^\theta} = \sin\theta(\bar{c}\,(I_{2y} - I_{1y})S_z + 2\bar{a}\,ZQ_xS_z). \tag{2.19}$$

and the observable signal is immediately obtained by application of Eq. (1.99) thus defining the measurable expectation value of the magnetization $\langle S\rangle$ of a nucleus S after a 90° x-pulse to be

$$\langle S_y\rangle = Tr[S_y\{\bar{c}\,(I_{1z} - I_{2z})S_y + \bar{d}\,ZQ_xS_y\}]. \tag{2.20}$$

As only these terms in Eq. (2.14) are related to S magnetization S_z. Analysis of the expectation value of the magnetization shows that $\bar{c}$ and $\bar{d}$ describe the amplitudes of spectral lines for an S-spin spectrum. As these coefficients govern the polarization transfer it is prudent to discuss the dependency of the coefficients on x, indirectly encoding field strength and y which is related to the molecular structure.

2.4.2 Matching conditions

The coefficients are repeated for convenience and it is

$$\bar{c}(x,y) = \frac{1}{2}\left(\frac{y+x}{1+(y+x)^2} + \frac{y-x}{1+(y-x)^2}\right) \tag{2.21}$$

$$\bar{d}(x,y) = \left(\frac{1}{1+(y+x)^2} - \frac{1}{1+(y-x)^2}\right). \tag{2.22}$$

Derivation of the extreme values of $\bar{c}(x,y)$ and $\bar{d}(x,y)$ is tedious and will not be shown. The upper and lower boundaries are $\bar{c} \in [-0.5; 0.5]$ and $\bar{d} \in [-1; 1]$.

It was first attempted to understand the behavior of $\bar{c}$ and $\bar{d}$ for the limits $x = 0$ and $y = 0$ corresponding to zero magnetic field $x = 0$ and identical values of the heteronuclear J-coupling constant. If y is assumed to be zero both $\bar{c}$ and $\bar{d}$ vanish and no further discussion in necessary.

If x is zero, as it is the case in zero magnetic field, $\bar{c}$ becomes

$$\bar{c} = \frac{y}{1+y^2}, \tag{2.23}$$

which is maximal for $y = 1$, thus defining the matching condition for zero magnetic field. For $y < 1$ the constant in the denominator is dominating and $\bar{c}$ never exceeds one. For $y > 1$ the term y^2 keeps $\bar{c}$ below 0.5 at all times. The maximum is obtained for $y = 1$ identical values of hetero- and homonuclear coupling, where $\bar{c} = 0,5$. This defines the matching conditions for low magnetic fields.

Regarding coefficient $\bar{d}$, inspection of Eq. 2.22 reveals that x cannot be neglected, because as a result of the

[55] where reasonable means being sure.
[56] high field NMR with the old PHIP setup didn't make any sense due to poor resolution.

−sign between terms one and two coefficient $\bar{d}$ vanishes for $x = 0$. For $x << 1$ the coefficient $\bar{d}$ is very close to zero and as a result no polarization transfer from this coefficient can be expected for low magnetic fields. Instead a magnetic field is a requirement and $\bar{d}$ becomes maximal if either of two cases is realized. The first possibility for coefficient maximization is realized when term two is as small as possible, or $1 + (y - x)^2$ has to be maximal, while the first term remains as large as possible, or $1 + (y + x)^2$ minimal, respectively. The largest value is obtained for $x = y$ thus defining the matching condition for high magnetic fields associated with coefficient $\bar{d}$.

2.4.3 Experimental Studies

A different approach relating immediately to an experiment is using y as a fixed parameter, as it is defined by the molecular structure and cannot be altered. x will take different values with different evolution fields and a value of x for which polarization transfer to heteronuclei occurs with highest efficiency may be determined by analyzing the dependence of $\bar{c}$ and $\bar{d}$ on x. For the experimental studies a procedure in analogy to the studies of ethoxyethylene has been used. The parahydrogen was generated using the BPHG090 system. The catalyst [1,4-Bis(diphenylphosphino)butane](1,5-cycloocta-diene)rhodium(I)tetrafluoroborate) was dissolved in 340 μL anhydrous acetone-d6 and 25 μL phenylacetylene were added. The samples are repeatedly frozen and degassed in vacuo prior to the experiment to avoid catalyst inactivation. The solution is subjected to 5 bar parahydrogen and shaken for 5 - 10 seconds at the fields given below. Data was recorded with a sampling rate of $3 \cdot 10^{-4}$s. Different values of the evolution field B_{evo} were chosen to vary x. The main reason for the choice of these values is that they can be conveniently and reproducibly realized. The first value was realized by shaking the sample for 10 seconds in residual magnetic field inside of a double layered μ-metal chamber, where $B_{evo} = 0.002$ G, with $x = 1.8 \cdot 10^{-4} \approx 0$. The second value is the Earth's magnetic field with $B_{evo} = 0.45$ G corresponding to an $x = 4 \cdot 10^{-2}$ and the third value is given the stray field just outside the magnet, just where it is possible to shake the sample. At this positions $B_{evo} \approx 5$ G and $x = 4.5 \cdot 10^{-1}$. It should be noted that an experiment that immediately transfers the sample from zero magnetic field to the magnet cannot be conducted, as brief exposure to the Earth's magnetic field cannot be avoided. The fourth value is defined by the magnetic field required to obtain a ^{13}C resonance frequency of 166 kHz, which corresponds to $B_{evo} = 155$ G or $x = 1.4$, which is identical to simply performing the low-field analogue of a PASADENA experiment. Using the values given prior to the discussion of the ^{1}H spectrum of styrene allows to calculate y for all ^{13}C positions in the vicinity of the double bond.[64]

For clarity $y_{S,I1,I2}$ is introduced, as there are nine possible values for the parameter y if the system of four coupled spins is approximated by superposition of three spin systems. Indices correspond to the position identifiers defined by Fig. 2.39. It is $y_{\mathrm{Ca,Ha,Hb}} = 7.0$, $y_{\mathrm{Ca,Ha,Hc}} = 4.5$, $y_{\mathrm{Ca,Hb,Hc}} = 2.25$, $y_{\mathrm{Cb,Ha,Hb}} = 7.3$, $y_{\mathrm{Cb,Ha,Hc}} = 4.4$, $y_{\mathrm{Cb,Hb,Hc}} = 2.7$, $y_{\mathrm{Cc,Ha,Hb}} = 0.4$, $y_{\mathrm{Cc,Ha,Hc}} = 1$, and $y_{\mathrm{Cc,Hb,Hc}} = 1.4$. From the low field matching condition associated with coefficient $\bar{c}$ strong enhancements are expected for all $y_{S,I1,I2} \approx 1$, whereas the high field matching condition associated with coefficient $\bar{d}$ is $x = y$. The problem is rather intricate as both coefficients are rather complex functions of x and y. $x = y$ is fulfilled at $B_{evo} =$ 5 G for $y_{\mathrm{Cc,Ha,Hb}}$, where $\bar{d} = -0.41$. However, the dependency on y cannot be neglected and for example for $y_{\mathrm{Cc,Ha,Hc}}$ it is $\bar{d} = -0.44$. Even if the spectra are recorded in low magnetic fields shuttling the sample through the stray field to the homogeneous volume leads to both low- and high-field matching conditions influencing the spectra.

It is rather surprising that a ^{13}C spectrum of styrene at a Larmor-frequency of 166 kHz can be obtained from a single transient (FID shown in Fig. 2.42), as the natural abundance of ^{13}C is only 1%. Nevertheless the spectrum shown in Fig. 2.43 obtained with 90° pulse excitation has five groups of peaks as a result of superposition of C_a and C_b isotopomer subspectra. The occurrence of five distinct groups in the spectrum can be described as a triplet of line groups for to the C_b isotopomer and a doublet of line groups for the C_a isotopomer. Figure 2.44 shows a magnified view of the $^{13}C_b$ isotopomer subspectrum. The heteronuclear coupling is anisochronous with $^1J_{\mathrm{HbCb}} \neq^1 J_{\mathrm{HcCb}}$ but the ^{1}H nuclei are nearly isogamous $\nu_{\mathrm{Hb}} = \nu_{\mathrm{Hc}} \approx 0.3Hz$ at the resonance frequency of 166 kHz. If J-coupling constants have similar magnitude ($^1J_{\mathrm{HbCb}} = 160.0$ Hz and

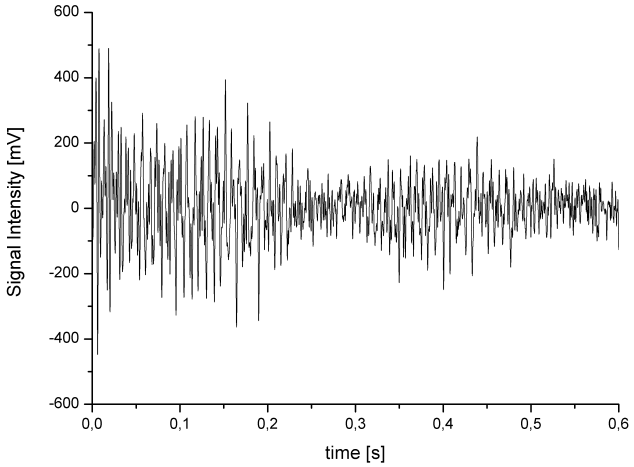

Figure 2.42: FID of ^{13}C in styrene at a resonance frequency of 166 kHz using para-hydrogen induced polarization and 90° pulse excitation. The SNR in a single scan is 16-19.

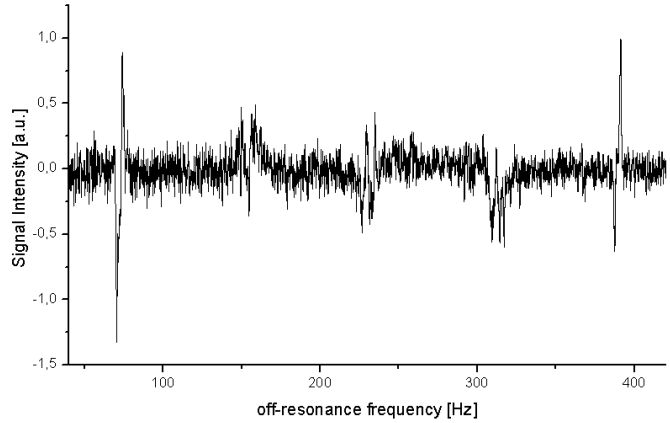

Figure 2.43: Spectrum of naturally abundant ^{13}C in styrene at a resonance frequency of 166 kHz with 90° pulse excitation using para-hydrogen induced polarization. The evolution field was 5 G, evolution time was 10 s. The spectrum shows five groups of peaks, one anti phase triplet and one anti-phase doublet (see text). High frequency peaks have reduced intensity because spectral bandwidth exceeds the width of the bandpass filter.

$^1J_{\mathrm{HcCb}}$= 154.6 Hz) the coupling pattern is a triplet, as observed in the spectrum. It is logical to assume that the triplet arises as a result of the $|\alpha\alpha\rangle$, $|\alpha\beta\rangle$ and $|\beta\beta\rangle$ state of protons $\mathrm{H_b}$ and $\mathrm{H_c}$. The frequency separation between the peaks is, however, exactly $^2J_{\mathrm{HaCb}}$ larger, as this heteronuclear coupling is too small to be resolved thus rendering ($^1J_{\mathrm{HC}} + {}^2J_{\mathrm{HC}}$) observable as heteronuclear coupling adds as line broadening shifting the observed frequency of the spectral line. Spectral parameters are more easily accessible from the lines at lowest and highest off-resonance frequencies and determination of spectral parameters from the spectrum is shown in Fig. 2.44. Regarding the structure of the two anti-phase doublets centered at 230 Hz off-resonance frequency the same analysis can be carried out, but the superposition of anti-phase doublets renders the peak at $\nu \approx 231.4$ Hz rather badly resolved. Nevertheless, identical spectral parameters can also be obtained by recognition of superimposed doublets.

The $^{13}\mathrm{C_a}$ isotopomer subspectrum is unfortunately less well resolved,[57] as several long range heteronuclear couplings of small magnitude, originating from the phenyl substituent as well as $\mathrm{H_b}$ and $\mathrm{H_c}$, result in fine structure below the resolution limit. The line broadening makes two line groups observable. Each of the line

[57] not shown in magnification.

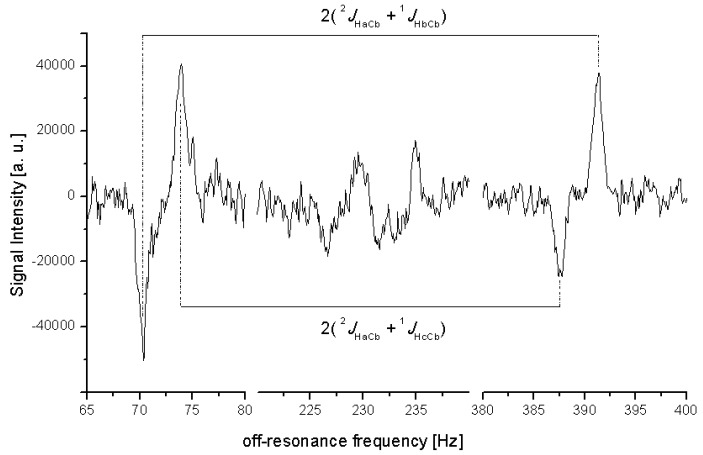

Figure 2.44: The anti-phase triplet corresponding to the C_b isotopomer subspectrum. All heteronuclear J-coupling constants can be obtained from the frequency separation between the the in phase doublets spaced by 2 ($^1J_{HC} + {}^2J_{HC}$). The peak group centered at 230 Hz is an anti-phase doublet of doublets. Assignment of ($^1J_{HC} + {}^2J_{HC}$) is more difficult because of anti phase peak superposition (see text for explanation).

groups separated by $^1J_{HaCa} = 154.0$ Hz of the $^{13}C_a$ isotopomer subspectrum is roughly a doublet. Fine structure is most likely mainly due to $^2J_{HcCa}$ = -4.5 Hz, where other very small long range heteronuclear coupling constants lead to the observed peak broadening. The center frequencies of the doublet of line groups and the triplet of line groups are shifted by approximately 4 Hz with respect to each other thus rendering the chemical shift difference $\delta_{Ca} - \delta_{Cb} = 23.6$ppm, corresponding to 3.9 Hz at 166 kHz Larmor-frequency, observable. ^{13}C spectra of styrene at other evolution fields show very similar spectral features as the spectra shown for the evolution field of 5 G with respect to line positions and SNR. This is most likely a result of the transfer process into the magnet where, as shown above, the high field matching condition is fulfilled for some spinpairs, whereas the low field matching condition is fulfilled in the Earth's field.

It is also possible to obtain spectra with an evolution field of 0 G is shown in Fig. 2.45. The spectrum

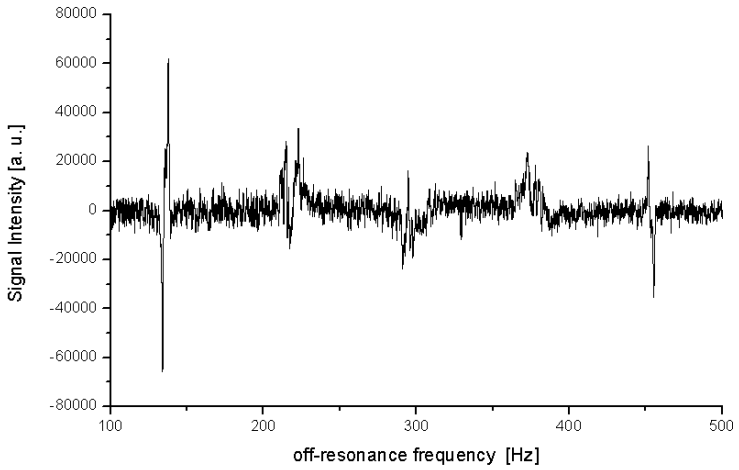

Figure 2.45: Spectrum of naturally abundant ^{13}C in styrene at a resonance frequency of 166 kHz with 90° pulse excitation and para-hydrogen induced polarization. The evolution field was 0 G, evolution time was 10 s. This spectrum shows five groups of peaks with identical relative positions but different phase. The triplet of the $^{13}C_b$ isotopomer subspectrum exhibits a down-up up-down pattern for the peaks at lowest and highest frequency, as opposed to the spectrum obtained at 5 G evolution field.

of styrene shown in Fig. 2.45 obtained after choosing an evolution field of 0 G, with experimental conditions

otherwise unchanged, contains the same information as the spectrum at an evolution field of 5 G but has a different appearance with respect to the relative phases of line groups. This is most notable by comparison of the highest and lowest frequency lines in Figs. 2.43 and 2.45, where the down-up down-up pattern at 5 G changes to an down-up up-down pattern for these four peaks. The third peak group in the center of also affected phase shift and due to superposition of anti-phase signals the peak group appears to be in dispersion.[58] From analysis of the three spin density matrix it is evident that the anti-Zeemann term largely responsible for anti-phase peak patterns is associated with coefficient $\bar{c}$ and thus the low field-matching condition, whereas coefficient $\bar{d}$ is associated with the intermediate to high field matching condition and the ZQ_xS_z spin order term and thus the J-coupling. Attempting an analysis of the four spin system with the three spin density matrix requires calculation of the coefficients in terms of a parametric discussion. It seems reasonable to assume that, as the protons referred to as H_a and H_b are the former para-hydrogen nuclei, coefficients associated with these y_{I1I2S} values should allow to predict and compare line amplitudes, but analysis of phase requires occupation and transition moments connecting the states which is not possible without the exact four-spin density matrix. For the relevant coefficients it is $\bar{c}_{\mathrm{CaHaHb}} = 0.14$ and $\bar{c}_{\mathrm{CbHaHb}} = 0.135$, where the dependency on x and y renders $\bar{c}$ identical at this specific value of the evolution field. The observed line intensities, nearly identical in Fig. 2.45 and Fig. 2.43, can thus be accounted for by the calculated coefficient value. As expected from the coefficient analysis $\bar{d}$ is negligibly small (10^{-6}) at both values of x and $\bar{d}$ seems to not contribute to the observed spectrum.

As a result the intensity of transition lines is rather similar at both 0 G and 5 G evolution field strengths. However the three spin density matrix is derived under the assumption that only S_z needs to be considered but experimental evidence suggests that evolution in the strong coupling regime does not allow to neglect the x and y-components of the S-spin operator. When placed inside the double layer μ-metal chamber the Larmor-frequency difference between ^{13}C and ^{1}H is several Hz, comparable to the homonuclear J-coupling. The spectrum obtained when choosing the Earth's as evolution field exhibits the same spectral features, where in this case the Larmor-frequency difference $\nu_{\mathrm{H}} - \nu_{\mathrm{C}}$ is approximately 1400 Hz, or 10 $^{1}J_{\mathrm{HC}}$. This is consistent with the conditions from where strong coupling may influence spactral appearance.[4] The mathematical models available are too limited to account for all observations made in this section. It should be noted that correct assignment of phase behavior can not be guaranteed considering the large spectral of the ^{13}C-spectra in this section. The behavior of the detector phase on the off-resonance frequency is unknown.

The three spin density matrix nevertheless allows for an explanation of the polarization transfer to heteronuclei observed under ALTADENA conditions. In this context it is especially enlightening to note that compounds structurally very similar to the ethoxyethylene (the authors subjected trimethylsilylacetylene to an ALTADENA experiment) used for the experimental proof of the three spin density matrix have been reported to exhibit strong ^{29}Si enhancements[25]. The observations made by Haake et al. fit perfectly to the polarization transfer conditions derived and described in terms of coefficient maximization. In the ethoxyethylene hydrogenation product the ^{29}Si isotopomer is exactly a three spin system. It would be expected that using the homonuclear J-coupling between H_a and H_b and the difference of the heteronuclear coupling constants of H_a and H_b to ^{29}Si the corresponding value of y should be very close to one and indeed $y \approx 0.8$ is obtained. The coefficient responsible for low field matching takes a value close to its maximum and correspondingly strong Silicium enhancements were observed.

[58] This phenomenon is reproducibly observable at Earth's magnetic field and in zero field and it is thus unlikely to be caused by the phase problem of the spectrometer.

Chapter 3

Conclusion and Outlook

The feasibility of a magnet system based on a combination of resistive coils yielding a shimmable electromagnet allowing for high resolution low field NMR spectroscopy was successfully demonstrated. The magnet system has been tested in a field range from 10-180 G. It was shown experimentally that the field homogeneity obtained at different frequencies remains in the sub-ppm regime and that it is largely independent of the flux density. With decreasing field strength external factors, such as positioning of paramagnetic or ferromagnetic metallic objects in the room is increasingly significant but sub-ppm homogeneity can nevertheless be maintained by careful shimming. High resolution spectra of nuclei with vastly different gyromagnetic ratios could be easily obtained by readjusting currents to match the frequencies defined by the filter settings of the lock-in amplifier stage. Adjustment of currents to the Larmor-frequency of a new nucleus is easily realized by multiplication of known currents with a factor defined by the ratio of gyromagnetic ratios. The only error source is the non-zero contribution of the Earth's magnetic field shifting the off-resonance frequency which can be easily adjusted manually. In order to facilitate the ease with which Larmor-frequencies may be changed a system making use of detection coil modules was developed and constructed. The rf-pulse excitation coil has been included in the probe rather than using a different coil for every detection coil. The time required to change from one nucleus to another at a different frequency has been improved from 30 minutes to less than five, constituting a great improvement over the experimental setup available in the initial stages of this thesis. Although the probe has been changed to make room for a new amplifier stage[1] the basic operating principles inspired by high field probes remain unchanged in the new setup. The electronically shimmable electromagnet with four separate shims and completely in-house optimized periphery, such as [2] current source and amplifiers does, at the moment, constitute one of the best-developed setups for NMR applications at this field range. The flexibility of the setup, where two different nuclei may be measured at the same Larmor-frequency simply by readjusting currents, is advantageous for SPINOE and PHIP experiments and allows to easily check for ^{13}C, ^{1}H enhancements. The large diameter of the rf-excitation coil leaves a lot of space for different layouts of probes, samples and gas-supply for hyperpolarization experiments. Due to a rather large homogeneous volume the experimental setup is robust to sample positioning variations between successive experiments. The large internal diameter of the mean field coil allows for great experimental flexibility and robustness to positioning errors of the sample was an essential factor for reproducibility of experiments making use of hyperpolarized gases.

In the following the newly constructed setup was used to investigate a possible application of hyperpolarized xenon for the polarization of ionic compounds and nuclei other than 13 C and 1 H. It could be shown that SPINOE is applicable to polarize ionic compounds despite the experimental difficulties in condensed phase. The current state of SPINOE theory was experimentally investigated and experimental results indicate that in order to obtain successful SPINOE the dynamic aspect of solution processes and the interdependence of solubility can not be neglected. It could be shown that the efficiency of SPINOE is very much solvent dependent. It is likely that in the future the applicability of SPINOE can be extended by making use of established quantum

[1] developed by M. Süfke and S. Appelt.

[2] I need to say this somewhere: quite ingeniously constructed.

chemical software packages. A better understanding of the important parameters for SPINOE, correlation times and interatomic distances, can be obtained rather easily by calculating interaction energies and equilibrium distances for xenon and target nucleus.

The parahydrogen section of this thesis was largely concerned with investigations regarding small spin systems with a low number of hydrogen nuclei in the vicinity of a hydrogenation site. Experiments allowing for not only derivation of the analytic description of a heteronuclear three-spin system polarized by parahydrogen, but also allowing for experimental proof of the theory were carried out. The results obtained in this section allow for solid understanding of polarization transfer phenomena to heteronuclei observed and reported under ALTADENA conditions, that is hydrogenation reactions in the Earth's magnetic field. The polarization transfer even in larger spin systems could be qualitatively explained by the matching conditions formulated and derived in this section.

In current developments low-field NMR spectroscopy has found increased attention, where many different factors contribute to this development. Advances in microelectronics and alternative detection schemes including atomic magnetometry and force or optically detected NMR allow to alleviate the signal to noise problem and hyperpolarization may be applied to further circumvent this problem. A solid theoretical understanding of strong coupling occurring in low and intermediate magnetic fields and advances in processor speeds have made simulation and understanding of more complex spectra viable. The possibility to construct probes and magnets in house and the affordability of low-field equipment and reduced operating costs over superconducting magnets make low field NMR research economically sensible.

With respect to hyperpolarization methodology it is my personal assessment that SPINOE is currently underused in NMR sciences. The possibility to recycle the gas mix necessary for Xenon hyperpolarization by constructing a closed cycle setup has not yet been explored. In the light of results presented by other groups, where liquid Xenon has been used as solvent for organic compounds[55] and reactions[61], raises the question whether is wouldn't be sensible to explore the use of hyperpolarized Xenon further. This could be carried out by accumulating Xe in a pressurized and cooled cell with automatized sample injection, mixing and transfer to the NMR. Helium and nitrogen would bypass the accumulation chamber as their melting points are well below the melting point of Xenon and residual organic traces in the gas should be quantitatively removable by cooling the gas flow to slightly above liquid nitrogen temperature.

With respect to PHIP methodology it is difficult to make an assessment about the state of the art and the future potential in the life and natural sciences. The most straightforward application is investigation of homogeneous phase hydrogenation reactions, where large signal enhancements would in theory allow to detect even minute quantities of byproducts or short lived intermediates in a much shorter timeframe than usual, in ideal cases a single scan. However, as PHIP polarization distribution over the molecule and appearance of the spectra is difficult to foresee some time will pass before it can be expected to be a routine application. As result of the difficulties involved in understanding PHIP, mainly to the intrinsically quantum mechanical nature of the involved singlet states, it is more likely that the methodology will find more applications in specific procedures warranting extensive optimization procedures from an economic viewpoint.

Bibliography

[1] A. Abragam. *Principles of Nuclear Magnetism.* Oxford University Press, 1961.

[2] R. Adams et al. "Reversible Interactions with para-Hydrogen Enhance NMR Sensitivity by Polarization Transfer". In: *Science* 323 (2009), p. 1708.

[3] S. Appelt et al. "Chemical analysis by ultrahigh resolution nuclear magnetic resonance in the Earths magnetic field". In: *Nat. Phys.* 2 (2006), p. 105.

[4] S. Appelt et al. "Paths from weak to strong coupling in NMR". In: *Phys. Rev. A* 81 (2010), p. 023420.

[5] S. Appelt et al. "Phenomena in J-coupled nuclear magnetic resonance spectroscopy in low magnetic fields". In: *Phys. Rev. A* 76 (2007), p. 023420.

[6] J. Barkemeyer, M. Haake, and J. Bargon. "Hetero-NMR Enhancement via Parahydrogen Labeling". In: *Journal of the American Chemical Society* 117 (1995), p. 2927.

[7] D. A. Barskiy et al. "The Feasibility of Formation and Kinetics of NMR Signal Amplification by Reversible Exchange (SABRE) at High Magnetic Field (9.4 T)". In: *Journal of the American Chemical Society* 136 (2014), p. 3322.

[8] R. S. Berry. "Correlation of Rates of Intramolecular Tunneling Processes, with Application to Some Group V Compounds". In: *J. Chem. Phys.* 32 (1960), p. 933.

[9] K. Bonhoeffer and P. Harteck. "Para- and ortho-hydrogen". In: *Z. physik. Chemie* B5 (1929), p. 292.

[10] C. Bowers and D. Weitekamp. "Parahydrogen and Synthesis Allow Dramatically Enhanced Nuclear Alignment". In: *Journal of the American Chemical Society* 109 (1987), p. 5541.

[11] C. Bowers and D. Weitekamp. "Transformation of Symmetrization Order to Nuclear-Spin Magnetization by Chemical Reaction and Nuclear Magnetic Resonance". In: *Phys. Rev. Lett.* 57 (1986), p. 2645.

[12] E. Brunner. "Solubility of hydrogen in 10 Organic Solvents at 298.15 K, 323.15 K and 373.15 K". In: *J. Chem. Eng. Data* 30 (1985), pp. 269–273.

[13] T. Carver and C. Slichter. "Polarization of Nuclear Spins in Metals". In: *Phys. Rev.* 92 (1953), p. 212.

[14] J. Colell. "Simulation, Aufbau und Signal-zu-Rausch-Verhältnis von Resonatoren und Konstruktion eines elektronisch shimmbaren Niederfeldkernspinresonanzspektrometers". Diplomarbeit. Forschungszentrum Jülich, 2010.

[15] J. Colell et al. "Fundamental Aspects of parahydrogen enhanced low-field nuclear magnetic resonance". In: *Phys. Rev. Lett* 110 (2013), p. 137602.

[16] C. Descamps et al. "Solubility of hydrogen in methanol at temperatures from 248.41 to 308.20 K". In: *Thermochimica Acta* 430 (2005), p. 1.

[17] R. Dronskowski. *Computational Chemistry of Solid State Materials.* Wiley-VCH Verlag GmbH, 2005.

[18] S. Duckett, C. Newell, and R. Eisenberg. "More than INEPT: parahydrogen and INEPT+ give unprecedented resonance enhancement to carbon-13 by direct proton polarization transfer". In: *J. Am. Chem. Soc.* 115 (1993), p. 1156.

[19] T. Eisenschmid et al. "INEPT in a chemical way. Polarization transfer from para hydrogen to phosphorus-31 by oxidative addition and dipolar relaxation". In: *Journal of the American Chemical Society* 111 (1989), p. 7267.

[20] H. Friebolin. *Ein- und zweidimensionale NMR-Spektroskopie*. VCH Verlagsgesellschaft, 1992.

[21] G. R. Fulmer et al. "NMR Chemical Shifts of Trace Impurities: Common Laboratory Solvents, Organics, and Gases in Deuterated Solvents Relevant to the Organometallic Chemist". In: *Organometallics* 29 (2010), p. 2176.

[22] Q. Gong, A. Gordji-Nejad, and S. Appelt. "Trace Analysis by Low-Field NMR: Breaking the Sensitivity Limit". In: *Anal. Chem.* 82 (2010), p. 7078.

[23] H. E. Gottlieb, V. Kotlyar, and A. Nudelman. "NMR Chemical Shifts of Common Laboratory Solvents as Trace Impurities". In: *J. Org. Chem.* 430 (1997), pp. 7512–7515.

[24] W. Schneider H. Bernstein J. Pople. "The Analysis of Nuclear Magnetic Resonance Spectra - I. Systems of Two and Three Nuclei". In: *Canadian Journal of Chemistry* 35 (1957), p. 65.

[25] M. Haake, J. Natterer, and J. Bargon. "Efficient NMR Pulse Sequences to Transfer the Parahydrogen-Induced Polarization to Hetero Nuclei". In: *J. Am. Chem. Soc.* 118 (1996), p. 8688.

[26] J. Halpern. "Mechanism and Stereoselectivity of Asymmetric Hydrogenation". In: *Science* 217 (1982), pp. 401–407.

[27] J. Halpern. "Mechanistic aspects of homogeneous catalytic hydrogenation and related processes". In: *Inorganica Chimica Acta* 50 (1981), p. 11.

[28] A. Harthun et al. "Rhodium- and palladium-catalysed proton exchange in styrene detected in situ by para-hydrogen induced polarization". In: *Chem. Commun.* (21 1996), p. 2483.

[29] R. van Heeswijk et al. "Hyperpolarized lithium-6 as a sensor of nanomolar contrast agents". In: *Magnetic Resonance in Medicine* 61 (2009), p. 1489.

[30] W. Heisenberg. "Mehrkörperprobleme und Resonanz in der Quantenmechanik. II." In: *Z. Physik* 41 (1927), p. 239.

[31] A. Hollemann and E. Wiberg. *Lehrbuch der anorganischen Chemie*. de Gruyter, 1995.

[32] S. Hommeltoft, D. Berry, and R. Eisenberg. "A Metal-Centered Radical-Pair Mechanism for Alkyne Hydrogenation with a Binuclear Rhodium Hydride Complex. CIDNP without Organic Radicals". In: *Journal of the American Chemical Society* 108 (1987), p. 5345.

[33] P. Hore, J. Jones, and S. Wimperis. *NMR: The Toolkit*. Oxford Science Publications, 2000.

[34] H. Bernstein J. Pople W. Schneider. "The Analysis of Nuclear Magnetic Resonance Spectra - II. Two Pairs of Two Equivalent Nuclei". In: *Canadian Journal of Chemistry* 35 (1957), p. 1060.

[35] J. D. Jackson. *Klassische Elektrodynamik*. de Gruyter, 1983.

[36] H. Kalinowski, S. Berger, and S. Braun. *13C-NMR Spektroskopie*. Georg Thieme Verlag, 1984.

[37] Martin Karplus. "Contact Electron Spin Coupling of Nuclear Magnetic Moments". In: *The Journal of Chemical Physics* 30 (1959), p. 11.

[38] Martin Karplus. "Vicinal Proton Coupling in Nuclear Magnetic Resonance". In: *Journal of the American Chemical Society* 85 (1963), p. 2870.

[39] L. D. Landau and E. M. Lifschitz. *Lehrbuch der theoretischen Physik III - Quantenmechanik*. Verlag Harri Deutsch, 1986.

[40] J. Leachman et al. "Fundamental Equations of State for Parahydrogen, Normal Hydrogen, and Orthohydrogen". In: *J. Phys. Chem. Ref. Data* 38 (2009), p. 721.

[41] M. Ledbetter et al. "Near-zero field nuclear magnetic resonance". In: *Phys. Rev. Lett.* 107 (2011), p. 107601.

[42] M. Levitt. *Spin Dymamics*. Wiley, 2008.

[43] F. Longpre et al. "Radical addition to ynol ethers". In: *Can. J. Chem* 86 (2008), p. 970.

[44] H. McConell, A. McLean, and C. Reilly. "Analysis of Spin-Spin Multiplets in Nuclear Magnetic Resonance". In: *Journal of Chemical Physics* 23 (1955), p. 1152.

[45] K. Miller et al. "Xenon NMR: chemical shifts of a general anesthetic in common solvents, proteins, and membranes". In: *Proceedings of the National Academy of Sciences* 78 (1981), pp. 4946–4949.

[46] J. Natterer and J. Bargon. "Parahydrogen induced polarization". In: *Prog. Magn. Res. Spec.* 31 (1997), p. 293.

[47] G. Navon et al. "Enhancement of Solution NMR and MRI with Laser-Polarized Xenon". In: *Science* 271 (1996), p. 1848.

[48] W. Nolting. *Grundkurs Theoretische Physik 3 - Elektrodynamik*. Springer, 2007.

[49] J. A. Osborn et al. "The Preparation and Properties of Tris(triphenylphosphine)halogenorhodium(I) and Some Reactions thereof including Catalytic Homogeneous Hydrogenation of Olefins and Acetylenes and their Derivatives". In: *J. Chem. Soc. A* 1 (1966), p. 1711.

[50] M. Packard and R. Varian. "Free Nuclear Induction in the Earths Magnetic Field". In: *Phys. Rev.* 93 (1954), p. 941.

[51] G. Pollack. "Solubility of xenon in n-alkanes: n-pentane through n-hexadecane". In: *Journal of Chemical Physics* 75 (1981), p. 5875.

[52] G. Pollack, J. Himm, and J. Enyeart. "Solubility of xenon in liquid n-alkanols: Thermodynamic functions in simple polar liquids". In: *Journal of Chemical Physics* 81 (1984), p. 3239.

[53] G. Pollack et al. "Solubility of xenon in 45 organic solvents including cycloalkanes, acids, and alkanals: Experiment and theory". In: *Journal of Chemical Physics* 90 (1989), p. 6569.

[54] M. Pravica and D. Weitekamp. "Net NMR alignment by adibataic transport of parahydrogen addition products to high magnetic field". In: *Chemical Physics Letters* 145 (1988), p. 255.

[55] P. Rentzepis and Douglass D. "Xenon as a solvent". In: *Nature* 293 (1981), p. 165.

[56] T. Room et al. "Enhancement of surface NMR by laser polarized noble gases". In: *Phys. Rev. B* 55 (1997), p. 11604.

[57] P. F. Seidler et al. "Synthesis of trinuclear alkylidyne complexes from dinuclear alkyne complexes and metal hydrides. CIDNP evidence for vinyl radical intermediates in the hydrogenolysis of these clusters". In: *Organometallics* 2 (1983), p. 1701.

[58] J. Sharma and L. Bouchard. "Strongly hyperpolarized gas from parahydrogen by rational design of ligand-capped nanoparticles". In: *Scientific Reports* 2 (2012), p. 1.

[59] C. P. Slichter. *Principles of Magnetic Resonance*. Springer, 1996.

[60] O. Sorensen et al. "Product Operator Formalism for the Description of NMR Pulse Experiments". In: *Prog. Nucl. Magn. Res. Spec.* 16 (1983), p. 163.

[61] M. Sponsler et al. "Liquid xenon: an effective inert solvent for carbon-hydrogen oxidative addition reactions". In: *Journal of the American Chemical Society* 111 (1989), p. 6841.

[62] M. Stephan et al. "13C PHIP NMR spectra and polarization transfer during the homogeneous hydrogenation of alynes with parahydrogen". In: *Magn. Reson. Chem.* 40 (2002), p. 157.

[63] P. Türschmann. "Inverser Dacheffekt und para-Wasserstoff induzierter Polararisationstranfer im Niederfeld". Masterarbeit. RWTH Aachen, 2012.

[64] P. Türschmann et al. "Analysis of para-hydrogen polarized spin systems in low magnetic fields". In: *Phys. Chem. Chem. Phys.* 16 (2014), p. 15411.

[65] F. Van den Ven and C. Hilbers. "A simple formalism for the description of multiple-pulse experiments. Application to a weakly coupled two-spin (I = 1/2) system". In: *J. Magn. Reson.* 54 (1983), p. 512.

[66] T. Weber et al. "Van der Waals bond lengths and electronic spectral ahifts of the benzene-Kr and benzene-Xe complexes". In: *Chemical Physics Letters* 183 (1991), p. 77.